National Library
of Canada

Bibliothèque nationale
du Canada

Canadian Theses Service

Service des thèses canadiennes

Ottawa, Canada
K1A 0N4

NOTICE

The quality of this microform is heavily dependent upon the quality of the original thesis submitted for microfilming. Every effort has been made to ensure the highest quality of reproduction possible.

If pages are missing, contact the university which granted the degree.

Some pages may have indistinct print especially if the original pages were typed with a poor typewriter ribbon or if the university sent us an inferior photocopy.

Reproduction in full or in part of this microform is governed by the Canadian Copyright Act, R.S.C. 1970, c. C-30, and subsequent amendments.

AVIS

La qualité de cette microforme dépend grandement de la qualité de la thèse soumise au microfilmage. Nous avons tout fait pour assurer une qualité supérieure de reproduction.

S'il manque des pages, veuillez communiquer avec l'université qui a conféré le grade.

La qualité d'impression de certaines pages peut laisser à désirer, surtout si les pages originales ont été dactylographiées à l'aide d'un ruban usé ou si l'université nous a fait parvenir une photocopie de qualité inférieure.

La reproduction, même partielle, de cette microforme est soumise à la Loi canadienne sur le droit d'auteur, SRC 1970, c. C-30, et ses amendements subséquents.

NL-339 (r. 88/04) c

Canada

National Library of Canada
Bibliothèque nationale du Canada

Canadian Theses Service
Service des thèses canadiennes

Ottawa, Canada
K1A 0N4

The author has granted an irrevocable non-exclusive licence allowing the National Library of Canada to reproduce, loan, distribute or sell copies of his/her thesis by any means and in any form or format, making this thesis available to interested persons.

The author retains ownership of the copyright in his/her thesis. Neither the thesis nor substantial extracts from it may be printed or otherwise reproduced without his/her permission.

L'auteur a accordé une licence irrévocable et non exclusive permettant à la Bibliothèque nationale du Canada de reproduire, prêter, distribuer ou vendre des copies de sa thèse de quelque manière et sous quelque forme que ce soit pour mettre des exemplaires de cette thèse à la disposition des personnes intéressées.

L'auteur conserve la propriété du droit d'auteur qui protège sa thèse. Ni la thèse ni des extraits substantiels de celle-ci ne doivent être imprimés ou autrement reproduits sans son autorisation.

ISBN 0-315-55443-6

Canada

THE UNIVERSITY OF ALBERTA

AN ASSESSMENT OF THE USE OF IMAGE ANALYSIS IN CARBONATE SEDIMENTOLOGY

by

BOONRASRI TONGPENYAI

©

A THESIS
SUBMITTED TO THE FACULTY OF GRADUATE STUDIES AND RESEARCH
IN PARTIAL FULFILMENT OF THE REQUIREMENTS FOR THE DEGREE
OF DOCTOR OF PHILOSOPHY

DEPARTMENT OF GEOLOGY

EDMONTON, ALBERTA
FALL, 1989

THE UNIVERSITY OF ALBERTA

RELEASE FORM

NAME OF AUTHOR BOONRASRI TONGPENYAI

TITLE OF THESIS AN ASSESSMENT OF THE USE OF IMAGE ANALYSIS IN CARBONATE SEDIMENTOLOGY

DEGREE FOR WHICH THESIS WAS PRESENTED DOCTOR OF PHILOSOPHY

YEAR THIS DEGREE GRANTED FALL, 1989

Permission is hereby granted to THE UNIVERSITY OF ALBERTA LIBRARY to reproduce single copies of this thesis and to lend or sell such copies for private, scholarly or scientific research purposes only.

The author reserves other publication rights, and neither the thesis nor extensive extracts from it may be printed or otherwise reproduced without the author's written permission.

(SIGNED) Boonrasri Tongpenyai

PERMANENT ADDRESS:

68/5 MOO 3, TUMBOL BANGKRABAOW
NAKORNCHAISRI, NAKORNPATHOM
THAILAND 73120

DATED April 27, 1989

THE UNIVERSITY OF ALBERTA

FACULTY OF GRADUATE STUDIES AND RESEARCH

The undersigned certify that they have read, and recommend to the Faculty of Graduate Studies and Research, for acceptance, a thesis entitled AN ASSESSMENT OF THE USE OF IMAGE ANALYSIS IN CARBONATE SEDIMENTOLOGY submitted by BOONRASRI TONGPENYAI in partial fulfilment of the requirements for the degree of DOCTOR OF PHILOSOPHY in GEOLOGY.

....

Supervisor

....

....

D. A. Craig

....

Charles F. Kahle

....

External Examiner

Date April 27, 1989

DEDICATION

To my parents, Buaros, Somthong, Thongyu; my husband, Yothin; and my daughter, Aimon.

ABSTRACT

Three image analysers, the density slicer, the automatic image analyser and the digitized graphic tablet, were used to study three quantitative geological problems. The results suggest that image analysis is a valuable tool for such studies, but each analyser has specific strengths and limitations. The density slicing technique is useful for delineating subtle variation in the grey tone of an image. Images comprising well-defined features, homogeneous in tone, can be analysed using an automatic image analyser. The digitized graphic tablet is useful if only the physical dimensions of a feature are needed.

Analysis of colour and black-and-white aerial photographs, using density-slicing technique in conjunction with field investigations, allowed the delineation of biological communities and substrate types in lagoons around Grand Cayman. Such aerial photograph maps are reliable with a 90% accuracy. The quantitative study of changes in the distribution of biologic communities and substrate types suggests an increased growth of *Thalassia* and a decrease in the volume of sand in the lagoons along the south coast during 1971 to 1985.

A digitized graphic tablet was used for size analysis of *Trypanites* and *Dendropoma (Novastoa) irregulare*?. The resulting information would be impossible to obtain using conventional methods. Size analysis of *Trypanites* from the Late Devonian Waterways Formation indicated that, in two dimensions, the size of boring is best described by its diameter. Size distribution obtained from the study of one thin section can be used to represent the distribution of the population, provided the thin section includes enough borings. Since the orientation of the boring affects the percent bored area, the average percentage should be calculated using numerous sections through the specimen.

Results from size analysis of vermetid gastropods suggest that the vermetid buildups around Grand Cayman are formed of one species, *Dendropoma (Novastoa) irregulare*?. The relationship between shell diameter and thickness indicates isometric

growth in the early stage and anisometric growth in the later stage. Based on size distribution of the vermetid gastropods and on radiometric dating, it is probable that coastal environmental conditions were more suitable for vermetid buildup 200 years ago than they were 600 years ago.

ACKNOWLEDGEMENTS

I am indebted to Dr. Brian Jones who served as my academic advisor, counsel, and friend for his patience, guidance, encouragement, and support during the course of my study. I am especially appreciative of his skillful editing which have improved this thesis considerably. I would like to thank my examining committee members, Drs. C. F. Kahle, D. A. Craig, R. A. Burwash, and S. G. Pemberton for their helpful suggestions and constructive criticisms.

I am grateful to the Thai Government for permission for a leave of absence during the course of study. I am greatly indebted to the Canadian International Development Agency (CIDA) who funded this study and made the completion of this thesis possible. Additional support for the research came from a National Sciences and Engineering Research Council of Canada (grant A6090 to Dr. B. Jones).

My thanks are extended to Mr. K. Campbell of the Remote Sensing Centre for his invaluable help and expertise with the density slicer; to George Braybrook for his help with the automatic image analyser; to Dr. S. Pawluk of the Department of Soil Sciences for permission to use the digitized graphic tablet; to Michael Abley for his technical assistance; to Dr. B. Jones and Ian Hunter for their help with photography. Thanks to Mr. Richard Beswick, Director of the Water Authority, Cayman Islands, for lending me some of aerial photographs used in this study. Underwater photographs were kindly provided by Dr. B. Jones, Ian Hunter, and Robert MacDonald. I sincerely thank Ian Hunter for his help in field investigations. Accommodation on Grand Cayman provided by Sam Ng is appreciated.

Many thanks are extended to Mr. J. W. Mossop, CIDA-Thailand Project Coordinator; Mr. B. Caldwell, CIDA Coordinator; and the staff at the International Centre of University of Alberta for their help and friendship that made my stay in Canada a pleasant one. My thanks are also extended to Elsie Tsang for her generous assistance in

various aspects and to Leni Honsaker for her friendship. My appreciation is extended to my fellow graduate students for their encouragement and moral support. Finally, special thanks go to Srilai, Kamol, Sumalee, and my family for their everlasting support.

TABLE OF CONTENTS

Chapter Page

I. INTRODUCTION 1

II. IMAGE ANALYSIS 3

A. BASIC DEFINITIONS 3

B. IMAGE ANALYSIS SYSTEM 4

C. ESSENTIAL STEPS IN IMAGE ANALYSIS 5

Image processing 7

Digitization 7

Image enhancement 8

Segmentation 8

Feature extraction 14

Measurement of features 14

Size measurement 15

D. SYNOPSIS 18

III. PREVIOUS WORK ON THE APPLICATION OF IMAGE ANALYSIS IN GEOLOGY 19

A. APPLICATIONS OF IMAGE ANALYSIS ON A MICROSCOPIC SCALE 19

B. APPLICATIONS OF IMAGE ANALYSIS ON A MACROSCOPIC SCALE 23

C. APPLICATIONS OF IMAGE ANALYSIS ON MAPPING 24

D. SYNOPSIS 25

IV. IMAGE ANALYSIS INSTRUMENTS 26

A. DENSITY SLICER 26

Fundamentals and basic operations 29

Sources of errors 31

Error caused by shading and scanner variations 31

Error caused by effect of stray light 36

Error caused by limitation of instrument 40

B. AUTOMATIC IMAGE ANALYSIS SYSTEM 42

Fundamentals and basic operations 42

Sources of errors 45

C. DIGITIZED GRAPHIC TABLET 46

Fundamentals and basic operations 49

Sources of errors 49

D. SYNOPSIS 52

V. STATISTICAL METHODS 54

A. BASIC DEFINITIONS 54

B. MODE AND MEAN 55

C. MEASURES OF VARIABILITY 56

D. PRECISION AND ACCURACY 57

E. SAMPLING TECHNIQUE 58

F. SAMPLE SIZE 61

G. HYPOTHESIS TESTING 62

t test 63

Analysis of variance 66

Mann-Whitney *U* test 69

H. CORRELATION AND REGRESSION 70

VI. APPLICATION OF IMAGE ANALYSIS TO MAPPING 72

A. INTRODUCTION 72

B. GENERAL PHYSICAL CONDITIONS ON GRAND CAYMAN 73

C. GENERAL GEOLOGY AND TECTONICS 77

D. MATERIALS 79

E. METHODS 81

Density-slicing technique 81

Automatic-image-analysis technique 82

Field work 83

F. COMPARISON OF THE TWO IMAGE ANALYSIS TECHNIQUES ...83

Aerial photograph map obtained via density-slicing technique 84

Aerial photograph map obtained via automatic-image-analysis technique 84

G. CLASSIFICATION OF AERIAL PHOTOGRAPH MAP 91

Primary classification of aerial photograph maps 91

Verification of primary classification of aerial photograph map 95

H. ACCURACY ASSESSMENT 111

Sampling technique 115

Results 116

I. FACTORS AFFECTING CLASSIFICATION 119

Limitation of conventional mapping technique 119

Lack of contrast in tone between different features 120

Basic assumption in mapping techniques 121

J. DETECTION OF BOTTOM FEATURES 121

K. DETECTION OF CHANGES IN COMMUNITIES THROUGH TIME 125

Changes of *Thalassia* community 126

L. INTERRELATIONSHIP BETWEEN COMMUNITIES 129

M. IMPLICATION OF CHANGES IN THE DISTRIBUTION OF *THALASSIA* COMMUNITY 129

N. SYNOPSIS 133

VII. APPLICATION OF IMAGE ANALYSIS TO SIZE MEASUREMENT 135

A. INTRODUCTION 135

B. APPLICATION - I: SIZE ANALYSIS OF *TRYPANITES WEISEI* IN THE DEVONIAN STROMATOPOROIDS 135

Materials 136
Geometry of boring 139
Methods used in study of trace fossils 139
Techniques used in this study 142
  Density-slicing technique 142
  Automatic-image-analysis technique 145
  Digitized-graphic-tablet technique 148
Comparison of the results obtained via graphic tablet technique with those obtained via conventional method 152
  Statistical test 152
  Discussion 159
Size distribution 167
Effect of orientation of boring on percent bored area 167
Orientation of geopetal structure 176
Synopsis 176
C. APPLICATION - II: SIZE ANALYSIS OF VERMETID GASTROPODS 177
Materials 177
Methods of study 177
Results on size measurement 181
Discussion 188
  Ontogenetic variation 188
  Size-frequency distribution 190
Synopsis 193
VIII. CONCLUSIONS 194
IX. REFERENCES 197

LIST OF TABLES

Table Page

IV-1 Summary of data on amount of halo error 38

IV-2 An example of area calculation 41

IV-3 Assessment of error involved in the measurements of area and major and minor axes, using digitized graphic tablet 51

V-1 Summary of sampling techniques 60

V-2 The analysis of variance table 67

VI-1 Summary of annual temperatures on Grand Cayman 76

VI-2 Summary of the detection of community categories from aerial photograph maps by means of density-slicing technique 112

VI-3 Summary of the distribution of communities in term of percent area with respect to the total area of each location 113

VI-4 Summary of the distribution of various communities in East Sound (North) as shown in published map by Rigby and Roberts (1976) 114

VI-5 Summary of modified data on the percent of biologic communities and substrate of East Sound (North) 114

VI-6 A map accuracy error matrix 117

VI-7 Summary of results of regression analysis 130

VII-1 Laboratory techniques for studying trace fossils 141

VII-2 Basic measurements made by the graphic tablet applicable to size analysis 149

VII-3 Summary of data on size measurement of *Trypanites* 153

VII-4 Summary of the results of *F*-test and *t*-test of length data of *Trypanites* 156

VII-5 Summary of the results of *F*-test and *t*-test on the cross-sectional area data of *Trypanites* 157

VII-6 Summary of the results of *F*-test and *t*-test of width data of *Trypanites* 158

VII-7 Assessment of error measured area by graphic tablet versus calculated area using rectangle and ellipse 164

VII-8 Data on size measurement used to evaluate the effect of shape of cross-sectional profile on percent error 165

VII-9 Summary of data on the number and percent of *Trypanites* 166

VII-10 Summary of data on width measurement of *Trypanites* from 12 thin sections 168

VII-11 Results of analysis of variance of diameter of *Trypanites* 169

VII-12 Summary of number of borings and percent bored area per thin section 174

VII-13 Summary of data on shell diameter and thickness of vermetid gastropods 183

VII-14 Summary of the results of the Mann-Whitney *U* test on diameter of vermetid gastropods 191

LIST OF FIGURES

Figure Page

II-1 Principle steps in image analysis 6

II-2 Example of logical operator comparing two binary images on a pixel for pixel basis and showing the result in the image area specified in mathematical expression 12

II-3 Diagram showing diameters used in image analysis 13

II-4 Example of erosion and dilatation transformations 16

II-5 Schematic diagram showing effect of erosion and dilatation on two sizes of features 17

IV-1 Schematic diagram showing set of test samples with various sizes 32

IV-2 Schematic diagram showing effect of scanner variations 35

IV-3 Schematic diagram showing effect of stray light on sample of size 2 x 2 cm and 10 x 10 cm 37

IV-4 Graphs showing relationship between amount of halo error, size, and number of feature in the field of view 39

IV-5 Set of test samples used in assessment of errors 50

V-1 Schematic diagrams showing various sampling techniques 59

V-2 Example of the stabilized probability plot 64

VI-1 Location map of Grand Cayman 74

VI-2 Geological map of Grand Cayman 78

VI-3 Community and bottom-type map of South Sound 92

VI-4 Community and bottom-type map of Blue Rock Bay 93

VI-5 Community and bottom-type map of East Sound 94

VI-6 Grey level histrogram of aerial photograph map 96

VI-7 Schematic diagram showing cross-section of blowout 122

VI-8 Schematic diagram showing succession development patterns of biologic communities and substrate 130

VI-9 Graphs showing cross-plots between communities 131

VII-1 Schematic diagram showing cross-sectional views of cylindrical boring with hemispherical cap cut at various angles and positions. 140

VII-2 Schematic diagram showing Feret's diameter. 151

VII-3 Graphs showing results of normality test of width of borings 155

VII-4 Frequency histrogram for length of borings 160

VII-5 Frequency histrogram for cross-sectional area of borings 161

VII-6 Frequency histrogram for width of borings 162

VII-7 Cross-plots of length of boring and percent error 165

VII-8 Schematic diagram of stromatoporoid head showing differential distribution of borings 171

VII-9 Schematic diagram showing orientation of boring with respect to vertical axis 172

VII-10 Frequency histrogram of orientation of borings with respect to vertical axis 173

VII-11 Diagrams showing orientation of geopetal structures in stromatoporoid heads X, Y, and Z 175

VII-12 Location map of Grand Cayman and schematic cross-sections of the coastal areas at Boddentown and Great Bluff Estates showing general setting of vermetid buildups 178

VII-13 Schematic diagram showing cross section of vermetid gastropod 182

VII-14 Size-frequency histograms of vermetid gastropods 185

VII-15 Graphs showing the results of normality test of samples of vermetid gastropods 186

VII-16 Frequency histograms of shell thickness of vermetid gastropods 187

VII-17 Cross-plots between diameter and shell thickness of vermetid gastropods 189

LIST OF PHOTOGRAPHIC PLATES

Plate		Page
IV-1	The modules of density slicer	27
IV-2	An example of shading error	33
IV-3	The modules of automatic image analysis system	43
IV-4	The modules of digitized graphic tablet	47
VI-1	Aerial photograph maps of biological communities and substrates of Frank Sound	85
VI-2	Aerial photograph maps of biological communities and substrates of East Sound (North), East Sound (South), and South Sound	87
VI-3	Aerial photograph maps of biological communities and substrates of South Sound and Blue Rock Bay	89
VI-4	Various distribution of *Thalassia* community	99
VI-5	Coral community	101
VI-6	Brown algae community - Rubble flat	103
VI-7	Brown algae community - Rocky floor	105
VI-8	Brown algae community - Rocky floor, and barren sand	107
VI-9	Transition zone	109
VI-10	*Thalassia* bank and blowout	123
VII-1	Negative photograph of thin section A showing the distribution of *Trypanites weisei.*	137
VII-2	Resulted image of thin section A obtained from density slicing technique	143
VII-3	Resulted image of thin section A obtained from automatic image analyzer	146
VII-4	Photograph of hand specimen of vermetid gastropods	179

I. INTRODUCTION

Quantitative geology is not a new subject since its roots can be traced back to the 1830's (Merriam, 1981). Although techniques have been developed through time, the basic steps involved in analysis are still the same. These steps are: (1) formulation of the problem, (2) acquisition of data, and (3) statistical analysis. The formulation of the problem and statistical analysis are problem-dependent while the acquisition of data is a general concern in any quantitative analysis. Jones (1988a) stated that two important concerns about the acquisition of data are: (1) selecting the proper parameter for the problem being considered, and (2) the accuracy of the measurements. In this study, attention will focus on these aspects.

Recently, with the advances in computer technology, modern image analysers show great potential for use in overcoming difficulties encountered in time-consuming conventional methods. The modern image analyser also offers several distinct advantages, such as a large amount of data can be acquired in a limited time and various parameters can be selected. Therefore, the accuracy of the analysis is improved since it partly depends upon the number of measurements used. In addition, the quality of an image (any two-dimensional pictorial representation of an object) can be improved using image-processing techniques. The term "image analysis" is used to denote all the processes involved in the quantitative analysis of an image.

The main objective of this study is to assess the use of image analysis in carbonate sedimentology. Three different image analysers were used, a density slicer, an automatic image analyser, and a digitized graphic tablet. Emphasis is placed on evaluating the efficiency of each instrument and the reliability of the results. The use of image analysis is demonstrated with respect to mapping and size analysis.

To test the application of image analysis to mapping, lagoons around Grand Cayman were selected as study areas. Sequential aerial photographs were studied to identify and describe the spatial patterns of the substrate and biological communities. Analyses of these aerial photographs were done by means of the density slicer and the automatic image analyser.

Although aerial photographs had been very useful in coastal studies (e.g. Hopley, 1978; Kelly and Conrod, 1969; Harris and Umbach, 1972), those studies had concentrated on qualitative analysis. The present study tries to establish the possibilities and limitations of the use of aerial photographs for the quantitative analysis of changes in the distribution of substrate and biologic communities through time. The accuracy of the maps derived from aerial photographs was tested by comparing them to the published maps of the area. Data from field investigations were used to verify the classification of aerial photograph maps. The relationships between the biological communities and substrate were determined using correlation and regression analyses.

For the application of image analysis to size measurement, the aim of the experiment was to investigate an appropriate method for measuring the sizes of features composed of nonuniform tones. All three image analysers were used. The use of image analysis is described by reference to two applications: (1) the analysis of size of borings in Devonian stromatoporoids, including the assessment of boring size and the percent of the bored area, and determination of the orientation of the borings and the orientation of the geopetal structures in the boring, and (2) the analysis of size of vermetid gastropods from Grand Cayman, including analysis of shell size and shell thickness. The reliability of the results obtained in this study was tested by comparing them with results obtained by conventional method and by different investigators. In order to determine whether the data obtained via two different methods belong to the same statistical population, various hypothesis-testing statistics were used.

II. IMAGE ANALYSIS

The term "image analysis" is used to denote the acquisition of numerical data on the basis of information extracted from images or image sequences (Bradbury, 1979; Swenson and Attle, 1979; Fabbri, 1984). For clarity and completeness, some basic definitions, background information, and relevant image analysis concepts are discussed in this chapter.

A. BASIC DEFINITIONS

An *image* is any two dimensional pictorial representation of an object, irrespective of the imaging device used to produce it. *Tone* and *texture* are two fundamental inherent properties of an image that have been widely used in image analysis. Tone, sometimes called grey-tone, refers to the varying shades of grey of the resolution cells in a black-and-white photographic image (Haralick *et al.*, 1973; Sabins, 1987). Drury (1987) included the different colours or relative brightness of parts of the surface making up an image in the concept of tone. In this study, tone is used in both senses, since both black-and-white and colour images were used. Texture describes the spatial distribution of tonal variations in any given area (Haralick *et al.*, 1973). These two ideas are intuitively related. Tone can be the predominate characteristic if an area shows slight changes in grey-tone. Conversely, if there is a large variation in grey tone the characteristic property is texture.

In a digital image, the smallest discrete point in a picture is termed a *picture element*, commonly known by the abbreviation *pixel*. A pixel usually has a number associated with it which denotes the *grey level* (or *grey value*). The grey level of a feature in an image may correspond to its density, absorbence, reflectance or transmittance, depending on how the feature is imaged. The range of this number depends on the type of instrument used. Two commonly used ranges are 0 to 63 (64 grey levels) and 0 to 255 (256 grey levels). However, ranges of 16 and 32 grey levels are also available. When analysing an image the features of interest is usually separated from surrounding features by using a binary image concept. A *binary image* is an image that has only two values of grey level, 1 or 0, which can be considered as black (features of interest) and white (background) or vice versa.

B. IMAGE ANALYSIS SYSTEM

Quantitative data can be gathered from images by: (1) manual methods (Thomson, 1930; Tomkeieff, 1945; Chayes, 1949, 1956; Gadgil, 1963; Underwood, 1970; Weibel, 1979; Russ, 1985), (2) semi-automatic methods (Schäfer *et al.*, 1981; Wilson, 1983; Kobluk and Kozelj, 1985; Klapper and Foster, 1986; Lazarus, 1986; Robertson, 1986), or (3) automatic methods (Minnis, 1984; Dilks and Graham, 1985; Ruzyla, 1986; Dorobek *et al.*, 1987).

The manual method (e.g. point counting) requires the superimposition of some form of test probe system of lines or points upon the image. The observer then records the numbers of points which fall on, or intersect with, the components of interest. The operator is responsible for the recognition, selection, and recording of the different categories of object in the images. This method generally allows analysis of complex images and images of low contrast and rather poor quality which are difficult to handle by automated systems. It is also convenient for small-scale problems involving relatively small numbers of points and small fields. However, this method is relatively time-consuming and the results of the analyses are dependent upon the skill of the analyst.

Semi-automatic systems of image analysis usually involve some form of digitizing tablet which allows the user to pass numerical digitized data directly into a computer. The recognition and delineation of components of interest is carried out by the user while the numerical data is acquired and processed by the computer. This systems allow the analysis of an image at any level of magnification either from photographic prints or images projected directly on the digitizer tablet. It is ideal for the measurement of physical dimensions of complex images (e.g. images with irregular shaped features or with nonuniform grey level) which cannot be analysed by automatic system. In terms of time, this system is intermediate between manual and automatic-image-analysis methods.

Fully automatic-image-analysis systems are based upon some form of image plane television scanning input which provides the signals for the detector and the central processing modules. The television camera is coupled to a suitable imaging device to produce an electronic video image. The image is then subjected to a detection process where features of interest in the image are separated from the background on the basis of their grey level or contrast differences. Image sources may take a variety of forms, such as an optical microscope, scanning electron microscope, photographic, or negative-imaging devices. The detected features are then counted, measured, and classified according to a wide range of geometric, densitometric, and textural criteria. The automatic-image-analysis system is an ideal tool for acquiring a large amount of data in a limited time. Dilks and Graham (1985) reported that the compositional analysis of sandstones required approximately 15 second per image field. Ruzyla (1986) reported that, in the study of pore spaces, only 1 hour was required for processing 15 to 20 SEM photographs on the automatic image analyser. This system may, however, have limitations when applied to complex images and images that lack grey-level discrimination.

C. ESSENTIAL STEPS IN IMAGE ANALYSIS

The essential steps in digital image analysis are: (1) image processing, (2) measuring the key parameters of each feature, and (3) interpreting the data statistically to quantify the image (Fig. II-1). In this chapter only the principle stages in the first two steps are discussed. For statistical analysis, different kinds of problems require different methods of statistical analysis. The statistical methods used in this study will be discussed separately in Chapter 5.

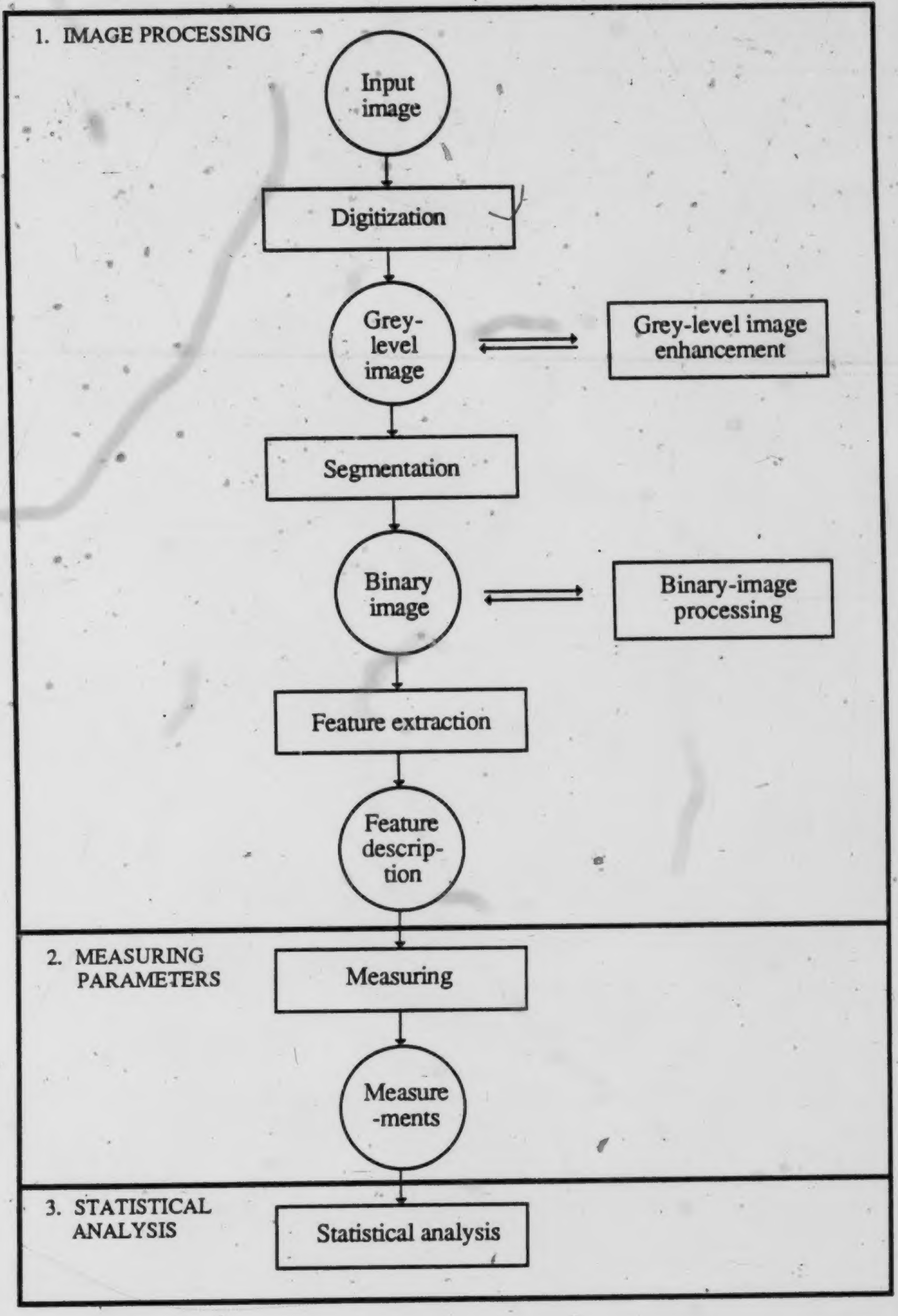
1. IMAGE PROCESSING
Input image
Digitization
Grey-level image
Grey-level image enhancement
Segmentation
Binary image
Binary-image processing
Feature extraction
Feature description
2. MEASURING PARAMETERS
Measuring
Measure -ments
3. STATISTICAL ANALYSIS
Statistical analysis

Figure II-1. The principle steps in image analysis.

Image processing

In general, the term "image processing" simply means improving an image so that it is easier for the human eye to interpret it without any quantification or analysis taking place (Joyce-Loebl, 1985; Robinson, 1985). Several text books discuss image processing methods in both concept and mathematical detail (e.g. Reeves, 1975; Gonzalez and Wintz, 1987; Castleman, 1979; Rosenfeld and Kak, 1982a, 1982b; Colwell, 1983; Fabbri, 1984). Numerous computer programs are readily available for most common image-processing tasks. Therefore, the analyst can omit the mathematical description of the process, and instead, concentrate on the principles of operation and the results they can achieve. Although numerous computerized image-processing methods have been developed, only digitization, image enhancement, image segmentation, and feature detection are discussed below.

Digitization

Images can be considered as continuous functions with the grey level being a continuous function of the position in the image (Rosenfeld and Kak, 1982a; Fabbri, 1984). Before such an image can be processed, it needs to be digitized. Digitization is the process of transforming the brightness function of a continuous image into an array of discrete grey levels (Rosenfeld and Kak, 1982a). This can be accomplished through the integration of the image brightness over some small region (sampling) and then assigning a grey level to represent this sampled value (quantization). This means that the range of grey values of the sample is divided into intervals and all the values within an interval are represented by a single value. Hardware to perform this task includes an input sensor (e.g. TV camera, flying spot scanner) and an analog-to-digital converter (Haberäcker, 1983; Fabbri, 1984). Rosenfeld and Kak (1982a) showed that the appropriate choice of number of sampling and quantization is dependent on the complexity of the image. They concluded that it is important to have fine quantization in an image with a small range of grey levels, but the sampling can be coarse. Conversely, in an image with a large range of grey levels (large amount of detail), it is necessary to sample finely but quantization can be coarse.

Image enhancement

Whenever an image is transformed from one form to another (e.g. scanned) the quality of the output image may be lower than the quality of the input. The purpose of image enhancement is to smooth or sharpen images for either visual inspection or further machine processing. Many enhancement techniques have been designed to compensate for the effects of these degradation process (Duda and Hart, 1973). These processes include methods of modifying grey level by sharpening (using high-pass filter) or smoothing (using low-pass filter). Smoothing processes average noise and may blur the image, while sharpening processes enhance the image and permit feature boundaries to be easily identified (Russ and Russ, 1984). Enhancement techniques can also be used to suppress selected features of an image, or to emphasize such features at the expense of other features (Duda and Hart, 1973).

Grey-level correction and grey-level transformation are two types of operations involved in modifying the grey levels of an image (Rosenfeld and Kak, 1982a). Grey-level correction modifies the grey level of the individual image point to compensate for uneven exposure when the image was originally recorded. This method can be employed only when the nonuniform exposure that produced the image can be determined. Grey-level transformation can be used to change grey levels in a uniform way throughout the entire image or selectively to increase contrast and make details of an image more easily visible.

Segmentation

One aspect of image analysis is to describe the interested features in the image in detail. In order to do that, the features must first be singled out from the background. This can be accomplished by segmenting an image into several distinct regions of uniform properties (e.g. grey level). This process is, in fact, the first step of image analysis which aims at either a description of an image or a classification of the image. It is a critical component of an image recognition system because errors in segmentation will propagate in feature extraction and classification.

Moore (1968) introduced the "phase" concept, allowing the analysis of complex images to be treated as a series of binary images. The patterns formed by the features of a single phase are then considered one at a time. The term "phase" refers to a set of points which includes all features of the same kind. Although many segmentation techniques have been investigated, there is no single standard approach (Fu and Mui, 1981). The segmentation algorithms are based on the concepts of similarity between neighbouring local regions or discontinuity. Three common techniques are: (1) region extraction, (2) edge detection, and (3) grey-level histogram thresholding.

Region extraction: The basic purpose of region extraction is to partition the image into homogeneous connected regions. The detail of region extraction has been documented by Zucker (1977), Browning and Tanimoto (1982), Lumia *et al.* (1983), Suk and Chung (1983) and Rosenfeld (1984). In general, this is done by: (1) a region-growing technique, or (2) a split-and-merge technique.

The region-growing technique starts with a seed location (with a given property). Then, an attempt is made to join neighbouring points to this growing seed. When no neighbours around a growing region can be joined to the growing seed another seed point is chosen. The process continues until every picture point is attached to a region.

The split-and-merge technique starts with an initial arbitrary partitioning the image into regions. Modifications can be made by splitting these regions if they are not sufficiently homogeneous and by merging pairs of adjacent regions if their union is still homogeneous. In this approach "homogeneous" means that a given property is approximately constant. Browning and Tanimoto (1982) developed the split-and-group with linking method that is a modification of the split-and-merge method. They concluded that their method is suitable for minicomputer technology and that larger images can be handled.

Region-extraction techniques, however, are not common in practice because they process the image in an iterative manner and usually involve a great expenditure in computation time and memory.

Edge Detection: Images can be segmented into regions by detecting the edges of regions. Ideally, the detected edges must be linked together to form closed contours (Bartlife, 1983). A number of edge-detection techniques have been documented by Davis (1975), Pavlidis (1977), Riseman and Arbib (1977), Fu and Mui (1981), and Rosenfeld and Kak (1982b). The aim of edge-detection techniques is to place the edge or boundary where there is a relatively abrupt change in grey level or where other local properties are evident in the image. Some of the problems associated with edge-detection techniques are: (1) not only the edge points have been detected, but also the noise, (2) in some cases, edges are detected where there is no transition from one region to another, and (3) the edge points may or may not have formed closed contours. However, these problems can be solved mathematically (Rosenfeld and Kak, 1982b).

The width of the detected edge lines usually comprise more than one pixel. In order to increase the accuracy of subsequent measurements, these edge lines are reduced to a width of one pixel (thinning processes) located precisely at the centre of the original (wider) lines (Rosenfeld and Kak, 1982b; Paler and Kittler, 1983; Fabbri, 1984). The edge-detection approaches may be desirable if some of the regions are small or there are regions with many different grey-level ranges (Davis, 1975; Fu and Mui, 1981).

Grey-level histogram thresholding: A grey-level histogram is a graphical display of the number of image pixels at each grey-level value. Ideally, a grey-level histogram of an image should display peaks corresponding to the number of regions that occupy different grey-level ranges. Although the formation of peaks or modes occurs for almost all simple images, it does not always clearly exist in the cases of complex images or when the grey level of different regions become more alike (Drury, 1987). As the number of regions increases, the peaks become harder to distinguish, and segmentation by thresholding becomes more difficult. This problem can sometimes be alleviated by smoothing the image before thresholding.

There have been a number of studies of threshold selection techniques (Duda and Hart, 1973; Brenner *et al.*, 1981; Rosenfeld and Kak, 1982b; Deravi and Pal, 1983). Some techniques use the lowest point between the peaks and others try a range of thresholds and choose the one for which the threshold image has some desired property. The threshold selected by using the lowest point between peaks seems to be the most commonly used method. However, this method has some disadvantages. First, the existence of many local minimums makes the selection of threshold values difficult. Second, no spatial information is used to select the threshold values so there is no guarantee that the segmented regions are continuous. Third, in histograms with broad and flat valleys it may be difficult to accurately locate the valley bottom. In order to achieve the best results with histograms, various methods have been proposed for sharpening the valleys between the peaks, enhancing the images and their histograms (Fu and Mui, 1981).

Serra (1982) developed the theory of transformations by means of "structuring elements" to detect features (binary image) in the image. This technique is normally referred to as "hit-or-miss transformations". The concept of this technique is to use the set theory to construct a picture algebra by developing criteria and models for image analysis. Logical operations and structuring elements are the two basic components. The logical operations used in binary system are U (union), I (intersection), C (component), and their combinations in set theory symbols. These operations are denoted by OR, AND, EOR, and NOT in computer terminology (Fig. II-2). The structuring element is a set of pixels that is swept across every pixel of an image where 0 - 1 values is changed according to the

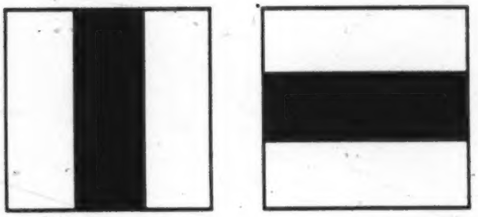

Binary image (B1) Binary image (B2)

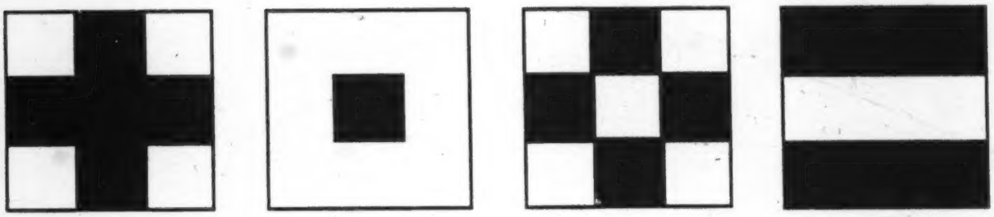

B1 OR B2 B1 AND B2 B1 EOR B2 NOT B2

Figure II-2. Example of logical operator comparing two binary images on a pixel for pixel basis (3 x 3 pixel areas) and showing the result in the image area specified in the mathematical expression.

B1 OR B2	The operator that computes an image as the result of the union between B1 and B2.
B1 AND B2	The operator that computes an image as the result of the intersection between B1 and B2.
B1 EOR B2	The operator that computes an image as the result of the union of non-overlapping subsets of B1 and B2.
NOT B2	The operator that computes a complement of an image B2.

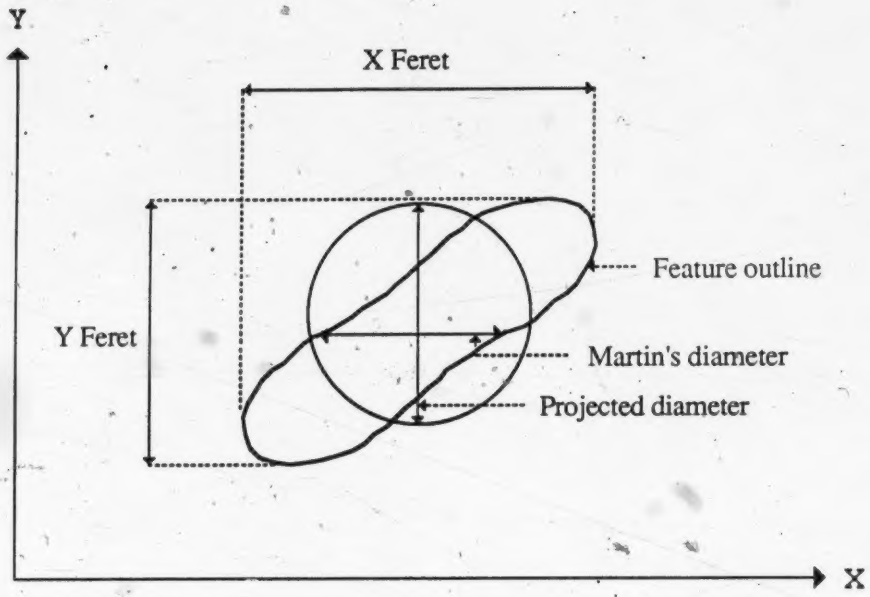
Y
X Feret
Feature outline
Y Feret
Martin's diameter
Projected diameter
X

Figure II-3. Diagram shows various diameters that can be used in image analysis.

degree of matching in its corresponding neighbourhood (Fabbri, 1984). The choice of structuring element is problem-dependent.

Feature extraction

Erosion and dilatation are image-processing techniques used to characterize the binary image in automatic image analysis (Fig. II-4). The concept of erosion is to contract the image by uniform inward movement of feature boundaries; dilatation expands the image by uniform outward movement of feature boundaries (Blume, 1967; Calabi and Hartnett, 1968; Duda and Hart, 1973; Serra, 1982; Fabbri, 1984).

Erosion can be used to simplify and separate touching features. Conversely, dilatation can be used to join discrete objects into a continuous feature. The combination of erosion-dilatation processes can serve a number of purposes. Fabbri (1984) used the term "opening" for an erosion followed by a dilatation and the term "closing" for a dilatation followed by an erosion.

Measurement of features

In image analysis, data may be collected in field and feature modes (Crutwell, 1974; Bradbury, 1979). In field mode, features are measured and analysed in terms of the sum of values obtained for all the detected features in one field. This type of data may be useful in assessing area fraction, for example, the percentage of inclusions of a phase in the total area of an image. In cases where the image is composed of discrete features in a single field of view, the measurement of such features may provide considerable information. In general, parameters such as area, perimeter, length and width, orientation, and location of features of a given phase are measured.

Practically, measurements of parameters are made from the binary image of selected features. Therefore, the grey-level image needs to be transformed into a binary image. The resulting binary image is much easier to understand and to handle than a grey-level image, and it is simpler to formulize topology from a binary image than from a grey-level image (Goetcherian, 1980).

Size measurement

Size measurement of individual features can be expressed in various ways such as projected area diameter, Martin's diameter, or Feret's diameter (Fig. II-3). Therefore, it is necessary to express the means of derivation of the measurement, so the degree of approximation can be understood.

The projected area diameter is the diameter of a circle having an area equal to the projected area of the feature. It can be calculated, without the need to create an equivalent circle, using the formula

$$A = \frac{\pi D^2}{4} ,$$

where A = area, D = diameter.

Martin's diameter is the length of a line that divides the feature into two equal areas. It is not easy to determine accurately and tends to overestimate average diameter (Joyce-Loebl, 1985).

Feret's diameter, proposed by Feret in 1931 (*in* Joyce-Loebl, 1985), is the maximum spacing between parallel tangents to a feature in a given direction. Feret's diameter is orientation-dependent. It has an advantage because it is possible to measure the Feret diameter at any angle to the horizontal by using the mathematical operation of co-ordinate transformation (Joyce-Loebl, 1985). However, in practice, only a fixed number of Feret diameters are measured because of the significant computing-time penalty for the measurement of multiple Feret diameters. For most purposes, the minimum number of eight is sufficient (Ruzyla, 1986). The maximum Feret diameter is normally considered to be the length, and the minimum Feret diameter is considered the width. Generally, the

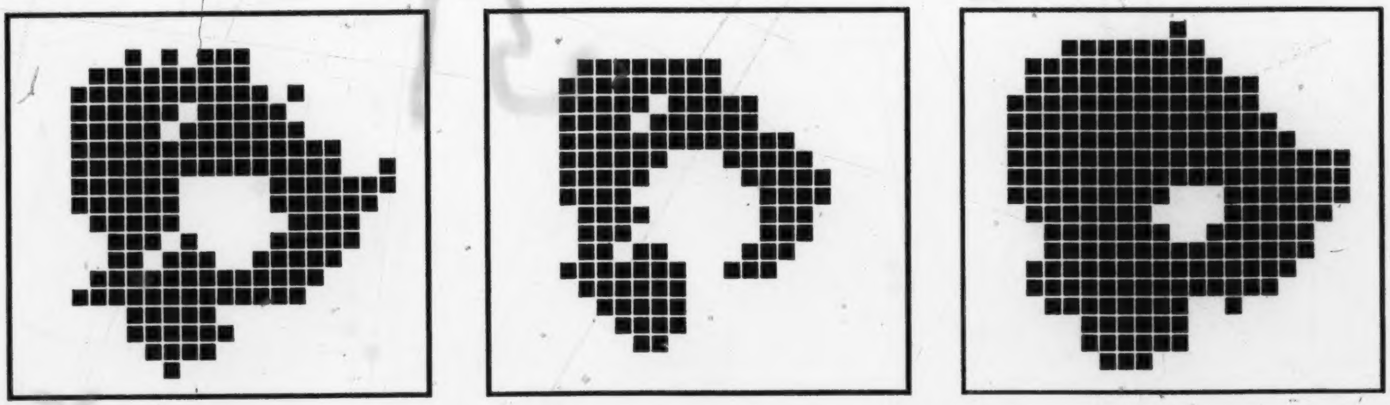

A. Original image

B. Erosion with n = 3

C. Dilatation with n = 3

Figure II-4. An example of erosion and dilatation transformations (modified after Russ, 1985).

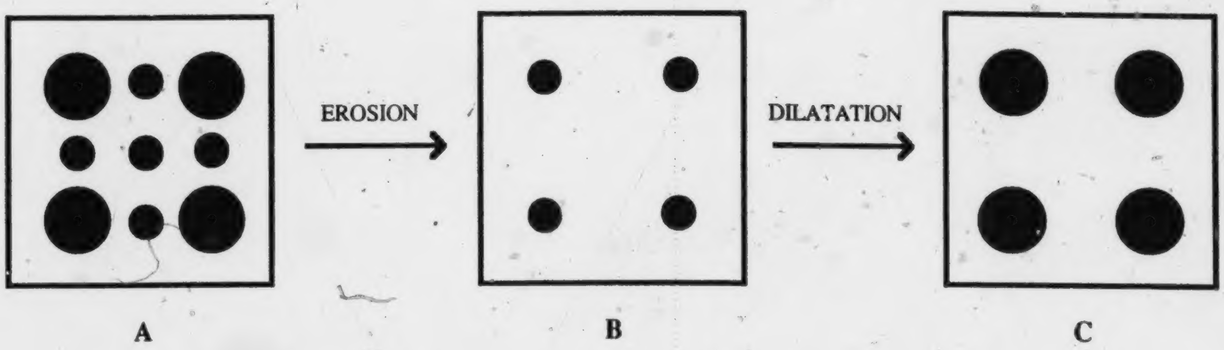

Figure II-5. Schematic diagram showing the effect of erosion and dilatation on two sizes of features, original image (A). After erosion (B), the smaller features are removed but the larger features remain for further dilatation (C). (modified after Ehrlich *et al.*, 1984)

error involved in length measurement is not a severe problem unless the feature is very long and skinny.

The opening and closing transformations have been used as an important element in the analysis of petrographic images (Rink, 1976; Serra, 1982; Ehrlich *et al.*, 1984; Fabbri, 1984; Dilks and Graham, 1985; Yuan, 1987). For example, those processes have been used to characterize pore geometry (Ehrlich *et al.*, 1984; Yuan, 1987) and to obtain information about pore size distribution (Ehrlich *et al.*, 1984; Fabbri, 1984; Yuan, 1987). Dilatation after erosion need not restore a feature to its original shape (Matheron, 1975 *in* Ehrlich *et al.*, 1984; Young *et al.*, 1981) because irregularities lost by erosion cannot be replaced by dilatation (Fig. II-5).

The use of erosion, dilatation, and their combinations in size analysis does not lead to successful results in the case of overlapping features; all the connected features will be counted as a single feature and that leads to an error in measurement. In this situation manual interaction is necessary. Two approaches are normally used: editing the image using an interactive editing pen and entering via graphic tablet.

D. SYNOPSIS

Quantitative data can be gathered from images by: (1) manual methods, (2) semi-automatic methods, or (3) automatic methods. There are many different processes involved in digital image analysis such as image processing, measuring the key parameters of features, and interpreting the data statistically. Therefore, there are no general procedures that specify how these processes should interact in carrying out a given task, in particular when a number of methods exist for performing each step of image analysis. Each method has both advantages and disadvantages. It would usually be desirable to implement several methods in order to obtain the best results. Sample preparation is also one of the keys for successful analysis. Sufficient contrast must be present between the features to be analysed, especially in automatic analysis.

III. PREVIOUS WORK ON THE APPLICATION OF IMAGE ANALYSIS IN GEOLOGY

Image analysis is not new to geologists because they have been doing it manually for many years (for example, point counting, Chayes, 1949, 1956; Ginsburg, 1956). Recently, automatic and semi-automatic analysis systems have been used widely as tools for extracting quantitative data in various geological problems. Besides being a time-saving technique, the results obtained from automatic and semi-automatic image-analysis techniques are known to be reliable. In this chapter only the use of automatic and semi-automatic analysis systems in geological study will be emphasized. Many researchers (e.g. Agterberg and Fabbri, 1978a, 1978b; England *et al.*, 1979; Kasvand *et al.*, 1981; Schäfer *et al.*, 1981; Chao *et al.*, 1982; Crelling, 1982; Ehrlich *et al.*, 1984; Fabbri, 1984; Minnis, 1984; Piepe and Steller, 1984; Dilks and Graham, 1985; Ruzyla, 1986) have shown that these image-analysis techniques can be used in problems of various scales.

A. APPLICATION OF IMAGE ANALYSIS ON A MICROSCOPIC SCALE

On a microscopic scale, emphasis has been placed on the study of the texture of grains and pores. The term "texture", as used herein, refers to the geometrical aspects of the component particles of a rock, including size, shape, and arrangement (Bates and Jackson, 1987).

Petruk (1976) and Pong *et al.* (1983) described the application of the automatic image analyser to quantitative mineralogical analysis. They noted that data on mineral quantities, size distributions, and other derived information (e.g. particle shape) can be obtained. Schäfer *et al.* (1981) used the Kontron Videoplan digitizing method in determining the size and shape of sand grains. They concluded that the results in size measurement obtained via the Videoplan method are close to those obtained by sieving.

Fabbri (1980, 1984) and Fabbri and Kasvand (1978) applied the Geological Image Analysis Program Package (GIAAP) to the study of thin sections of granulite and amphibolite. Parameters such as area, perimeter, length and width, orientation, and the distribution of particle profiles were measured directly using morphological opening transformations. In addition to the data obtained from direct measurement, other information was derived from the measured data, such as shape of grains determined by their circularity (area/perimeter) or aspect ratio (length/width).

Minnis (1984) reported that the spatial distribution of the minerals and bulk mineralogical analysis of sandstone can be performed using scanning electron microscope equipped with a LeMont Scientific Image Analysis System. The closeness of the results obtained via this technique compared with those obtained via X-ray diffraction and optical petrography depends on the complexity of the sample. Samples with simple mineralogy show closer correspondence between the values obtained from the different analytical approaches. Minnis (1984), however, indicated that even the trace amount of the mineral present can be detected and located. This information cannot be obtained from X-ray diffraction and optical petrography.

Dilks and Graham (1985) used a Kontron SEM-IPS image, coupled directly to a JEOL JXA 733 SEM equipped with an annular, back-scatter electron detector to extract quantitative data for both compositional and morphological mineralogical characterization of sandstones. They concluded that the results of compositional analysis from the back-scatter electron images, using the image-analysis system, are in good agreement with those obtained via point counting analysis using electron-probe microanalysis from a 500 point array. Dilks and Graham (1985) indicated there are limitations: the back-scatter electron cannot, by itself, distinguish between different minerals having the same intensity in the image.

Dorobek *et al.* (1987) used the General Image Processing System (GIPSY) to determine the abundance of grains and cement in carbonate rocks. They reported that the total and specific stages of calcite cementation, as defined by the cathodoluminescent zonation present in the cements, can be quantified. Thus, the amount of porosity loss during specific cementation stages, which may be useful in understanding and predicting reservoir characteristics, can be estimated. They pointed out several limitations of the techniques which stem from either the sample preparation procedure or from the complexity of the sample itself. However, this technique has been proven to work well when examining simple nonluminescent-to-bright-to-dull cathodoluminescent zonation (Grover and Read, 1983; Dorobek, 1987).

Mazzullo and Kennedy (1985) used the microprocessor-controlled image-analysis system, ARTHUR II, to measure the nominal sectional diameters (the diameter of a circle equal in area to the area of the grain in the plane of its largest and intermediate diameters, Wadell, 1934) of sedimentary particles.

In addition to determining the microscopic texture of grains, geometrical analysis of pore structure can provide information in formation evaluation because the physical properties of sedimentary rocks depend on the geometrical structure of their pores. Rink and Schopper (1978) used image analysis in a detailed study of pore space in sedimentary rocks with a Leitz microphotometer supplied with a computer-driven scanning stage. The quantitative data were derived by means of the "cut" process developed by Rink (1976). The porosity measurements obtained by this technique were in fair agreement with those determined volumetrically. Rink and Schopper (1978) claimed that deviations in the data were dependent mainly on inhomogeneities in the samples. The quality of the input image also played a role in the deviations.

Ehrlich *et al.* (1984) used the Petrographic Image Analysis (PIA) system to estimate the porosity, pore roughness or tortuosity of sandstones from resin-impregnated thin sections. Three types of data can be obtained through erosion and dilatation techniques, namely, total pixels of the scene, total pore pixels, and total pore perimeter. Porosity of rocks can be computed by dividing total pore pixel by total pixels of the scene. In addition, the ratios of total pore area to the total pore perimeter can provide information concerning pore roughness or tortuosity. The porosity values obtained by this method are more closely linked to effective (interconnected) porosity rather than to total porosity (Ehrlich *et al.*, 1984). This is due to the penetrating power of epoxy impregnation and to microscopic resolution. Ehrlich *et al.* (1984) pointed out that, in some cases, the transparence and/or translucence of the minerals in sedimentary rocks can affect porosity estimation. The presense of porosity below the upper plane of the thin section may increase the apparent proportion of porosity because blue-dyed pores can be seen through some mineral grains. Rink and Schopper (1978) suggested that Wood's alloy and a reflected light microscope should be used instead of pigmented epoxy and a transmitted light microscope. Yuan (1987) used the same system as Ehrlich *et al.* (1984) to study the correlation between pore size and throat size and the effect of this correlation on the porosity-permeability relationship. Dietterich and Full (1986) used the PIA system to study pore analysis and to obtain information needed for a detailed description of a reservoir.

Ruzyla (1986) applied image analysis on SEM photographic images of polished epoxy-impregnated samples. From his study, image analysis proved to be a rapid method for obtaining direct measurements of porosity, specific surface of pore (defined as the interstitial surface area of the pores per unit of bulk volume of porous material, Collins, 1961), pore size and pore shape from rock sections. Porosity values obtained from back-scatter electron images were in good agreement with conventional volumetric measurements of core analysis (Ruzyla, 1986). He also used samples impregnated with epoxy to which a fluorescent dye had been added. These samples showed much better grey-level histogram (clearly separated modes for rock grain and pore space) when using fluorescent light than when using plane-polarized light.

Coal lithotype has proved useful in a number of applications. For example, it can be used in the correlation of coal seams, in determination of coal rank, in studying the environment of coal deposition, and in evaluating coal for mining and coal preparation. The constraint is that manual coal lithotype analysis is time consuming and requires a skilled petrographer. Recently improved image analysis systems for microscopy may overcome this problem. The potential use of image analysis in coal petrography has been demonstrated by several researchers (e.g. England *et al.*, 1979; Chao *et al.*, 1982; Crelling, 1982; Piepe and Steller, 1984). The macerals and minerals are analysed on the basis of differences in reflectance. The polished section of coal can be used as an input material. The published results show that each maceral groups yield a characteristic reflectance histogram. Also, lithotype variation within the image and the distribution of maceral groups, mineral occurrences, texture analysis, and cracks can be quantified by statistical manipulation of the reflectance data. The results obtained from image analysis are in good agreement with those obtained by manual methods. Davis *et al.* (1983) showed that automatic-reflectance mapping of polished coal surface appears to be a potentially useful technique, particularly in cases where two-dimensional detailed petrographic information is needed for samples of relatively small size.

The graphic tablet digitizer, coupled with a microcomputer, has been proved to work well in examining size and shape of microfossils (Kobluk and Kozelj, 1985; Klapper and Foster, 1986; and Lazarus, 1986). Kobluk and Kozelj (1985) used the HiPad digitizing tablet of resolution 125 μm interfaced to an Apple III microcomputer to measure the cross-sectional area of the macroboring in growth framework reef cavities, Bonaire, Netherlands Antilles. Lazarus (1986) reported that three-dimensional measurements of microfossil morphology (length, area, and perimeter) of radiolarian can be achieved with an accuracy of approximately 1 μm using a graphic tablet digitizer. Klapper and Foster (1985) used a HiPad digitizer to study quantitative shape analysis of conodonts, resulting subsequently in improvements in taxonomy.

B. APPLICATION OF IMAGE ANALYSIS ON A MACROSCOPIC SCALE

Image analysis has also been used in the study of macropaleontology. Wilson (1983) used a graphic tablet digitizer connected with an Apple II Plus microcomputer to study the shape of shark's teeth. He noted that the accuracy of measurement depended upon the user's ability to position the digitizer's cursor precisely. Hageman (1988) showed that the numerical data of principal characteristics (length, area, angle) used in fenestrate bryozoan taxonomy (for generic and specific identification) can be obtained via digitizing package "Magic" and a Macintosh Plus computer. Foster *et al.* (1988), in the study of coral *Trachyphyllia bilobata* (Duncan), obtained data on surface area, length, width, and columella size by digitizing landmark points on photographs of the upper surface of each coral.

C. APPLICATION OF IMAGE ANALYSIS ON MAPPING

Image analysis can be considered as a tool for systematic analysis of geologic maps. Image analysis techniques have been used in the study of spatial correlation of stratigraphic units digitized from maps for the statistical analysis of tectonic and mineral-deposit data (Agterberg and Fabbri, 1978a, 1978b; Agterberg, 1981; Fabbri, 1981; Kasvand *et al.*, 1981). Generally, for this type of study, the geologic maps are quantified, therefore the binary image of stratigraphic units can be used to study the geographic framework. Then, geophysical and geochemical map patterns are considered in conjunction with the geological images in order to determine the probability of the occurrence of combined events which described the environment of mineralization. The algorithms for quantification of map patterns and image analysis may be based on concepts of mathematical morphology. Switzer (1976) developed a method for estimating algebraically the spatial dependence of map patterns and the accuracy of digital maps. Srivastava (1977) proposed optical processing method to quantify structural contour maps in the form of "zebra maps". He noted that his technique can be used in analysing pictorial data including aerial photographs, rock-fabric diagrams and thin sections.

D. SYNOPSIS

Recent advances in computerized quantitative image analysis have made rapid analysis possible in various aspects of geological problems. There is no doubt that image analysis allows the gathering of a large amount of data with accuracy. The limitations of image analysis are normally due to the complexity of the sample itself and/or sample preparation which produces images that lack grey-level discrimination or images with multi-grey levels. A prerequisite for the automatic image analysis is good optical contrast between the features to be studied and all other surrounding components. The graphic tablet digitizer and microcomputer, on the other hand, seems to serve well in the analysis of complex images.

IV. IMAGE ANALYSIS INSTRUMENTS

Three different image analysis systems, namely density slicer, automatic image analyser, and digitized graphic tablet were used during this study. Consequently, this chapter describes these instruments, their basic operating concepts (summarized from the manual for each instrument), and the sources of errors associated with each system.

A. DENSITY SLICER

Density slicing is an image enhancement technique that converts the continuous tone of an image into a series of density intervals, or slices, each corresponding to a specific range of density. Density slicing can be undertaken either by using density slicing films (photographic density slicing) or by using electronic systems. Since photographic density slicing depends upon chemical reactions that are difficult to control precisely it can be difficult to obtain quantifiable results (Thomson, 1973; Simonett, 1974; White, 1977). With electronic systems, an image can be sliced electronically by selecting the signal levels that correspond to specific ranges of image density. The individual slices so derived (corresponding to signal levels) can then be assigned different colours. Density slicing techniques can be used to delineate the boundary between adjacent areas of different density, (i.e. edge enhancement).

The electronic density slicer, DATACOLOR model 703 (Plate IV-1), located at the Remote Sensing Centre, Alberta, was used in this study. The system consists of:

(1) a high-resolution Vidicon television camera that views the image and converts the transmitted light into an electrical video signal,

(2) a light table with a top glass plate and fixed and adjustable masks. A light table provides a constant (±5%) illumination of over 1000 foot-candles,

PLATE IV-1

The modules of density slicer comprise of a high-resolution Vidicon television (v), a light table (lt), an electronic colour analyser console (ca), and television monitor.

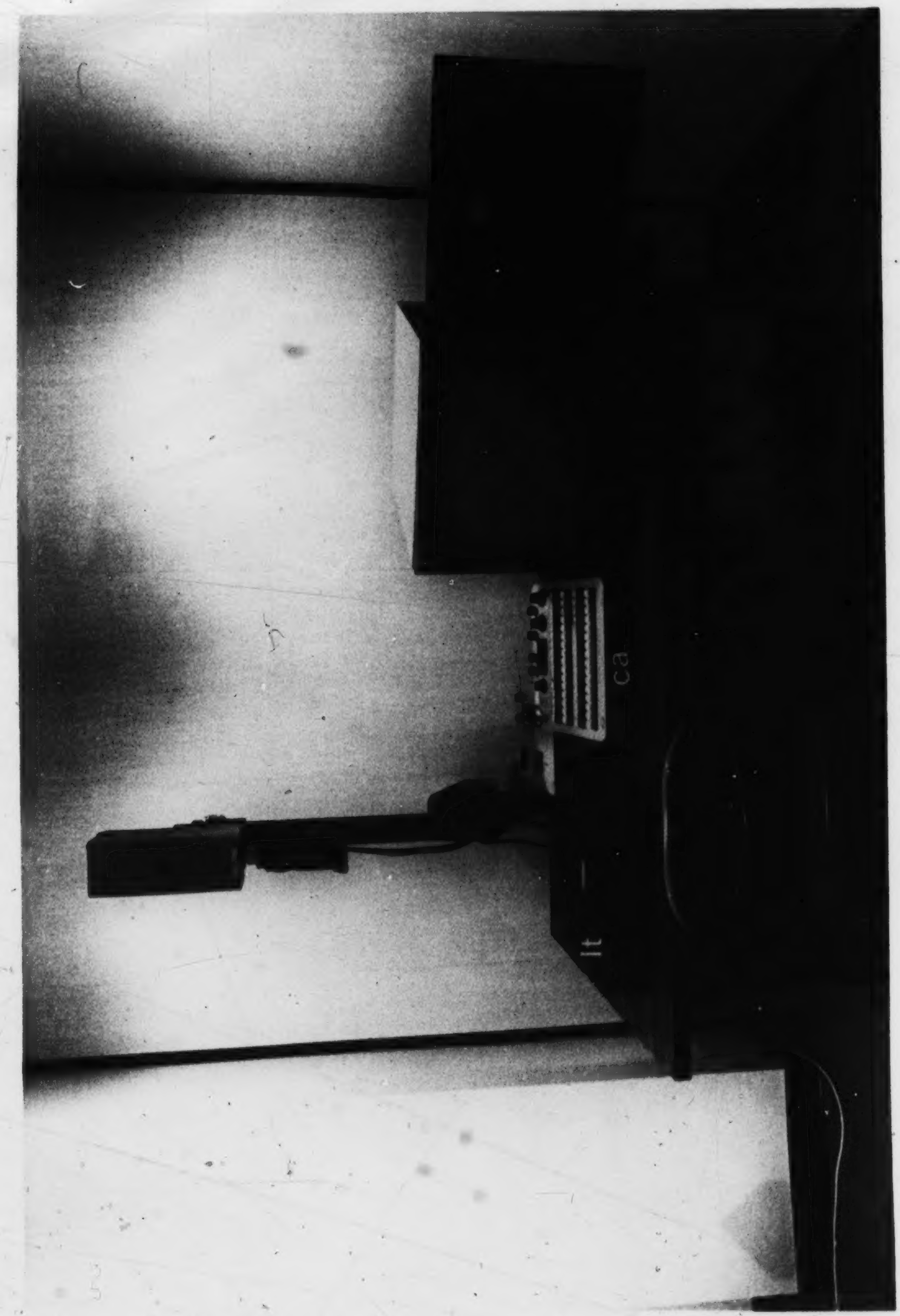
ca
lt

(3) an electronic-colour analyser console that separates the shades of tone into as many as 32 levels and encodes colour video signals for each level. This unit comprises:

  - a logarithmic amplifier that converts the camera signal to a signal that is proportional to the film density,
  - an analog-digital converter that digitizes the density signal into as many as 32 levels,
  - D_{min} and D_{max} controls that control the adjustment for the minimum and maximum density of the image,
  - control keyboard for controlling the colour-analysis levels, the number of colours displayed, and the electronic planimeter.

(4) a colour television monitor being a rectangle of 512 x 256 pixels.

Fundamentals and basic operations

Basically this instrument digitizes the image density into as many as 32 levels. The image density, D, is related to the transmittance, T, by

$$D = \log (1/T)$$

where the transmittance, T, is the quotient of the intensity of light entering and that leaving the transparent medium. The transmittance has a value from 0 to 1. The television camera converts the image density, D, to a video signal that is then digitized into 32 levels of unique colour through a colour analyser. Each band represents an equal interval of image density, i.e. equidensity area. The 32 colours are in a fixed order starting with very light yellow, representing the brightest or lowest density part of the image and proceeding through 3 more shades of yellow, and then through four shades of cyan, green, orange, magenta, violet, red, and blue. Dark blue represents the darkest or highest density parts of the image. The colours always represent equal-density intervals no matter how many are used. The density step for each colour can be read directly. These colours are then displayed on a colour television monitor in a form of colour image. Image focus and magnification are controlled by a focus knob and standard 25 and 55 mm lenses. The maximum and minimum density of each input image are set using D_{max} and D_{min} controls. This adjustment ensures that the D_{max} and D_{min} of input image are set at the proper positions.

Before performing any analyses, the equipment should be properly calibrated so that the data obtained from different sets of measurement can be correlated relative to the same standard. The density step wedge tablet which has a density interval of 0.15 between steps corresponding to the 15 steps of the D_{min} and D_{max} controls is used for calibration. These calibration levels ensure that the equipment is set at the correct extreme positions.

Practically, the image to be analysed must be properly framed by black masks. Uncovered areas, even out of the field of view, may cause incorrect results due to stray reflections. Lison (1953), Goldstein (1970), and Jarvis (1981), noted that the measured values of transmittance can be altered by stray light. Black is used to preclude transmissions from unwanted area. In addition, the mask helps to separate the areas of interest from the background.

The area represented by each colour or combination of colours can be computed using a digital planimeter. To measure an area, the planimeter must be adjusted to zero and full scale for the image size (total area for the image being analysed). The area of any one or more colours is, then, measured with respect to the full scale of the image.

The size of a particular feature can be measured by the video micrometer which is connected to the system. The feature is measured by two calibrated reference marks that can be adjusted across the screen. The calibrations can be made in millimetres, metres or kilometres. The measurement is, however, limited to only horizontal and vertical distances.

The system allows the analysis of images ranging from 35 mm film to approximately 30 x 40 cm. Although the numerical data is acquired and processed by the system electronics, the operator is responsible for recording the data. The basic operating procedures are initiated via the keyboard.

Sources of Errors

Besides operator error there are three possible sources of error involved in the measurement of features: (1) error caused by shading and scanner variations, (2) error caused by effect of stray light (halo error), and (3) error caused by the limitations of the instrument. A set of test samples (Fig. IV-1), assumed to have the same optical properties, were used to determine these errors.

Error caused by shading and scanner variations

The term "shading", as defined by Swenson and Attle (1979), is a nonuniform electrical response across what appears to be a uniform field of view. Shading causes features of the same grey level to be interpreted electronically as having different grey levels in different regions of the image. Cole (1971) and Swenson and Attle (1979) noted that shading can produce inaccurate measurements.

Swenson and Attle (1979) documented two types of shading that exist in image analysis systems: system shading and specimen shading. System shading may arise from three principal sources: (1) nonuniform illumination in the image source, (2) lens shading due to light path variations through the lens, and (3) scanner shading resulting from nonuniformity in the photosensitive layer of the scanner. Specimen shading may result from artifacts in the sample preparation process such as the unequal staining of thin sections.

In testing procedures, the test sample 10 x 10 cm in size was placed at the centre of the light table. Normal operating procedures for density slicing technique were employed

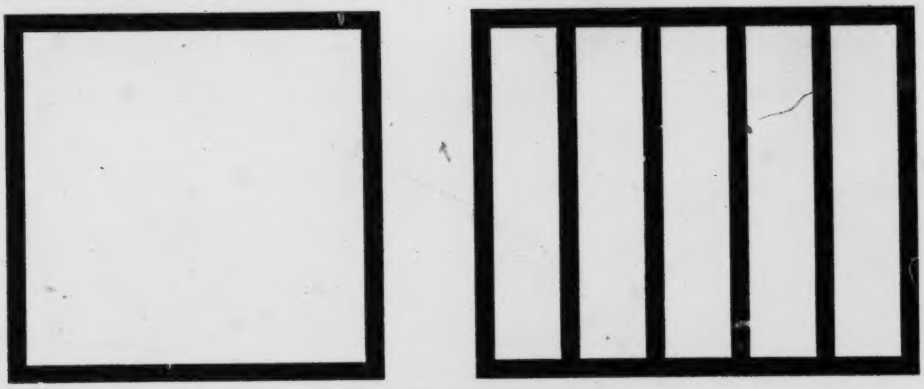

A. sample size 10 x 10 cm.

B. sample size 10 x 2 cm.

C. sample size = 2 x 2 cm.

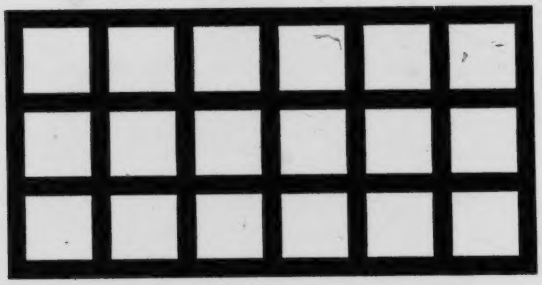

D. sample size = 1 x 2 cm.

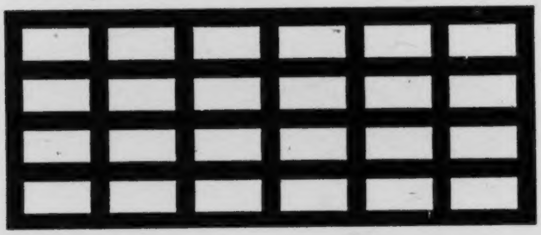

Figure IV-1. Schematic diagram showing set of test samples with various sizes used in determining errors caused by shading and scanner variations, and stray light. Scale = 1 : 2.

PLATE IV-2

An example of shading error caused by effect of nonuniform illumination (A), and effect of lens shading or scanner shading or the combination of both (B).

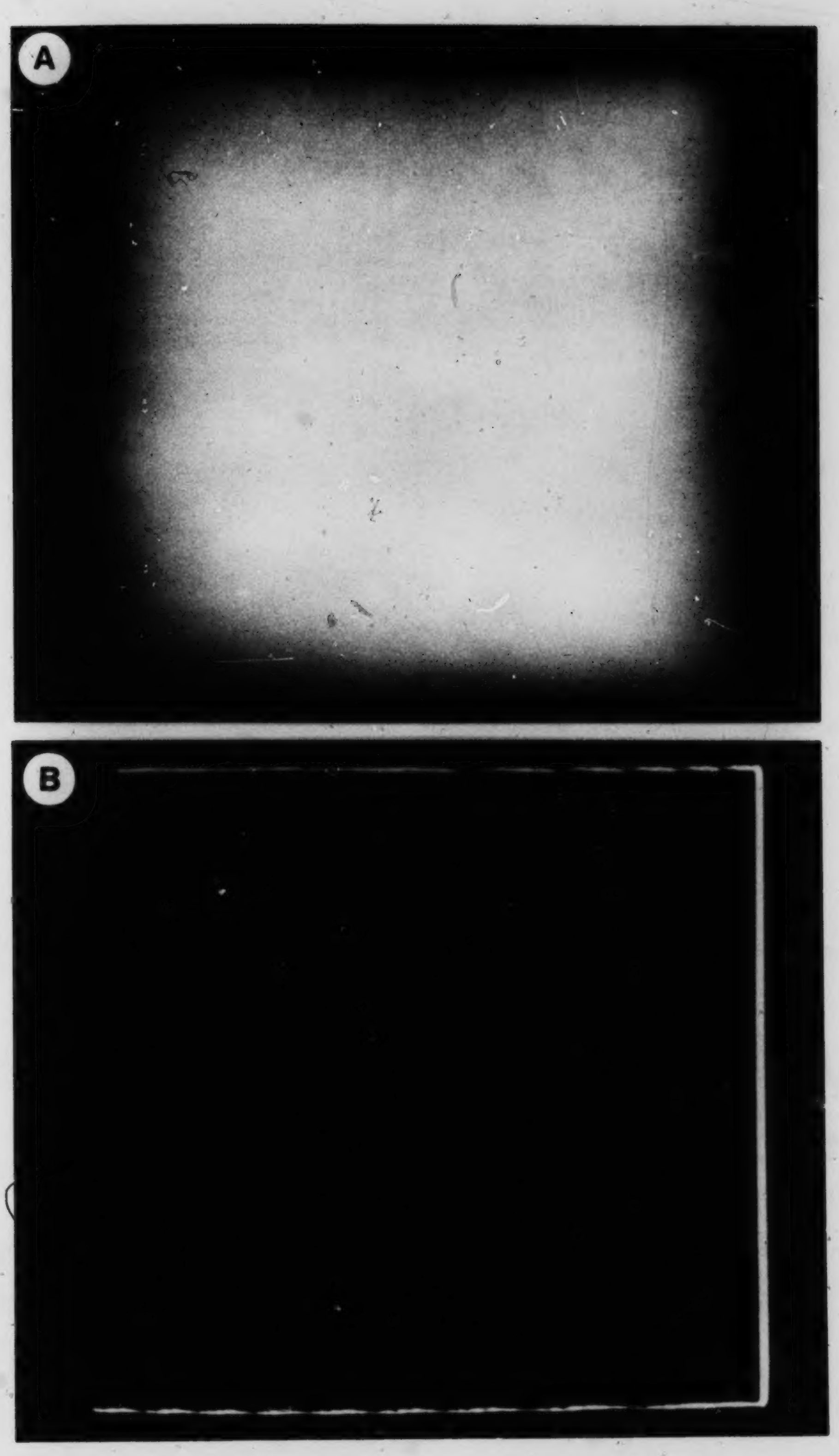
A
B

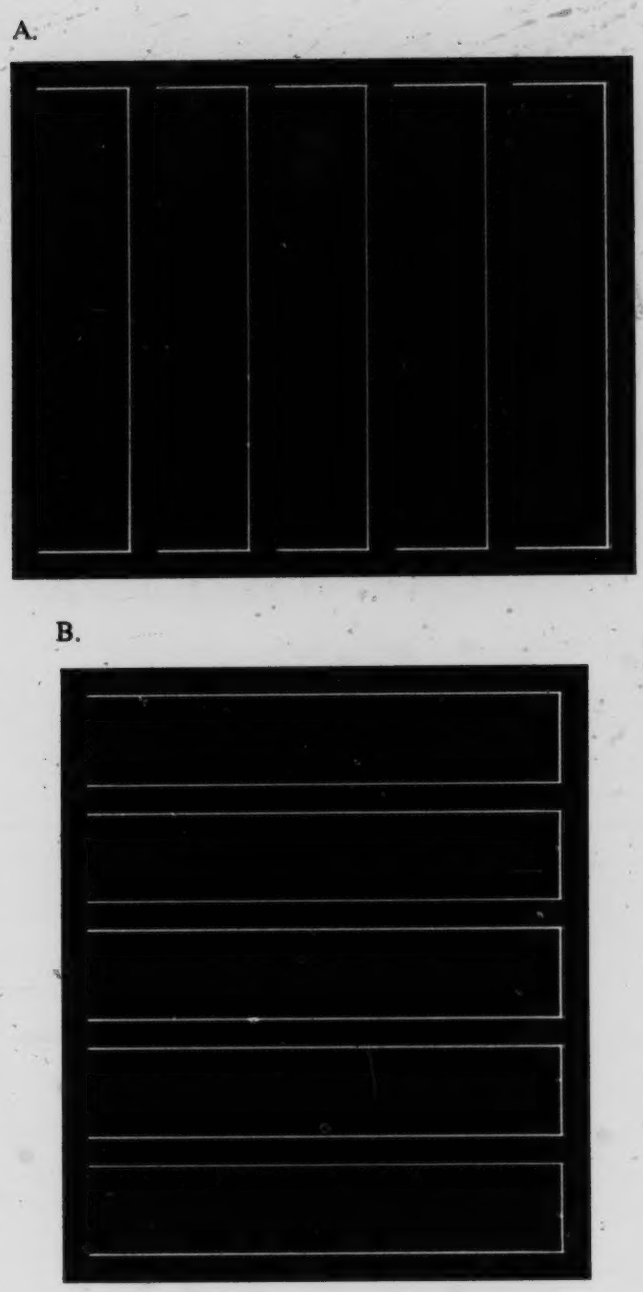

Figure IV-2. Schematic diagram showing effect of scanner variations. The left edge of the image is always missing no matter how the image is rotated. Features in B are rotated 90° from those in A.

and all 32 grey-level density were used. Density level 1 represents the major area in the output image while density level 2 to 32 occur as distinct colour strips along the edges of the images (Plate IV-2A, B). Visually, the area at the lower right corner is brighter than the rest of the image. This may due to effect of nonuniform illumination. The left edge of the output image was always missing no matter how the input image was rotated (Fig. IV-2). This suggests that the missing edge may be due to lens shading or scanner shading or a combination of both (K. Campbell, 1987, pers. comm.). Although shading can be minimized by careful calibration of the instrument and by placing the input image at the centre of the light table, it cannot be eliminated.

Error caused by effect of stray light

The occurrence of distinct colour strips along the edge of an image (boundary between blackened and unblackened areas) is somewhat similar, in the reverse sense, to those first described by Schwarzschild and Villiger (1906, p. 286-287) in their study of microdensitometry of the photographic image of the sun. They stated

> If photometric measurements are made upon a very opaque portion of a plate in the immediate neighborhood of a larger area which is very slightly opaque, the very bright light which then passes through the unblackened area is in part reflected at the objective of the observing microscope, and illuminates from in front the dark portion of the plate, so that it appears too bright.

This phenomenon, referred to as a "halo effect" (Cole, 1971; Petruk, 1976), expands the area of the black portion of the image. In other words, this error reduces the area of the bright portion. The amount (%) of halo effect can be calculated with respect to the total area of features in the field of view. When features are being viewed in transmitted light, both the thickness and the light-absorbency of the transparent medium will have an influence on the amount of stray light (Joyce-Loebl, 1985). Results from the analysis of

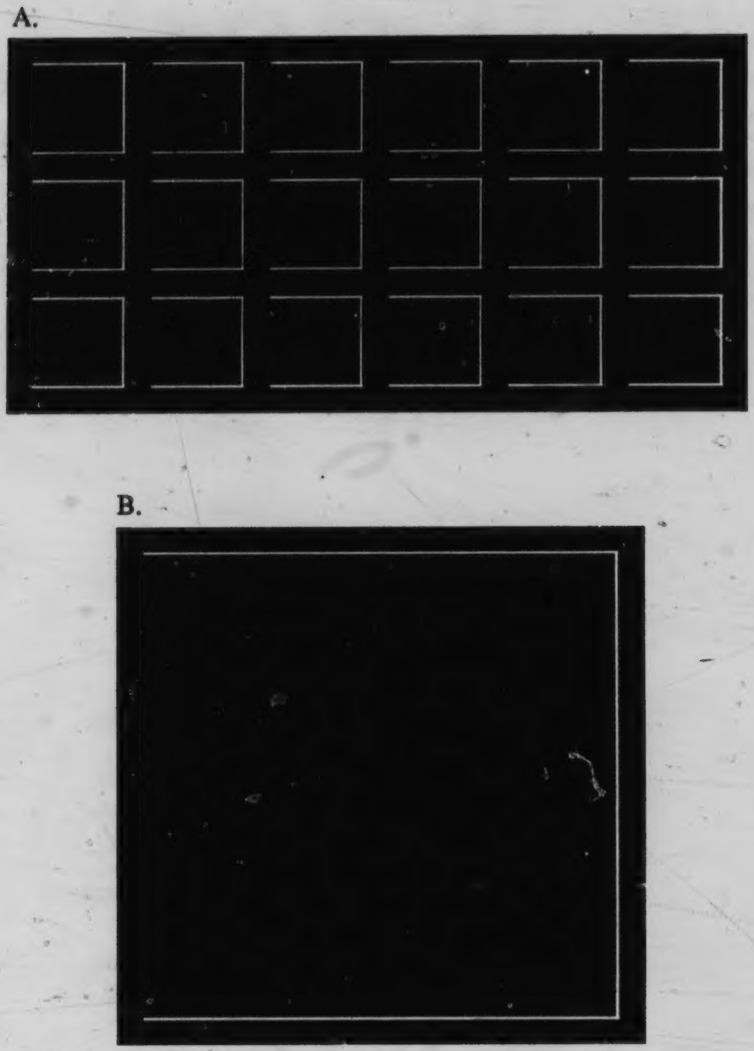

Figure IV-3. Schematic diagram showing effect of stray light on sample of size 2 x 2 cm (A) and 10 x 10 cm (B). The width of halo error is relatively constant regardless of the size of features.

Table IV-1. Summary of data on amount of halo error. The percentage of halo error is calculated with respect to total area. For sample numbers see Figure IV-1.

Sample Number	Number of object	Size (perimeter, cm)	Total perimeter (cm)	% halo error
Sample A	1	40	40	1.50
Sample B	1	24	24	3.94
	2	24	48	4.05
	3	24	72	4.06
	4	24	96	4.18
	5	24	120	4.40
Sample C	1	8	8	6.56
	2	8	16	6.58
	3	8	24	6.60
	4	8	32	6.77
	5	8	40	6.70
	6	8	48	7.00
	7	8	56	7.13
	8	8	64	7.06
	9	8	72	7.08
	10	8	80	7.32
	11	8	88	7.30
	12	8	96	7.31
	13	8	104	7.30
	14	8	112	7.35
	15	8	120	7.28
	16	8	128	7.23
	17	8	136	7.34
	18	8	144	7.42
Sample D	1	6	6	9.67
	2	6	12	9.76
	3	6	18	9.84
	4	6	24	9.88
	5	6	30	9.91
	6	6	36	9.76
	7	6	42	9.72
	8	6	48	9.74
	9	6	54	9.73
	10	6	60	9.90
	11	6	66	9.78
	12	6	72	9.92
	13	6	78	9.83
	14	6	84	9.74
	15	6	90	9.89
	16	6	96	9.84
	17	6	102	9.78
	18	6	108	9.76
	19	6	114	9.87
	20	6	120	9.88
	21	6	126	9.86
	22	6	132	9.87
	23	6	138	10.02
	24	6	144	9.97

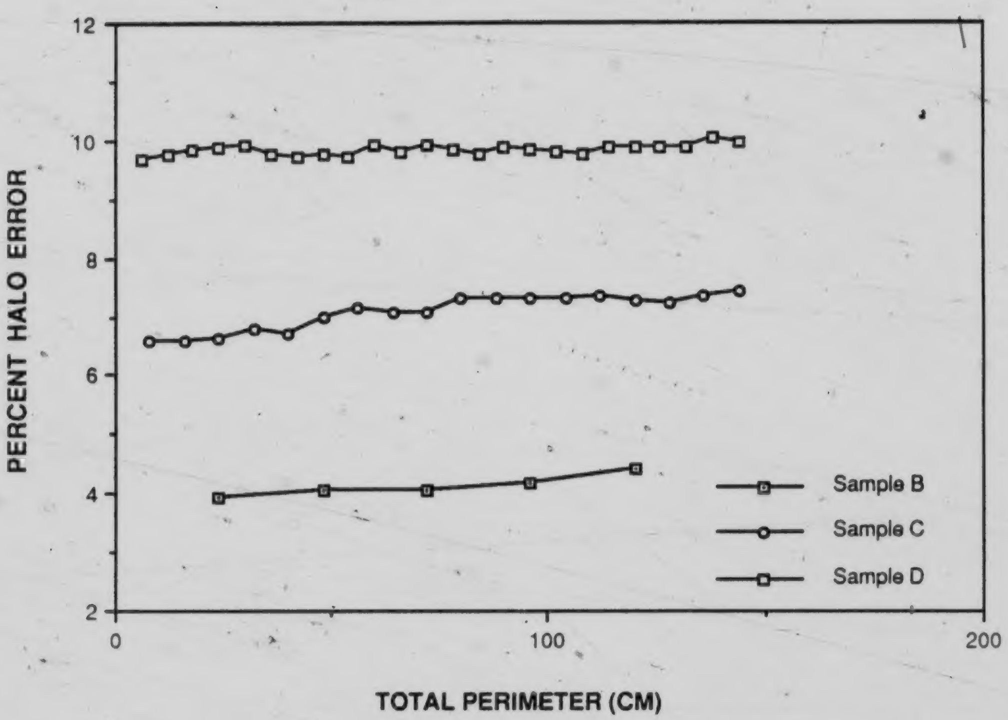

Figure IV-4. Graphs showing relationship between amount of halo error, size, and number of feature in the field of view. For sample numbers see Figure IV-1.

colour and black-and-white aerial photographs showed that the amount of stray light is slightly more pronounced for colour negatives than for black-and-white negatives (approximately 2 and 4 percent, respectively). This is probably due to the complex sensitivity of each emulsion layer in colour film (K. Campbell, 1987, pers. comm.).

In addition to the nature of the transparent medium, the amount of stray light also depends upon the size of features in the image. The width of colour strips is relatively constant regardless of the size of the feature being measured (Fig. IV-3). Experimentation on test samples showed that as the size of the measured feature decreases, the amount of halo error increases (Table IV-1). This suggests that the effect of halo error is more significant on the measurement of small features (Table IV-1, Fig. IV-4). The amount of halo error increases slightly (less than 1%, Table IV-1) as the number of features in the field of view increases. However, it is not clear whether the increase of halo error is caused by the increasing of features or experimental error. Effect of shading may be responsible for increasing halo error.

Error caused by limitation of instrument

In area measurement, it was found that the sum of the area measured on each colour band does not equal the total area obtained when the 32 colour bands were measured simultaneously. The associated error is caused by the limitation of the equipment since the digital readout can only give figures to one decimal place. This problem may be overcome by using the following procedures:

(1) Performing three different sets of area measurements: (i) measuring the area of each colour, (ii) measuring the area of each group of colours (yellow, cyan, green, orange, magenta, violet, red, and blue groups), and (iii) measuring the area of 32 colours simultaneously.

Table IV-2. An example of area calculation. Errors caused by effect of stray light and limitation of the instrument are taking into account. The corrections are made in two steps: (1) the difference between the subtotal and sum of the areas subgroup is equally distributed (c), and (2) the difference between the total and the sum of corrected areas is equally distributed (d). The measured area are adjusted to 100% (e) if necessary. Then, the halo error is corrected (f).

Density level	Colour level	(a) Measured area	Measured subtotal area	(b) Sum of subgroup area	(c) Corrected area at sub-group level	(d) Corrected area for full scale equal to 70	(e) Corrected area adjusted to 100%	(f) Corrected area (100%) after halo error correction
1	yellow - 1	0.1	6.6	6.4	0.150	0.1813	0.2589	0.3440
2	yellow - 2	0.6			0.650	0.6813	0.9732	1.0583
3	yellow - 3	2.5			2.550	2.5813	3.6875	3.7726
4	yellow - 4	3.2			3.250	3.2813	4.6875	4.7726
5	cyan - 1	4.5	19.0	18.9	4.525	4.5563	6.5089	6.5940
6	cyan - 2	5.4			5.425	5.4563	7.7946	7.8797
7	cyan - 3	4.9			4.925	4.9563	7.0804	7.1655
8	cyan - 4	4.1			4.125	4.1563	5.9375	6.0226
9	green - 1	4.2	18.6	18.5	4.225	4.2563	6.0804	6.1655
10	green - 2	4.1			4.425	4.4563	6.3661	6.4512
11	green - 3	4.5			4.525	4.5563	6.5089	6.5940
12	green - 4	5.4			5.425	5.4563	7.7946	7.8797
13	orange - 1	5.8	22.0	21.7	5.875	5.9063	8.4375	8.5226
14	orange - 2	5.7			5.775	5.8063	8.2946	8.3797
15	orange - 3	6.4			6.475	6.5063	9.2946	9.3797
16	orange - 4	3.8			3.875	3.9063	5.5804	5.6655
17	magenta - 1	1.5	2.1	2.0	1.525	1.5563	2.2232	2.3083
18	magenta - 2	0.4			0.425	0.4563	0.6518	0.7369
19	magenta - 3	0.1			0.125	0.1563	0.2232	0.3083
20	magenta - 4	+			0.025	0.0563	0.0804	
21	violet - 1	+	0.3	0.3	0.075	0.1063	0.1519	halo error = 1.6168
22	violet - 2	+			0.075	0.1063	0.1519	
23	violet - 3	+			0.075	0.1063	0.1519	
24	violet - 4	+			0.075	0.1063	0.1519	
25	red - 1	+	0.2	0.2	0.050	0.0813	0.1161	
26	red - 2	+			0.050	0.0813	0.1161	
27	red - 3	+			0.050	0.0813	0.1161	
28	red - 4	+			0.050	0.0813	0.1161	
29	blue - 1	+	0.2	0.2	0.050	0.0813	0.1161	
30	blue - 2	+			0.050	0.0813	0.1161	
31	blue - 3	+			0.050	0.0813	0.1161	
32	blue - 4	+			0.050	0.0813	0.1161	

+ area of individual colour which is too small to be measured
(a) Full scale of the output image is 70
(b) sum of each measured subgroup area
(c) Corrected area at subgroup level
  = measured area + (measured subtotal area - sum of subgroup)/4
  = 0.1 + (6.6 - 6.4)/4
  = 0.150
(d) Corrected area for full scale = 70
  = corrected area at subgroup + (full scale - total corrected area at subgroup level)/4
  = 0.150 + (70 - 69)/4
  = 0.1813
(e) Corrected area adjusted to 100%
  = corrected area for full scale x 100/70
  = 0.1813 x (100/70)
  = 0.2589
(f) Corrected area (100%) after halo error correction
  = corrected area adjusted to 100% + (halo error/number of density level representing features in image)
  = 0.2589 + (1.6168/19)
  = 0.3440.

(2) The corrections are made in two steps (Table IV-2) based on the assumption that the error is distributed equally in every measurement. First, the correction is made at the subgroup level. The difference between the measured subtotal area and sum of subgroup area of subgroup was equally distributed to each measurement in subgroup (see (c) in Table VI-2). Second, the difference between the total and the sum of corrected areas was equally distributed to 32 measurements (see (d) in Table VI-2).

(3) In the case that the full scale is not equal to 100%, the measured areas were adjusted to 100% (see (e) in Table VI-2).

(4) The correction for halo error was performed when necessary (see (f) in Table VI-2).

B. AUTOMATIC IMAGE ANALYSIS SYSTEM

The automatic image analyser, located at the Deaprtment of Entomology, University of Alberta, used in this study was a Tracor Northern TN-5000 (Plate IV-3). The modules of the instrument are: (1) microcomputer (1 Mb RAM), (2) Vidicon television camera, (3) light table, (4) a black-and-white television monitor to display "live" images, and (5) a colour monitor to display digitized and subsequently manipulated images.

Fundamentals and basic operations

The principle steps in image analysis, as described in Chapter 2 (Fig. II-1), can be performed using this system. Input images can be acquired from a television camera, from electron microscope detectors (using the microscan scan generator), or from the X-ray analyser. Thus, the image to be analysed may be a print, a negative, or a "live" image from the light-microscope, electron microscope, or X-ray analyser. The signal from the scanner is passed to a detector module and then to a monitor for display.

PLATE IV-3

The modules of automatic image analysis system comprise of microcomputer (m), Vidicon television camera (v), light table (lt), and black-and-white and colour television monitors.

PERIODIC CHART OF THE ATOMS

The digitized image is displayed on the colour television monitor with a screen rectangle of 512 x 256 pixels. The resolution of the image, however, can be specified by the operator. Four different levels of resolution are available: 1024 x 1024, 512 x 512, 256 x 256, or 128 x 128 pixels. Since the number of pixels in the image is used to define the resolution of the image, the greatest resolution is achieved with the highest number of pixels.

The software used was the Image Processing Program (IPP); a Flextran program used to construct digital images according to the intensities of the input image. The program provides an extensive array of image processing functions for modification and enhancement of an image (e.g. smoothing, sharpening, edge detection, grey-level transformations, and erosion-dilatation processes). The operation is performed by typed command or through keyboards.

A binary image can be created through a grey-level-segmentation process. Eight basic colours, black, red, green, blue, yellow, magenta, cyan, and white, can be assigned to the different phases existing in the image.

Measurements, such as area, perimeter, Feret's diameter, average diameter, length and width, and orientation are normally made from the binary image within a guard region to reduce error caused by measurements of features cut by the frame. The guard region, a border around the outside of the image, should be set at least one half the diameter of the largest feature to be measured.

Sources of errors

Instrument errors such as that caused by the effect of stray light (halo error) and by shading and the scanning system (as described in density slicer) are to be expected with the automatic image-analysis system. Practically, variations of illumination across the field of view and scanner variation can be reduced by: (1) using a shading corrector software (Ruzyla, 1986), and (2) by reducing the fraction of the field of view over which the measurements are taken (Cole, 1971). The shading correction software, however, was not available at the time this study was conducted.

Operator error normally occurs as a result of improper segmentation of the image. Practically, the binary image of the feature of interest is segmented from the background using grey-level thresholding. The threshold is usually set by selecting the lowest point between peaks of the histogram. In the case of images with low grey-tone contrast and small features (i.e. grey-level histogram does not show distinct peaks), it may be better to try a range of thresholds and choose the one for which the threshold image has some desired property. Besides error involved in image segmentation, error in size measurement can also occur as a result of using improper parameters to describe the feature.

C. DIGITIZED GRAPHIC TABLET

The digitized graphic tablet is an image analysis system in which the data acquisition and computation of geometric characteristic can be made by tracing the outlines of images placed on a digitizing tablet. Only the measurements of the physical dimensions, not the density of features, can be obtained. The digitized graphic tablet can be attached to an automatic image-analysis system or it can be coupled with a microcomputer. The system used in this study (Plate IV-4), a Mop-Videoplan graphic tablet, located in the Department of Soil Sciences, University of Alberta, comprised: (1) a digitizing tablet with a maximum measuring surface of 28 x 28 cm, (2) a microcomputer (64 Kbyte) with monitor, and (3) a printer. In addition to the basic units, a microscope can be connected to the system through a video camera. The system can be used to analyse an image in both photographic and transparent media. The advantage of this system is that additional sample preparation, e.g. staining techniques, may not be necessary if features to be measured can be visually recognized. The digitized graphic tablet is ideal for a complex image that cannot be analysed by an automatic image analyser.

PLATE IV-4

The modules of digitized graphic tablet comprise of microcomputer (m), tablet digitizer with pen cursor (dt), and printer (p). This system can be connected to microscope through a video camera.

Fundamentals and basic operations

In this system, data are entered by drawing on the tablet with a stylus that is electronically connected to the tablet's circuitry. This stylus also contains a sensing coil. Basic operating procedures are controlled by the software, Kontron CP/M, which is stored on a floppy disk supplied with the tablet. The measuring program enables the operator to measure numerous geometric parameters, including area, perimeter, size, orientation, and location of features in the image. Statistics such as sum, mean, standard deviation, and percentage values can be calculated. A range of functions can be selected via the keyboard and the menu located on the tablet.

The basic measuring units for this equipment is in millimetres; thus, before performing any analysis, the tablet must be calibrated in user-selected units. The input image is placed on the digitizing tablet, suitable geometric parameters are selected, and the features to be measured are traced on the tablet using the stylus. On lifting the stylus, parameters pertaining to the traced feature will be calculated and displayed on the monitor. For microscopic features, the images can be measured either by using photomicrographs and the graphic tablet or by projecting the image into the computer monitor via the video camera.

Sources of Errors

Errors encountered in the digitized graphic tablet technique arise from both software limitation and operator error. For example the measurement of irregularly shaped features is limited by the available equipment. In order to measure the dimension of irregularly shaped features, the features must be assumed to have forms such as circles or ellipses. Thus, the obtained values of such features are only approximations of the true values. If the shape of a given feature is significantly different from the assumed model, large errors in measurements may result.

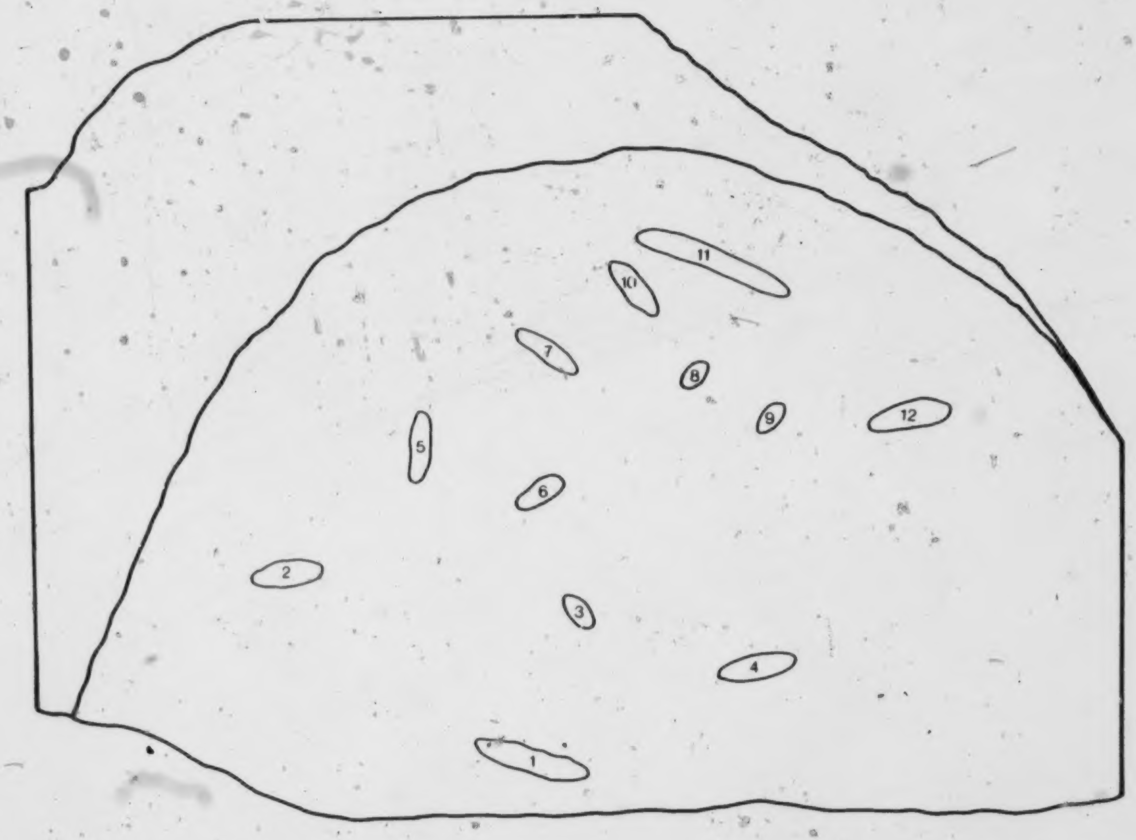
1
2
3
4
5
6
7
8
9
10
11
12

Figure IV-5. Set of test samples used in assessment of errors. The features were selected from thin section A of stromatoporoid head (see detail in Chapter 7).

Table IV-3. Assessment of error involved in the measurements of area, major axis and minor axis for unit types delineated on Figure IV-5, as measured using digitized graphic tablet. Scale in millimetres.

unit code	Minimum Area	Maximum Area	Mean Area	Standard Deviation	Coefficient of Variation
1	7.599	7.901	7.758	0.094	1.216
2	5.085	5.455	5.193	0.134	2.574
3	2.162	2.396	2.260	0.090	3.987
4	4.948	5.176	5.079	0.082	1.608
5	4.358	4.683	4.499	0.114	2.532
6	3.109	3.266	3.181	0.050	1.579
7	4.022	4.347	4.139	0.098	2.378
8	1.761	1.905	1.826	0.054	2.979
9	1.908	2.066	1.970	0.048	2.442
10	4.135	4.332	4.224	0.069	1.642
11	9.207	9.656	9.543	0.133	1.442
12	5.282	5.562	5.409	0.093	1.725

unit code	Minimum Major axis	Maximum Major axis	Mean Major axis	Standard Deviation	Coefficient of Variation
1	6.657	7.248	6.893	0.202	2.928
2	4.103	4.241	4.145	0.043	1.048
3	2.350	2.561	2.432	0.072	2.951
4	4.151	4.310	4.208	0.046	1.104
5	4.187	4.286	4.227	0.035	0.818
6	2.984	3.202	3.098	0.660	2.119
7	4.098	4.237	4.195	0.044	1.041
8	1.918	2.205	2.039	0.088	4.321
9	1.957	2.200	2.091	0.100	4.770
10	3.782	4.085	3.925	0.093	2.378
11	9.931	10.489	10.080	0.184	1.789
10	4.607	4.925	4.821	0.117	2.429

unit code	Minimum Minor axis	Maximum Minor axis	Mean Minor axis	Standard Deviation	Coefficient of Variation
1	1.404	1.491	1.453	0.030	2.075
2	1.562	1.696	1.619	0.038	2.326
3	1.123	1.279	1.216	0.049	4.000
4	1.450	1.603	1.528	0.044	2.907
5	1.130	1.431	1.368	0.035	2.551
6	1.286	1.363	1.330	0.025	1.906
7	1.236	1.301	1.264	0.024	1.870
8	1.070	1.216	1.150	0.048	4.133
9	1.145	1.312	1.238	0.059	4.799
10	1.332	1.453	1.391	0.033	2.360
11	1.217	1.308	1.255	0.030	2.365
12	1.381	1.510	1.450	0.054	3.748

Operator error normally occurs as a result of inconsistency in tracing the outline of a feature. During tracing, care must be taken to ensure that the stylus is not lifted before completing the tracing. An assessment of the degree of error likely to be involved can be evaluated statistically. The measurement error can be expressed in term of standard deviation and coefficient of variation. In an attempt to evaluate error (combination of instrument and operator errors) and give an assessment of the degree of error likely to be involved, test samples (Fig. IV-5) were measured. The parameters AREA and DELL AB were used to measure area, major and minor axes of each feature. According to Hayward (1977), ten repeat measurements of the same feature is acceptable for practical purposes of evaluating the precision of an instrument. In this study each feature was traced fifteen times in succession. The statistics of measurements, namely minimum and maximum values, mean values, standard deviation, and coefficient of variation (see Chapter 5) of each parameter, were calculated (Table IV-3). The degree of instrument and operator error likely to be involved is less than 5% as suggested by coefficient of variation (Table IV-3).

D. SYNOPSIS

The basic concept of density slicers and automatic image analysis systems is essentially the same. That is, a television camera converts the image density to a video signal and those signals are passed to a detector module and then to a monitor for display. However, the density slicer can be used only for enhancing the detail of images by assigning different colours to different grey tone. It is useful for delineating the boundary between the area where subtle differences in image tone occur. This instrument has a limitation in size measurement.

On the other hand, the automatic image analyser is useful in analysis when the image comprises of a well-defined feature, is homogeneous in tone, has continuous delineations. This system has the limited value in analysis of features which are touching, overlapping, or have a noisy background. In such cases, additional image processing techniques are needed. Care must be taken that image-processing techniques do not, in any way, alter the apparent dimensions of the features to a significant extent.

Only the physical dimensions of the features can be measured using a digitized graphic tablet since the data are entered by tracing the profile of the feature with a stylus. The digitized graphic tablet is an ideal system for complex images that cannot be analysed by an automatic image analyser.

V. STATISTICAL METHODS

An important aspect of image analysis is the statistical interpretation of the data obtained during such a study. Since the major concern of this study is to assess the use of image-analysis techniques in geology, the statistical discussion will concentrate on the hypothesis-testing methods which are applicable in evaluating the reliability of the results obtained via image-analysis techniques. Also, the concept of correlation and regression analysis will be considered. Full descriptions of these techniques can be found in statistical textbooks (e.g. Cochran, 1963; Hoel, 1982; Dalton *et al.*, 1975; Till, 1974; Freund and Williams, 1977; Silk, 1979; Maxwell, 1983; Davis, 1986; Wall, 1986).

A. BASIC DEFINITONS

Two important concepts in statistics are the *population* and the *sample*. A population consists of a well-defined set (either finite or infinite) of elements while a sample is a sub-set of elements taken from that population (Davis, 1986). In general, the population can be considered as a set of measurements of a specified property of a group of objects. For reason of economy (time and/or money), the small sub-set of the population (sample) is normally chosen to be a representative of the population. In other words, the properties of the sample are used as an estimate of the population parameters (statistical inference). The statistical formulae presented in this chapter concern the sample.

The choice of using statistical methods in a given situation is based on the *scales of measurement*. Four primary scales of measurement are: (1) the nominal scale, (2) the ordinal scale, (3) the interval scale, and (4) the ratio scale. The nominal scale is normally expressed by symbols or names, e.g. colour. It is used for classification only. The ordinal scale, or ranking scale, is used when measurements can be ranked or classed on some basis. The length of the steps between classes need not to be constant. The interval scale is a level of measurement where there is equality of length of steps between classes.

Therefore, the ratio of any two intervals is independent of the units of measurements. The ratio scale has a true zero in addition to the properties of the interval scale. The ratio scale has the maximum information and allows most statistical tests to be used.

Two main types of statistical methods are ***parametric*** and ***nonparametric*** statistics. The parametric statistics, such as *t* test and analysis of variance, are employed when the conditions about the parameters (e.g. distribution of the population, equality of variances, and scales of measurement) of the population from which the sample was drawn can be specified. There are cases, however, where the parametric statistical methods may not be applicable. For example, some paleoecological measurements on communities produce skewed distributions. In such cases, the nonparametric statistics are used. No estimates of parameters or distributional assumptions are necessary for nonparametric statistics. For this reason nonparametric statistics are commonly referred to as distribution-free statistics. Nonparametric statistics can be applied to all scales of measurement. Most parametric statistics are paralleled by nonparametric statistical techniques.

It may appear that nonparametric statistics have some advantages in certain aspects. However, nonparametric statistics are less power efficient. For example, nonparametric methods do not give estimates of means. Also, the sample size required for a particular nonparametric statistical test will be greater than the sample size required for the corresponding parametric statistical test. The statistical methods presented in this chapter, except for the Mann-Whitney *U* test, are parametric statistics.

B. MODE AND MEAN

There are situations (e.g. pursuing further analysis) when it is desirable to use a single value to represent a set of data. This single value is normally an average value about which the distribution of measurements is centred (known as a measure of central tendency). The mode and mean are the two measures of central tendency used in this study.

The mode are the values that occur most frequently in a distribution, corresponding to the highest point on a frequency curve. It is easy to determine and no computation is involved. However, the mode has some disadvantages: (1) it is not derived mathematically so it cannot be used in further analyses, (2) it is based only on frequency and only the observations with a highest frequency actually determine its value so it may not be a representative value, and (3) it is inappropriate for bimodal or polymodal distributions.

The best known measure of central tendency is the arithmetic mean. It is frequently called the mean or sometimes the average. In this study the term mean is used for the arithmetic mean. The mean is defined as the sum of the measurements divided by the number of measurements

$$\bar{X} = \frac{\sum_{i=1}^{n} X_i}{n}$$

where X_i = the value of the i^{th} measurement (i = 1, 2, 3........n), and $\bar{X}$ = mean.

The mean has certain advantages over the mode as a measure of central tendency. It is more representative of all the data since every measurement is used in the computation of the mean. Thus, the mean may be used in further computations. However, the mean is more affected by extreme measurement, especially when only a few measurements are considered.

C. MEASURES OF VARIABILITY

The presentation of the amount of variability in the data is important because it gives some information about the degree to which the average is representative of the data. There are several statistical descriptors of variation. In this study, three measurements are used: range, variance, and standard deviation.

Range is the simplest way to describe the spread of observations in a distribution. It is the difference between the highest and lowest values in the data set. Although the range is easy to calculate, it does not contain any information about how the data are distributed.

An important characteristic of a distribution curve is the spread or dispersion about the mean. The common measure of this is the variance and its square root which is termed the standard deviation.

The variance is defined by the equation

$$s^2 = \frac{\sum_{i=1}^{n} (X_i - \bar{X})^2}{n - 1}$$

where s^2 = variance, X_i = the value of the i^{th} measurement ($i = 1, 2, 3, \ldots\ldots\ldots n$), and $\bar{X}$ = mean. The standard deviation (s) can be calculated from

$$s = \sqrt{\frac{\sum_{i=1}^{n} (X_i - \bar{X})^2}{n - 1}}$$

D. PRECISION AND ACCURACY

Two properties which are normally concerned in any measurement process are precision and accuracy. Precision refers to the repeatability of a measurement. It is an estimate of the reproducibility of a method. Precision is estimated by the standard deviation of the distribution. It can also be presented as the coefficient of variation, which expresses the standard deviation as a percentage of the mean value

$$c = \frac{100s}{\bar{X}}$$

where c is coefficient of variation, s is standard deviation, and $\bar{X}$ is mean.

The coefficient of variation is more informative than the standard deviation because it is independent of the unit of measurement. Consequently, it can be useful in comparisons between different sets of measurements.

The accuracy is an estimate of how close to the true value is the measured value. It gives an estimation of bias in the measurement. In practice, accuracy is difficult to estimate because most of the time the true value of measurements is not known. However, accuracy can be estimated with reference to defined standards.

E. SAMPLING TECHNIQUE

In statistical analysis, the choice of sampling technique is important since the population parameters are estimated from the sample. The main concern in the selection of sampling techniques is to avoid bias. Practical sampling techniques (Fig. V-1) include random sampling, systematic sampling, stratified sampling, cluster sampling, or combinations of those techniques (Cochran, 1963; Dalton *et al.*, 1975). In random sampling each object in the population has the chance of being selected every time an object is taken. This is different from systematic sampling technique in which, the first unit is selected at random, but subsequent units are chosen at a prescribed and uniform interval from the first. The stratified sampling technique involves the selection of individual points either randomly or systematically in pre-arranged sub-areas (based on some criterion). In cluster sampling, the samples are selected from sub-areas determined randomly, not purposely as for stratified sampling.

There are three main sampling units: points, lines or traverses, and quadrants or areas (Fig. V-1). Each sampling technique has both advantages and disadvantages (Table V-1). Thus, the purpose of a sampling technique is to secure a sample which will reproduce the characteristics of the total population as closely as possible.

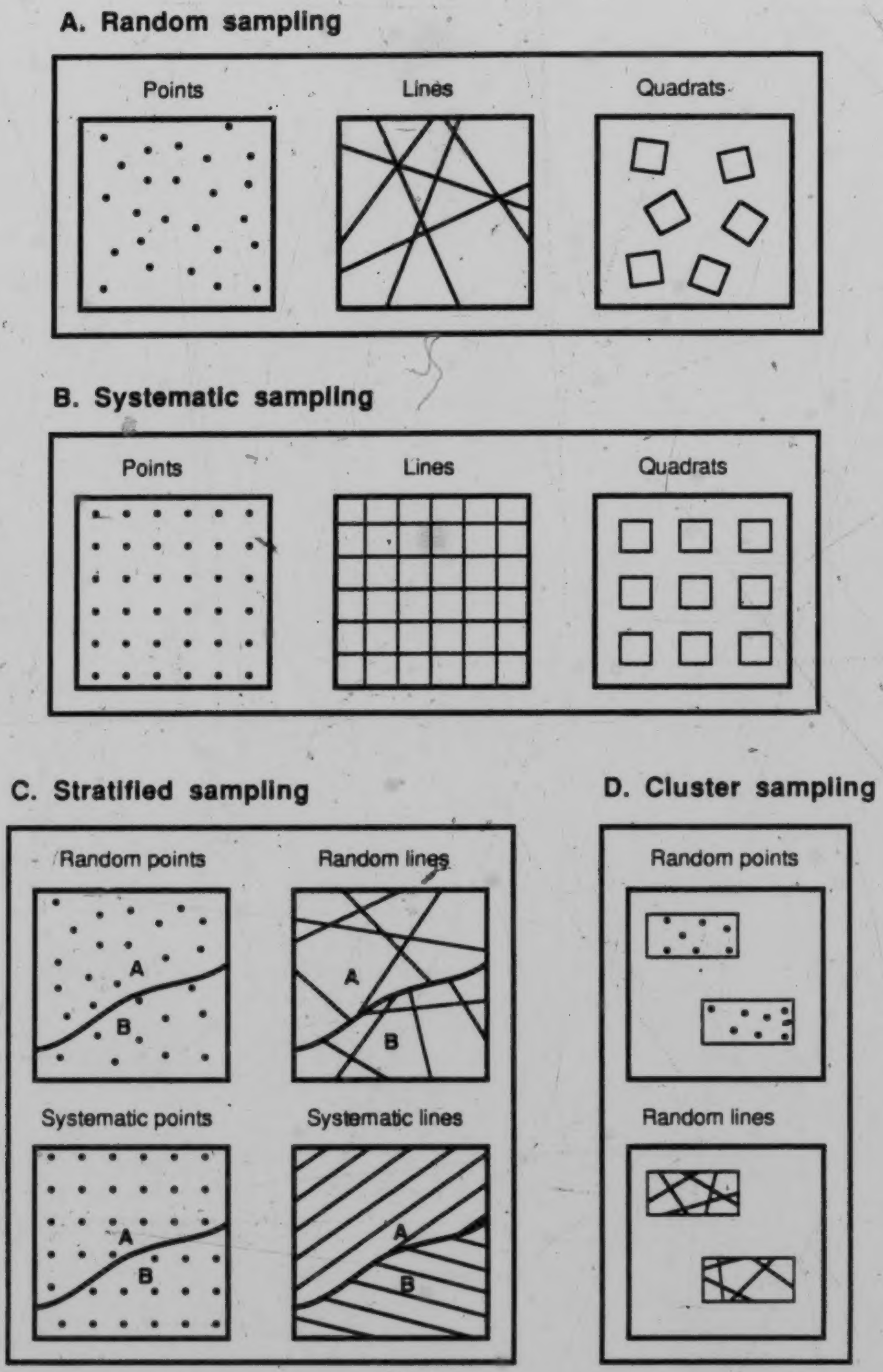
A. Random sampling
Points
Lines
Quadrats
B. Systematic sampling
Points
Lines
Quadrats
C. Stratified sampling
Random points
A
B
Random lines
A
B
Systematic points
A
B
Systematic lines
A
B
D. Cluster sampling
Random points
Random lines

Figure V-1. Schematic diagrams showing various sampling techniques.

Table V-1. Summary of sampling techniques.

Technique	Advantage	Disadvantage	References
Random sampling	each object in the population has the same chance of being selected; unbiased technique	difficult in practise; must ensure that every part of the area has an equal chance of select; no deliberate choosing of any unit which looks as if it is "average" must be allowed	Cochran, 1963 Dalton *et al.*, 1975 Freund and Williams, 1977 Silk, 1979
Systematic sampling	faster and simpler to use than the random sampling; sample spread more evenly over the entire population	all parts of the area do not have an equal chance of selection once the first point has been established; cannot be used for a recurring periodic feature in the distribution; might yield bias results	Cochran, 1963 Dalton *et al.*, 1975 Freund and Williams, 1977 Silk, 1979
Stratified sampling	suitable when a heterogeneous area is being investigated; smaller area can be satisfactorily represented; higher degree of precision than a simple random of the same size	problem in choosing the basis of stratification, number of strata, and sample sizes to allocate to the different strata; how should the samples within the strata be taken	Cochran, 1963 Dalton *et al.*, 1975 Freund and Williams, 1977 Silk, 1979
Cluster sampling	cheap to operate	usually not as reliable as estimates based on simple random sample of the same size	Cochran, 1963 Dalton *et al.*, 1975 Freund and Williams, 1977

F. SAMPLE SIZE

Results are subject to statistical fluctuations because the population parameters are normally estimated using statistical inference. Thus, any estimate will not be exact but will have an associated error. In any sampling technique, sample size must be specified since it is directly related to the accuracy of the results. The larger the number of samples, the more precise will be the estimation. However, an error as small as desired can be obtained by using sufficient samples. In practice, the allowable error is generally specified, and this information is used to determine the required samples.

Sample size for the normal distribution approximation to the binomial distribution (distribution of two mutually exclusive numbers or sets of conditions) can be estimated by:

$$n = \frac{pq}{E^2} z^2_{(1-\alpha/2)}$$

where n = the sample size

p = the percentage of area in a certain category

q = the percentage of area not in that category

E = the maximum allowable error in estimating p

$1 - \alpha$ = the desired probability or confidence level that the estimated proportion q does not differ from p by more than $\pm E$

$z_{(1-\alpha/2)}$ = the $(1 - \alpha/2)100$ percent point of a standard normal distribution

(from Hahn and Shapiro, 1967).

In order to compute the sample size, p, q, E, and $z_{(1-\alpha/2)}$ must be specified. For example, if $p = 0.2$, and $q= 0.8$, the desired confidence level is $1 - \alpha = 0.95$, then $\alpha = 0.05$ and $z_{(1-\alpha/2)} = 1.96$. Therefore, the estimate of the required sample size is

$$n = \frac{(0.2)(0.8)}{(0.05)^2} (1.96)^2 = 246$$

This approximation is generally adequate, except when np or $n(1 - p)$ is less than 5 (Hahn and Shapiro, 1967).

G. HYPOTHESIS TESTING

In most statistical analyses, decisions are based on incomplete information so there is a possibility of making erroneous conclusions. Hypothesis testing is a technique which allows the operator to reduce the probabilities of making a wrong decision. The aim of hypothesis testing is to formulate a set of rules which leads to a decision in acceptance or rejection of statements about population parameters.

The hypothesis which is formulated for the purpose of possible rejection is called the *null hypothesis*. The hypothesis against the null hypothesis is called the *alternative hypothesis*. Generally, a null hypothesis is an explicit statement while an alternative hypothesis is a general statement. The null hypothesis and the alternative hypothesis are determined by the question posed in the statement of a problem.

In the following, some of the statistical terminologies related to the hypothesis testing are discussed. The error of rejecting a null hypothesis which is in fact true is called a *type I error*. The probability of committing this error is denoted by alpha (α). The alpha (α) is also referred to as the level of significance of the test. The error of accepting a null hypothesis which is in fact false is called a *type II error*. The probability of committing this error is usually denoted by beta (β). Ideally both α and β should be very low.

The value which separates the acceptance and rejection regions is called the *critical value*. The region containing values greater than the critical value is called the *rejection region* whereas the region containing values less than the critical value is called the *acceptance region*. In other words, the null hypothesis is accepted if the calculated value of the hypothesis-testing technique is less than the critical value of such test. In contrast, the null hypothesis is rejected if the calculated value of the hypothesis-testing technique is larger than the critical value of such test.

The *degrees of freedoms* (υ) are denoted to the number of observations in excess of those necessary to estimate the parameters of the distribution. In other words, the degrees of freedom are the number of observations minus the number of estimates made from them.

In the following, the parametric hypothesis testing techniques, *t* test and analysis of variance, and nonparametric, Mann-Whitney *U* test will be discussed.

t test

The *t* test is useful for establishing the probability that a given sample could be a member of a population with specified characteristics, or for testing hypotheses about the equivalency of two samples. Three assumptions are implicit to this test: (1) the samples were selected at random, (2) the populations from which the samples were drawn are normally distributed, and (3) the variances of the two populations are equal.
The assumption that the populations from which the samples were drawn are normally distributed can be verified by using the *stabilized probability plot* (Michael, 1983). The plot shows the maximum deviation of the plotted points from their theoretical values (Fig. V-2). The values for the abcissa and the ordinate are the transformed values of the theoretical and data values, respectively. By transformation of the data values, the variances of the ordinates are approximately equal. This allows the acceptance region (for a specified confidence interval) to be added to the plot by simply drawing two straight lines. The middle line is the line where the data values are all equal to the theoretical values of a normal random variable. The two boundary lines show the 95% confidence interval. If all the plotted points fall between the two boundary lines, the data value is taken to have a normal distribution at the specified confidence level.

The equality of variances of the two populations can be checked by conducting an *F* test. The value of *F* is obtained by

$$F = \frac{s_1^2}{s_2^2}$$

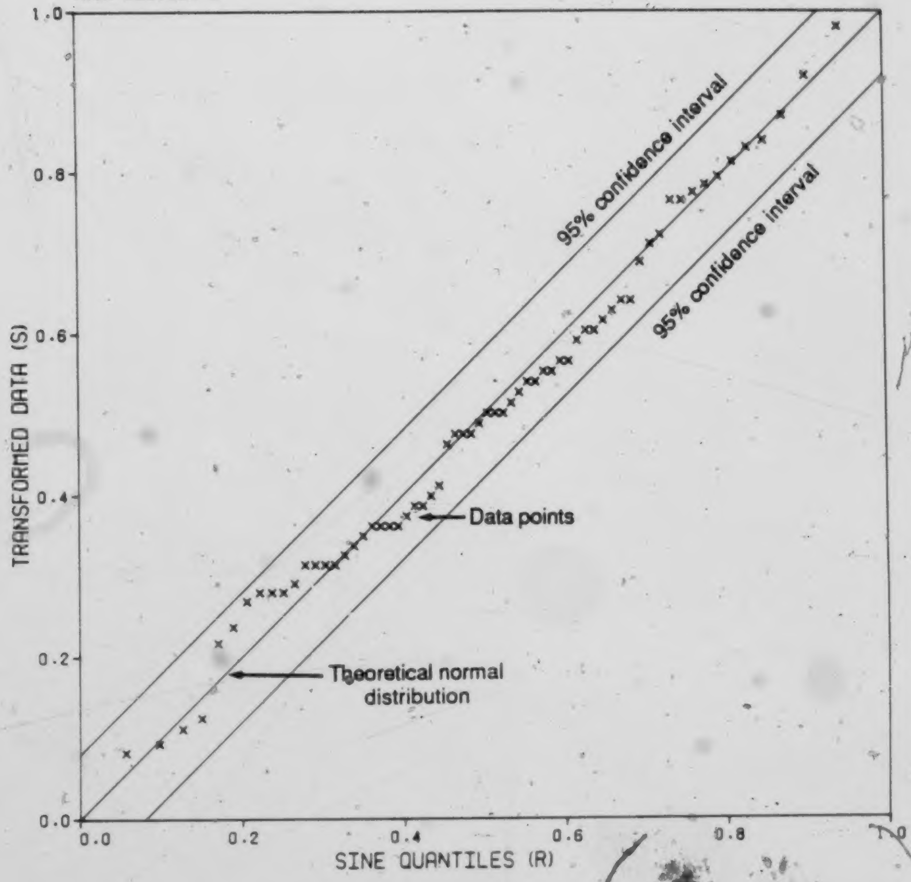

Figure V-2. Example of stabilized probability plot (data from thin section E in Chapter 7).

where s_1^2 and s_2^2 are sample variances from two populations.

If the two population variances are equal, the ratio of the two sample variances, based upon sample size of n_1 and n_2, will follow the *F* distribution with $\upsilon_1 = (n_1 - 1)$ and $\upsilon_2 = (n_2 - 1)$ degrees of freedom. This is the theoretical distribution of values that would be expected by randomly sampling from a normal population and calculating for all possible pairs of sample variances. In other words, the conclusion that the variances of these two populations are equal, at a specified confidence level, can be made when the value of *F* test is less than the critical value of the *F* distribution (obtained from table of critical value for *F*).

When all the assumptions for *t* test are satisfied, the *t* test can be performed using the formula below. For the two samples with mean $\bar{X}_1$ and $\bar{X}_2$ and size of n_1 and n_2, respectively, the formula for *t* can be written as

$$t = \frac{\bar{X}_1 - \bar{X}_2}{S\sqrt{\frac{1}{n_1} + \frac{1}{n_2}}}$$

where *S* (the pooled sample variance) is equal to

$$S = \sqrt{\frac{n_1 s_1^2 + n_2 s_2^2}{n_1 + n_2 - 2}}$$

with $n_1 + n_2 - 2$ degree of freedom.

Like the *F* test, it can be concluded that means of two populations are equal at a specified confidence level if the value of *t* test is less than *t* critical value (obtained from table of critical values for *t*).

Analysis of variance

Analysis of variance (ANOVA) is the statistical method used for comparing groups of measurements by simultaneously considering both differences in means and variances. The ANOVA used in this study is one-way analysis of variance; a method used to compare means under the basis of a single criterion. The one-way analysis of variance technique involves separating the total variance of measurements into various components or sources.

Three assumptions must be verified before performing the analysis of variance: (1) each set of replicates represents random samples from different populations, (2) each parent population is normally distributed, and (3) each parent population has the same variance.

The total variance of a data set is broken into two parts: *within-sample variance* and *among-sample variance*. The total variance is the variation of all measurements about their mean. The within-sample variance is the total variation of each sample about its own mean, and the among-samples variance is the variation of the sample means about the grand mean. The results of analysis of variance are usually tabulated in an analysis of variance table (Table. V-2).

The sum of squares of total variance of all observations (SS_T) for the group of measurements comprising *m* sample and *n* replicates per sample is defined by

$$SS_T = \sum_{j=1}^{m} \sum_{i=1}^{n} X_{ij}^2 - \frac{(\sum_{j=1}^{m} \sum_{i=1}^{n} X_{ij})^2}{N}$$

where X_{ij} is the i^{th} replicate of the j^{th} sample, and N is the number of replicates per sample times the number of samples, i.e. $N = n \times m$.

The sum of squares of within-samples variance (SS_W) is

$$SS_W = \sum_{j=1}^{m} \sum_{i=1}^{n} X_{ij}^2 - \sum_{j=1}^{m} \left(\frac{(\sum_{i=1}^{n} X_{ij})^2}{n} \right).$$

Table V-2. The analysis of variance table (from Davis, 1986).

Source of variation	Sum of squares	Degree of freedom	Mean squares	*F* Test
Between samples	SS_A	$m - 1$	MS_A	MS_A/MS_W
Within samples	SS_W	$N - m$	MS_W	
Total variation	SS_T	$N - 1$		

The sum of squares of among-samples variance (SS_A) is

$$SS_A = \sum_{j=1}^{m} \left(\frac{(\sum_{i=1}^{n} X_{ij})^2}{n} \right) - \frac{(\sum_{j=1}^{m} \sum_{i=1}^{n} X_{ij})^2}{N} .$$

The number of degrees of freedom for variance in the total data set is $N - 1$. Degrees of freedom for variance among the samples is $m - 1$. The difference between the two is the degree of freedom of variance for within-samples ($N - m$).

In order to obtain variances (or mean squares), the quantities, SS_T, SS_W, and SS_A must be divided by the appropriate degrees of freedom. The total variance, mean squares of among-samples and mean squares within-samples can be calculated by

$$\text{Total variance} = \frac{SS_T}{N - 1}$$

$$\text{Variance among-samples} = MS_A = \frac{SS_A}{m - 1}$$

$$\text{Variance within-samples} = MS_W = \frac{SS_W}{N - m} .$$

Then, F test can be calculated by

$$F = \frac{MS_A}{MS_W} .$$

If the F test is less than F critical at a specified confidence level, it can be concluded that the samples belong to the same population.

Mann-Whitney *U* test

The Mann-Whitney U test is the nonparametric equivalent of the parametric t test. It is used to test the equality of the means of two samples when the necessity conditions about the parameters of the population from which the sample was drawn required for t test cannot be specified. When two samples are to be tested whether they come from the same population, the two sets of observations are combined and sorted in decreasing order (or reverse). Each observation is assigned a rank, the smallest is rank 1 and so on up to the largest observation. If the two samples have been drawn randomly from the same population, the observations from one of the samples would be scattered more-or-less uniformly through the ranked sequence.

$$U = n_1 n_2 + \frac{n_1 (n_1 + 1)}{2} - R_1$$

where n_1 and n_2 are the first and second sample sizes and R_1 is the sum of the ranks assigned to the values of the first sample. Under the null hypothesis that the $n_1 + n_2$ observations come from identical populations, then the sampling distribution of U has the mean (μ_u) equal to

$$\mu_u = \frac{n_1 n_2}{2}$$

and the standard deviation (σ_u) equal to

$$\sigma_u = \sqrt{\frac{n_1 n_2 (n_1 + n_2 + 1)}{12}}$$

Furthermore, if n_1 and n_2 are both greater than 8 (some statisticians prefer that both be greater than 10), the sampling distribution of U can be approximated closely with a normal curve. Hence, the null hypothesis is rejected at the level of significant α if

$$z = \frac{U - \mu_u}{\sigma_u}$$

is either less than $-z_{\alpha/2}$ or greater than $z_{\alpha/2}$.

H. CORRELATION AND REGRESSION

The two concepts which are extensively used to study the relationship between variables are correlation and regression. Correlation and regression are bivariate and multivariate statistical methods.

The purpose of correlation is to determine if a relationship exists between two variables. The correlation coefficient is a measure of the strength of that relationship. The most frequently used measure of linear correlation between two variables is called the Pearson product-moment correlation coefficient, expressed mathematically as

$$r = \frac{\dfrac{\sum (X - \bar{X})(Y - \bar{Y})}{n - 1}}{\sqrt{\dfrac{\sum (X - \bar{X})^2}{n - 1} \; \dfrac{\sum (Y - \bar{Y})^2}{n - 1}}}$$

or

$$r = \frac{\text{covariance}(X,Y)}{\sqrt{\text{variance } X \;.\; \text{variance } Y}}$$

where r is the correlation coefficient, $\bar{X}$ and $\bar{Y}$ are the means values of X and Y, and n is the number of sample. The value of r ranges from 0 (no correlation) to plus or minus 1 (perfect correlation).

The purpose of regression analysis is to describe the relation between variables in quantitative terms, i.e. finding an equation to describe the relation between variables. The predicted variable is normally referred to as the dependent variable. The variable upon which the prediction is based is referred to as the independent variable.

The most frequently used technique is the least-squares method. In the least-squares method it is assumed that the dependent variable is not subject to error. The regression equation can be expressed as

$$Y = a + bX$$

where *a* is an intercept and *b* is the slope.

The value of *a* and *b* can be calculated by

$$a = \bar{X} - b\bar{Y}$$

$$b = \frac{\sum XY - \frac{(\sum X \sum Y)}{\mathrm{n}}}{\sum X^2 - \frac{(\sum X)^2}{n}} .$$

VI. APPLICATION OF IMAGE ANALYSIS TO MAPPING

A. INTRODUCTION

Aerial photographs have been widely used as a basis for geologic mapping. Patterns on aerial photograph results from the spatial arrangement of the different tones and textures. In aerial photographs, tone is a measure of the relative amount of light reflected by objects on the surface (Verstappen, 1974; Avery, 1977; Paine, 1981; Drury, 1987; Sabins, 1987). Variation in the photographic tone of an object is governed by the characteristics of the object, geographic latitude, angle of reflected light, sensitivity of film, and photographic processing. However, under ideal circumstances, objects of different colour have different qualities of light reflectances and, therefore, register in varying shades or tones on photographs. For example, research results have shown striking differences in the spectral reflectance curve of different soils and geologic material (Hoffer and Johannsen, 1969). It has also been suggested that if changes in relative photographic tone are present on a photograph, the interpreter should expect those changes to be geologically significant (Stone, 1956; Drury, 1987).

The interpretation of aerial photographs is mainly a matter of subjective assessment. Factors influencing the interpretation of aerial photographs are: (1) the quality of the aerial photographs, (2) the scale of the aerial photographs, (3) photography interpretation techniques, and (4) the skill of the photo interpreter. Generally, the interpretation of aerial photographs is based on the fundamental recognition of various properties evident on the photograph (e.g. tone, texture, shape, size, pattern) and the relation of associated features (Ray, 1960; Avery, 1977; Paine, 1981; Drury, 1987; Sabins, 1987). Although quantitative information such as height and difference in altitudes can be obtained using a stereoptic viewer, those fundamental elements are primarily qualitative attributes. For example, various areas of aerial photographs are normally characterized as light, intermediate, or dark in tone. It is difficult, however, to consistently and accurately discriminate between some of the more subtle differences in image tone when a manual classification procedure is used.

The present study tried to extract quantitative information from aerial photographs by means of various image-analysis techniques. Lagoons around Grand Cayman were selected for this purpose because: (1) four different sets of aerial photographs are available, (2) human disturbance is at a minimum, (3) there was an opportunity to do field work to check on the interpretation of aerial photographs, and (4) extensive research programs are currently being conducting in this area so additional data could be obtained. Relying on the assumption that different surface materials have different spectral reflectance, the pattern on the aerial photographs is taken as reflection of the different substrates and biologic communities in the lagoons around Grand Cayman.

The objectives of this study are:

(1) to identify the substrate and biological communities in the lagoons around Grand Cayman from aerial photographs by applying image-analysis techniques in conjunction with field investigations and to measure the area occupied by each substrate and biologic community,

(2) to detect changes in the distribution of biological communities and substrate and the implications of such changes over a period of time, and

(3) to determine any interrelationships that may be present between the biological communities and substrate.

B. GENERAL PHYSICAL CONDITIONS ON GRAND CAYMAN

Grand Cayman, the largest of the Cayman Islands, is approximately 280 km north-northwest of Jamaica between the latitudes of 19° 16' and 19° 24' north and longitudes 81° 05' and 81° 25' west (Fig. VI-1A). The island is a peak on the Cayman Ridge which is a submarine extension of the Sierra Maestra Range of Cuba (Rigby and Roberts, 1976). The

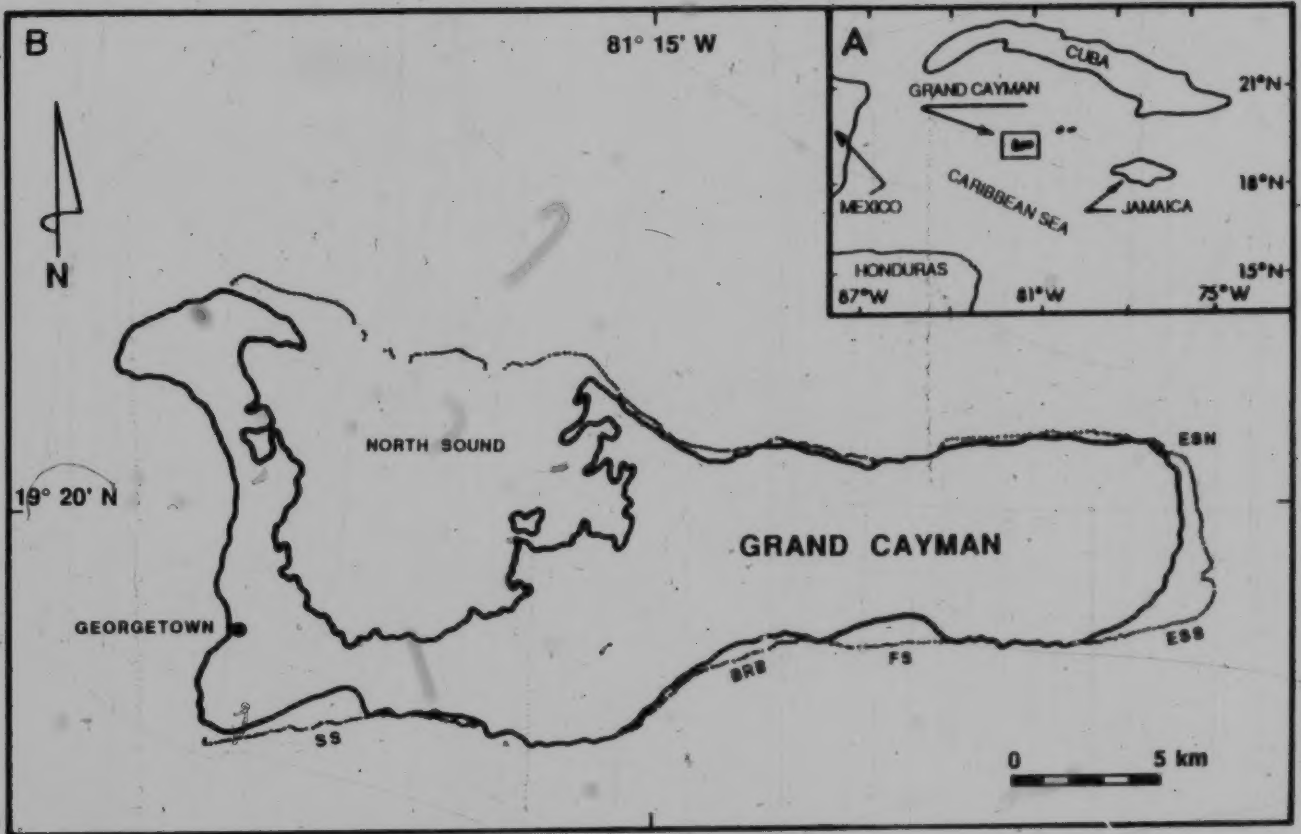
B
81° 15' W
N
19° 20' N
NORTH SOUND
GEORGETOWN
GRAND CAYMAN
ESN
ESS
FS
BRB
SS
0
5 km
A
CUBA
GRAND CAYMAN
21°N
MEXICO
CARIBBEAN SEA
18°N
JAMAICA
HONDURAS
15°N
87°W
81°W
75°W

Figure VI-1. Location map of Grand Cayman. Dotted lines offshore show position of coral reefs and boulder-based barrier ridges. SS = South Sound, BRB = Blue Rock Bay, FS = Frank Sound, ESS = East Sound South, ESN = East Sound North (modified after National Geographic Map of the Caribbean, 1975).

island is 35 km long and is between 6 and 14 km wide (Fig. VI-1B), with an area of 197 km^2 (Woodroffe, 1981).

Topographically, Grand Cayman is relatively flat. Most of the island is less than 3 m above sea level, with a maximum elevation of 20 m (Jones *et al.*, 1984). Coral reefs and boulder-based barrier ridges developed at the abrupt break along the shelf margin along the island, except for the western coast. The lagoons, located between the reefs and coasts (Fig. VI-1B), are shallow and have a relatively uniform depth of 2 to 3 m with the maximum depth of approximately 5 m in North Sound (Roberts and Sneider, 1982) and up to 7 m in East Sound (B. Jones, 1988, pers. comm.). In general, those lagoons are less than 1 km wide, except for North Sound and the southern portion of East Sound.

The water surrounding Grand Cayman is clear, except for areas where the organic-rich water of the surrounding mangrove swamps enters the lagoons. The salinity of the Caribbean Sea water near the Cayman Islands is 35 to 38‰ and the chlorinity of 19.9 to 20.9‰ (Moore, 1973). The salinity of the lagoonal waters around Grand Cayman, however, depends upon local conditions, e.g. amount of rainfall as well as shoreline geography and wind-driven circulation in the sound (Roberts and Sneider, 1982). Salinity varies from normal salinity sea water in East Sound to the maximum salinity of 42‰ in North Sound (Rigby and Roberts, 1976).

Based on temperature data recorded by the United States Meteorological Station during 1970 - 1986 (Table VI-1), the average annual temperatures on Grand Cayman ranged from 26 to 27°C. The average temperature of the warmest month during summer (May to November) was about 28°C and the average temperature of the coldest month during the winter (December to April) ranged from 22 to 26°C. However, the difference between the highest and lowest temperatures was about 21°C (Table VI-1). No detailed data on water temperature are available; however, the trend of water temperatures approximates the trend of the land temperatures (K. C. Ng, 1988, pers. comm.). Water temperatures in shallow water areas, measured during field investigation in February 1988,

Table VI-1. Summary of annual temperatures on Grand Cayman from 1970 to 1986 (Data from United States Meteorological Station, Owen Roberts International Airport, Grand Cayman).

Year	Highest temperature (°C)	Lowest temperature (°C)	Average annual (°C)	Average warmest month temperature (°C)	Average coldest month temperature (°C)
1970	33.3	12.8	26.2	28.2 (June)	23.8 (February)
1971	32.7	12.2	26.2	no data	no data
1972	33.0	12.8	26.5	27.9 (July)	24.6 (March)
1973	33.0	13.3	26.4	28.0 (July)	23.9 (December)
1974	33.0	16.1	26.1	27.8 (July, August)	23.3 (February)
1975	33.5	15.0	26.2	28.2 (June)	24.3 (February)
1976	33.9	15.0	26.3	28.1 (August)	23.7 (January)
1977	34.1	13.3	26.9	28.4 (July)	24.3 (January)
1978	33.6	15.0	15.0	28.4 (August)	23.8 (February)
1979	34.1	13.3	26.4	28.1 (July)	24.6 (February)
1980	34.1	13.9	26.8	28.9 (July)	23.7 (February)
1981	33.6	12.8	26.3	28.4 (July)	21.9 (January)
1982	33.9	13.9	26.7	28.3 (July)	25.3 (February)
1983	no data	no data	27.0	28.9 (July)	24.9 (February)
1984	no data	no data	26.8	28.4 (July)	24.8 (January)
1985	33.6	12.9	26.7	28.7 (July)	23.6 (January)
1986	33.6	13.9	26.8	28.6 (July)	24.4 (February)

varied from 26 to 28°C. In the shallow coastal waters of Frank Sound, water temperatures as high as 34°C were recorded in July 1986 (B. Jones, 1987, pers. comm.).

Studies of physical processes around Grand Cayman show that the island is exposed to a wave regime which originates primarily in response to the northeast trade wind system (Roberts *et al.*, 1975). The dominant direction of waves throughout the year shifts from northeast through east, while the occasional short term winds are from the north. The difference in wave energy between the windward and leeward sides of the island is significant, over two orders of magnitude as reported by Roberts and Sneider (1982). Currents on the shelf are controlled by both the mean drift and tides and the westward component seems to be the dominant one (Rigby and Roberts, 1976). The coral reefs and boulder-based ridges protect the shelf lagoon from the direct influence of waves and currents.

C. GENERAL GEOLOGY AND TECTONICS

The Cayman Islands are peaks on a submarine ridge which is bordered to the north by the Yucatan Basin and to the south by the Cayman Trench (Rigby and Roberts, 1976). The Cayman Islands have undergone localized uplift since the middle Miocene (Perfit and Heezen, 1978). It has been suggested that the three Cayman Islands have been relatively stable since the last interglacial (Emery, 1981; Woodroffe *et al.*, 1983). Two submarine terraces occur around the islands with breaks in slope at 8 m and 15 m (Rigby and Roberts, 1976). The lagoons along the shores of Grand Cayman are related to shallow terraces cut into the bedrock.

Grand Cayman is composed of a core of the Oligocene-Miocene Bluff Formation and surrounded by Pleistocene carbonates of the Ironshore Formation (Fig. VI-2). The Bluff Formation, named by Matley (1926), is formed of cream to light tan coloured, dense, microcrystalline dolomite (Folk *et al.*, 1973; Jones *et al.*, 1984; Pleydell, 1987; Pleydell and Jones, 1988) which can be divided into the Oligocene Cayman Member (Oligocene)

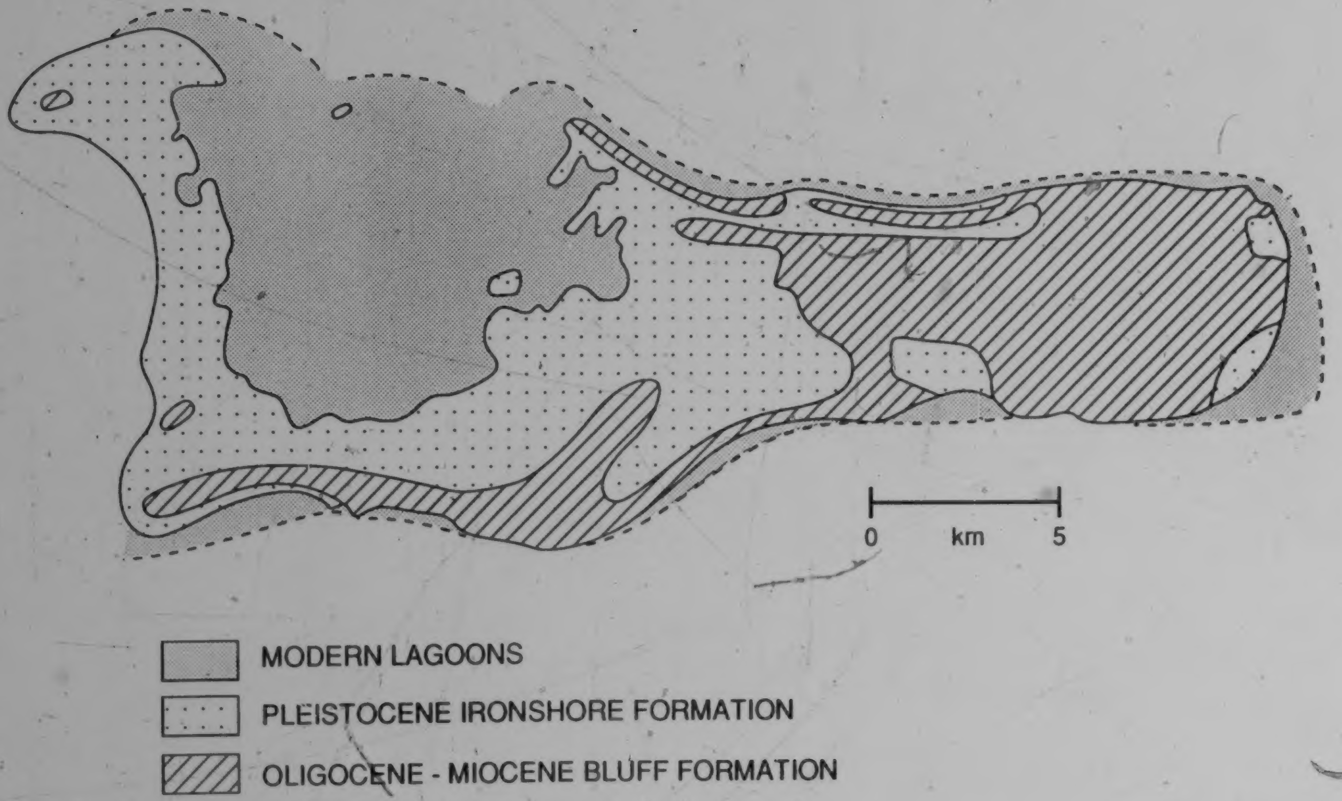
0
km
5
MODERN LAGOONS
PLEISTOCENE IRONSHORE FORMATION
OLIGOCENE - MIOCENE BLUFF FORMATION

Figure VI-2. Geological map of Grand Cayman (modified after Brunt et al., 1973).

and the overlying Miocene Pedro Castle Member (Jones and Hunter, 1989a). These two members were distinguished based on the lithology, differences in diagenetic styles, and the fauna (Jones and Hunter, 1989a). The boundary between these two members is a disconformity.

Brunt *et al.* (1973) divided the Pleistocene Ironshore Formation, named by Matley (1926), into five depositional environments: reef, back reef, lagoonal, shoal and beach ridge facies based on the lithology and biota. The work by Jones and Goodbody (1984), Pemberton and Jones (1988), and Jones and Pemberton (1989) provided further information concerning depositional systems associated with the Ironshore Formation. Recently, Hunter and Jones (1989) defined the depositional regimes of the Ironshore Formation into: (1) lagoonal environment - bivalves facies, (2) lagoonal environment - ooid facies, (3) lagoonal environment - patch reefs and interreef limestones, and (4) reef tract.

In addition to these two formations there are unconsolidated modern deposits which occur around the island and consist of coral reef, lagoonal sediments, beach rock, storm berms, and boulder ramparts. The recent biologic communities and sediments of the lagoons have been well described by Rigby and Roberts (1976), and Roberts (1971a, 1971b, 1976). The succession from a coral reef to a *Thalassia*-covered plain to mangrove forest as described by Welch (1963) is evident on Grand Cayman.

D. MATERIALS

Five lagoons around Grand Cayman were selected for this study: South Sound, Blue Rock Bay, Frank Sound, the southern portion of East Sound, and the northern portion of East Sound (Fig. VI-1B). The southern portion and northern portion of East Sound are hereafter referred to as East Sound (South) and East Sound (North), respectively.

Four sets of vertical aerial photographs of Grand Cayman, in 9 x 9 inch format, were used in this study, namely:

(1) black-and-white aerial photographs, scale 1: 12,500, taken in 1971,

(2) black-and-white near-infrared aerial photographs, scale 1: 10,000, taken in 1977,

(3) colour aerial photographs, scale 1: 50,000, taken in 1979, and

(4) colour aerial photographs, scale 1: 10,000, taken in 1985.

Colour and black-and-white negatives of the aerial photographs were reproduced in a 4 x 5 inch format. Colour negatives were reproduced using a Hasselblad camera and Kodak Vericolor II Prof. type L (6013) film; black-and-white negatives were reproduced using a 4 x 5 inch Sinar copy camera and Ektapan Kodak 4 x 5 film.

In general, by visual examination, the quality of aerial photograph of the study areas are good and free of cloud and sun reflections which can potentially alter the surface characteristics. Colour aerial photographs show a greater contrast between features than black-and-white aerial photographs. There was no difficulty, however, in locating the study areas and determining general lagoon outlines on the aerial photographs. The clarity of water in the lagoons allows the depiction of features below the water surface in depths over 20 m (Lepley, 1968; Rigby and Roberts, 1976).

The vertical aerial photograph is normally subjected to scale distortion as a result of any tilt in the aircraft at time of photography or to radial displacement due to relief. However, the scale distortion as a result of radial displacement may be considered to be minimal due to the general lack of relief of Grand Cayman.

There are several ideas about the scale of aerial photograph needed for the study of coastal areas. For example, Kelly and Conrad (1969) found advantages from photography at a scale of 1: 50,000; Harris and Umbach (1972) suggested an optimum scale of 1:15,000 for stereomapping of the ocean bed in a reef area; Hopley (1978) found that a scale of about 1:25,000 has the most consistent advantages in mapping morphological features in the Great Barrier Reef. The scales used in this study range from 1:10,000 to 1:50,000, falling within the range which has been suggested by several workers.

E. METHODS

The classification of substrate and biologic communities and the measurement of an area occupied by each community, as it appeared on aerial photographs, was carried out by means of image-analysis techniques in conjunction with field investigations. Two image-analysis techniques were used in this study, namely density-slicing and automatic-image-analysis techniques. Operating procedures were kept as constant as possible throughout the study in order to minimize operator error.

Density-slicing technique

Logically, the density-slicing technique partitions the lagoonal area into a few equidensity regions, each of which represents a different type of surface material. Only the negatives of aerial photographs were used as an input image and were analysed as follows:

(1) For each negative, all areas not including in the analysis were shaded black to reduce the effect of nonuniform illumination and to separate the lagoon from background which has a similar photographic tone. Due to the irregular outline of the lagoon, the rigid fixed and adjustable masks supplied with the equipment cannot be used to frame the input image effectively. Thus, additional preparation was needed and special masking procedures were used. A transparency was overlaid on the negative, so that all areas on the negative, except the lagoon, were blackened using Indian ink. The landward boundary of the lagoon was marked by the coast line while the seaward boundary was marked by the water break at the reef crest.

(2) The density slicer was calibrated using a density step wedge tablet. Throughout the study, the logarithmic amplifier (see Chapter 4) was set at 1.42 and *f* stop 2.8.

(3) The input image was placed at the centre of the light table, and the image was magnified approximately 4 times. All 32 density levels were used. The

maximum and minimum density of each input image were set by adjusting D_{max} and D_{min}. The density range (D_{max} - D_{min}) for each colour and black-and-white negative is consistent (1.2D and 0.75D, respectively).

(4) The area occupied by each colour was measured using the electronic planimeter. The computed areas were recalculated by taking into consideration all the errors that affect the area measurement, i.e. errors caused by the limitation of instrument and effects of halo error.

(5) Photographs were taken from the television monitor using Kodak Vericolor VR-G 100 at shutter speed of 1/2 of a second and *f* stop 5.6.

Automatic-image-analysis technique

Using the automatic-image-analysis system the aerial photographs were analysed as follows:

(1) Both aerial photographs and their negatives were used as an input image. The input image was prepared in essentially the same way as for the density-slicing technique.

(2) The input image, placed at the centre of the light table, was digitized and stored as "image 1". In order to minimize the variation of illumination across the input image, a white background image was used. The background image was digitized and stored as "image 2".

(3) The image resulting from the intersection of "image 1" and "image 2" was the image to be analysed. It was stored as "image 3". A high-pass filter was used to sharpen the appearance of "image 3". Gamma densities were used where they could improve the density contrast as the result of stretching the density ranges. The "image 3" was then segmented into different phases by using a grey-level histogram thresholding. Colours were assigned to

differentiate various communities. The area of each colour was measured from the binary image of each phase.

(4) Photographs were taken from television views using Kodak Vericolor VR-G 100 at shutter speed of one second and *f* stop 8.

Field work

Field work was conducted during February 12-22, 1987 and February 1-7, 1988. Ground observation data were collected to supplement the existing information of the area. Traverses and spot investigations were made using a small boat and by swimming (Figs. VI-3, VI-4, VI-5, and Plates VI-1). Substrate and biologic communities and their distribution were described. The tones of substrate and biologic communities were observed from the water surface and from a distance in order to assess changes in relative tone. Data from field investigations were used to verify the classification of aerial photograph maps. In addition, underwater photographs were taken to provide a permanent record of the actual distribution and field relationships of various communities.

F. COMPARISON OF THE TWO IMAGE ANALYSIS TECHNIQUES

After some experience with the work it was found that only black-and-white and colour aerial photographs can be used to delineate the substrates and biological communities. For black-and-white near-infrared aerial photographs, only the reflectance of the substrates in the very shallow water can be detected. This is because, in the near-infrared photographs, water acts almost like a perfect black body and absorbs virtually all incident energy (Drury, 1987). Therefore, the black-and-white near-infrared aerial photographs were not used in this study. The maps obtained from aerial photographs are hereafter referred to as aerial photograph maps. The quality of aerial photograph maps depends mainly on the quality of the original aerial photograph (input image).

Aerial photograph map obtained via density-slicing technique

The aerial photograph maps obtained by density-slicing technique were automatically divided into equidensity areas represented by 32 colours (Plates VI-1A, B, VI-2, VI-3). It was found that the same features on aerial photograph maps derived from different sets of aerial photographs, either from colour or black-and-white aerial photographs, are represented by the same levels of colours. This is because after the maximum and minimum densities of each aerial photograph were set at the extreme positions, the range of density was divided equally into 32 density levels and each level is represented by a unique colour in fixed order. Therefore, the minimum density area of each aerial photograph is represented by shades of yellow and the maximum density area is represented by shades of blue. The intermediate density levels are represented by shades of cyan, green, orange, magenta, violet, and red. In this way, the aerial photograph was systematically partitioned into subareas, and the comparison between different sets of aerial photograph maps of the same area can be made on the same basis.

Aerial photograph obtained via automatic-image-analysis technique

Since the grey-level histogram of aerial photograph maps (e.g. Plate VI-1C) does not show distinct peaks, the threshold selected by using the lowest point between peaks is not an appropriate method. The aerial photograph map was segmented by setting thresholds at the point where the binary image has some desired property (when compared to the original aerial photograph). It is difficult to segment the image (with certain) because of the complexity of grey tones in aerial photographs.

The aerial photograph map obtained by the density-slicing technique seems to provide more detailed information on the distribution of communities and substrates than the aerial photograph map obtained by automatic-image-analysis technique because the subtle grey tone can be delineated. Therefore, in the following, discussion will concentrate on the classification of the aerial photograph map obtained via density slicer.

PLATE VI-1

Aerial photograph map of biological communities and substrate of Frank Sound reproduced from colour aerial photograph (1985) using density-slicing technique.

Density levels and colour levels are indicated by numbers (e.g. 1C), where Y = yellow, C = cyan, G = green, O = orange, M = magenta, V = violet; numbers indicate relative shades of colour, 1 = very light, 2 = light, 3 = medium, 4 = dark. These density levels and colour levels were used to represent various communities on aerial photograph maps of Plates VI-2, VI-3, and Table VI-2.

Dash lines represent traverses of 1988 investigations. The white stripe indicates missing area between two sections of the map.

0
1 km
N

PLATE VI-2

Aerial photograph map of biological communities and substrate of:

(A) East Sound (North) reproduced from colour aerial photograph (1979) using density-slicing technique.

(B) East Sound (South) reproduced from black-and-white aerial photograph (1971) using density-slicing technique.

(C) South Sound reproduced from colour aerial photograph (1985) using automatic image analyzer.

For legend of colours see Plate VI-1 and Table VI-2.

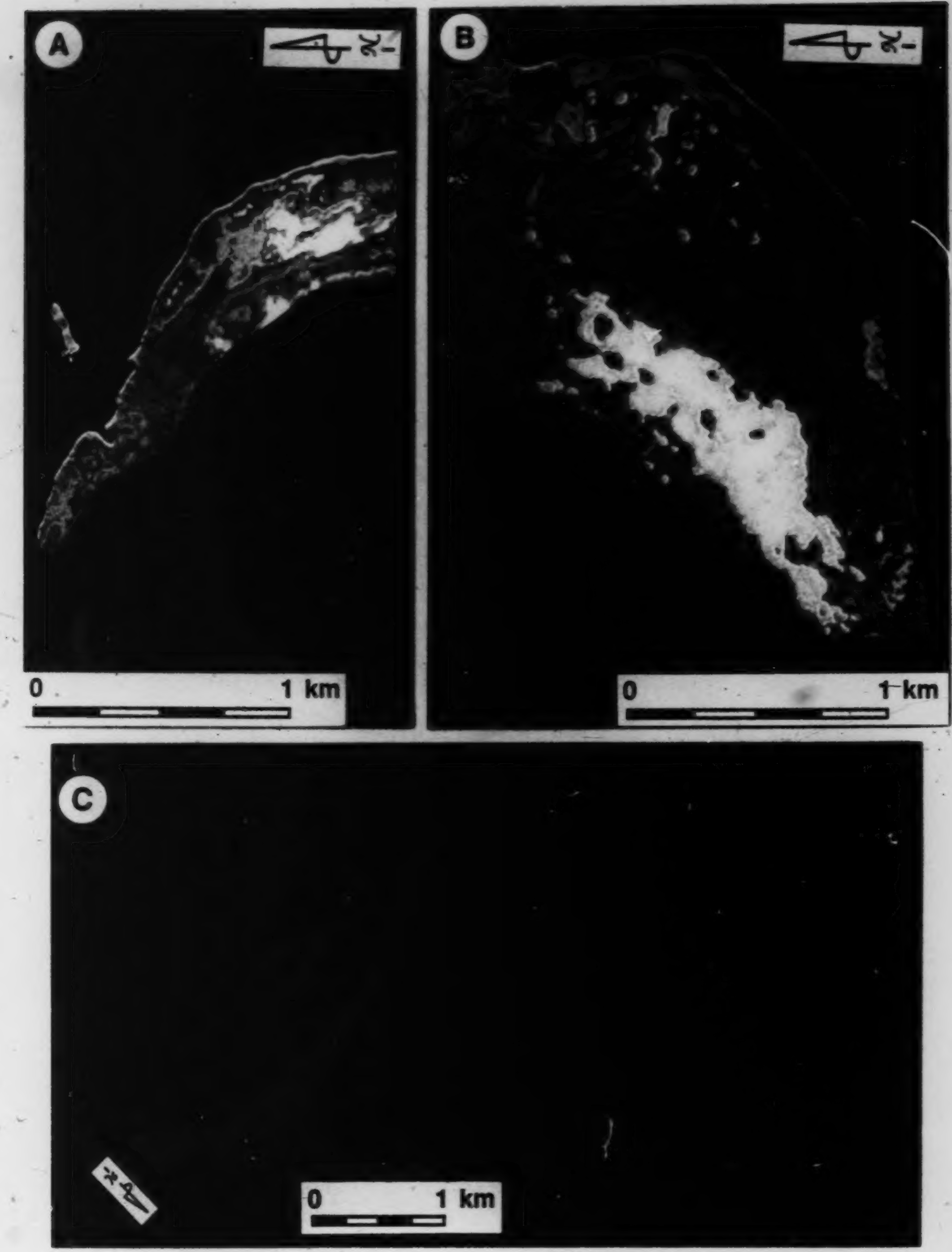
A
0
1 km
B
0
1 km
C
0
1 km

PLATE VI-3

Aerial photograph map of biological communities and substrate of:

(A) South Sound reproduced from colour aerial photograph (1985) using density-slicing technique. Note the series of blowout (b) and patches of *Thalassia* (p).

(B) Blue Rock Bay reproduced from colour aerial photograph (1985) using density-slicing technique.

For legend of colour see Plate VI-1 and Table VI-2.

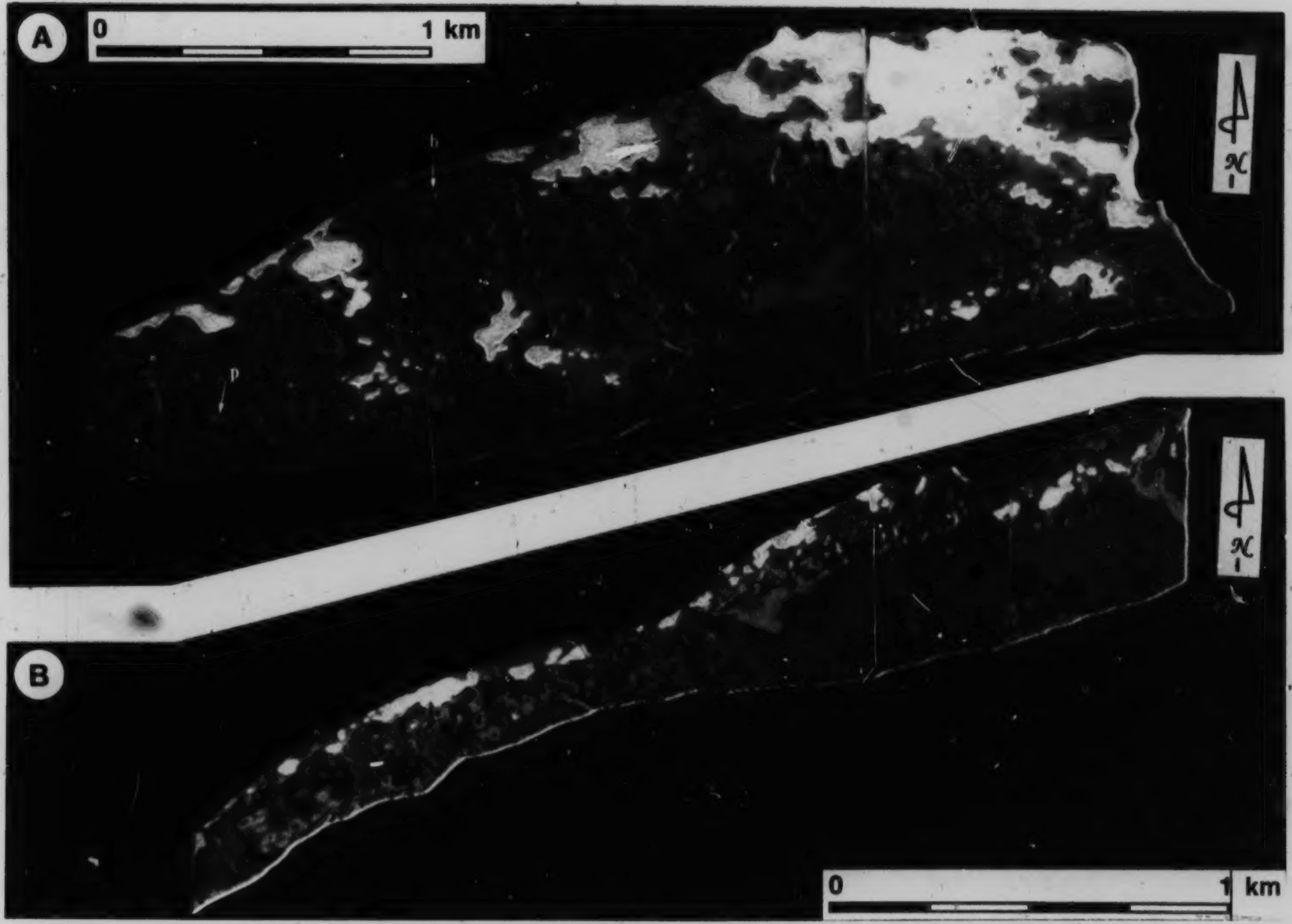
A
0
1 km
N
b
p
B
0
1 km
N

G. CLASSIFICATION OF AERIAL PHOTOGRAPH MAPS

One of the objectives of the study was to assign the various colour(s) to the corresponding community. This was achieved by: (1) comparing the spatial distribution of colour(s) with the spatial distribution of each community on published maps, (2) considering the grey-level histograms derived from an aerial photograph map, (3) examining information from aerial photographs documented by Rigby and Roberts (1976), and (4) considering information derived from field investigations.

Classification of the aerial photograph map was done in two stages. The primary classification was based on data from published maps, grey-level histograms of the aerial photograph map, and information from aerial photographs documented by Rigby and Roberts (1976). Second, the data obtained from field investigations were used to verify the primary classification. The relative tonal differences between different surface materials, not absolute tone, was used in classification since the absolute tones of the same features vary among the different sets of aerial photographs.

Primary classification of aerial photograph maps

The published maps used to provide basic geologic information were obtained from substrate and community distribution maps of offshore Grand Cayman developed by Rigby and Roberts (1976). Those published maps (Figs. VI-3, VI-4, and VI-5) were constructed on the basis of information obtained from aerial photographs, sample traverses, and spot investigations (Rigby and Roberts, 1976). It is assumed, in the study, that those maps represented the substrate and biologic community distribution in 1967, since much of the investigation was done in that year (Rigby and Roberts, 1976).

The bottom communities in the lagoons which have been delineated on the published maps of South Sound, Blue Rock Bay, East Sound (South) and East Sound (North) are: *Thalassia*, sand, *Montastrea annularis*, alcyonarian, gravel bed, and rock and

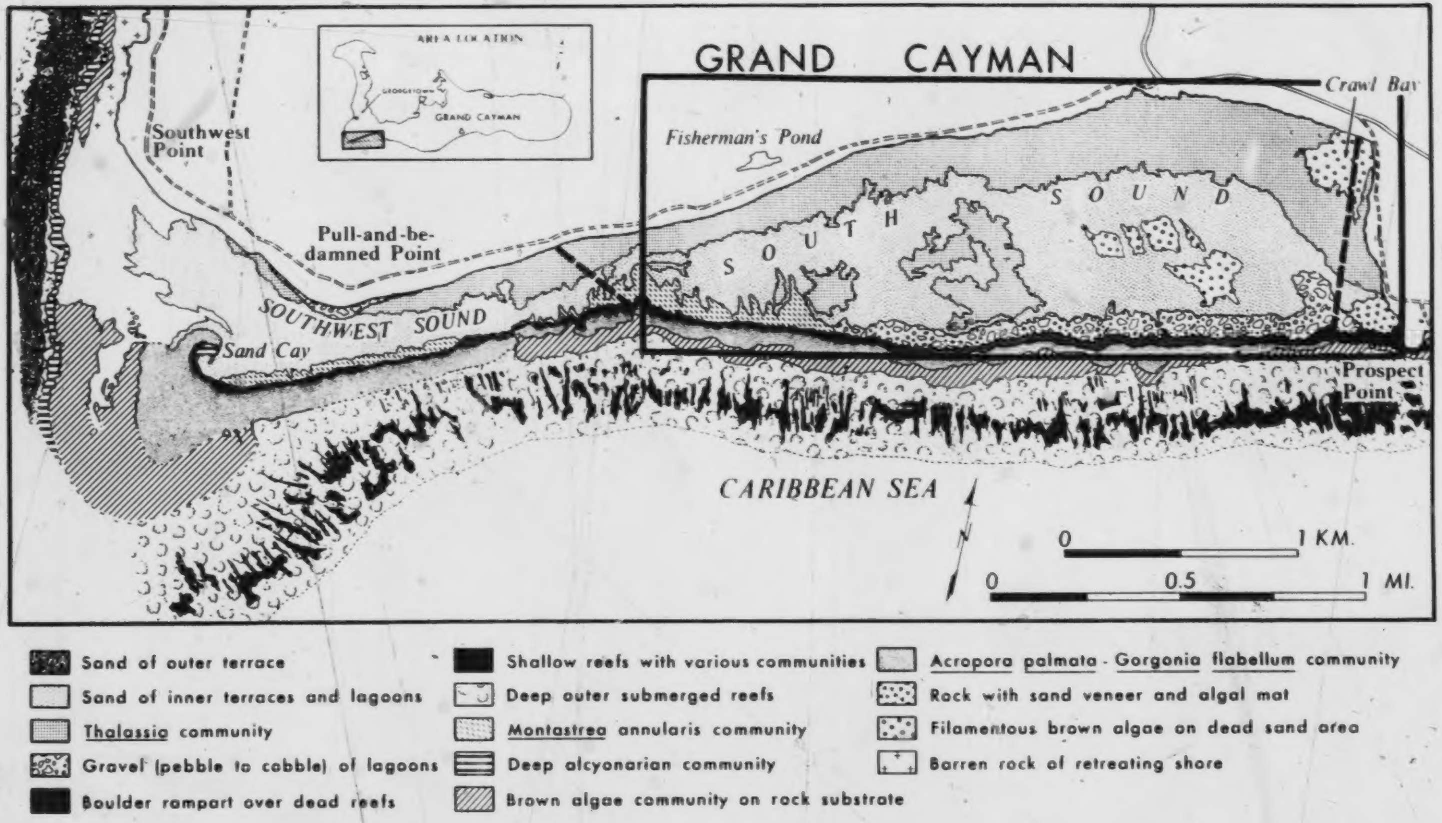
GRAND CAYMAN
AREA LOCATION
GEORGETOWN
GRAND CAYMAN
Southwest Point
Pull-and-be-damned Point
Fisherman's Pond
SOUTH SOUND
Crawl Bay
SOUTHWEST SOUND
Sand Cay
Prospect Point
CARIBBEAN SEA
0
1 KM.
0
0.5
1 MI.
Sand of outer terrace
Sand of inner terraces and lagoons
Thalassia community
Gravel (pebble to cobble) of lagoons
Boulder rampart over dead reefs
Shallow reefs with various communities
Deep outer submerged reefs
Montastrea annularis community
Deep alcyonarian community
Brown algae community on rock substrate
Acropora palmata - Gorgonia flabellum community
Rock with sand veneer and algal mat
Filamentous brown algae on dead sand area
Barren rock of retreating shore

Figure VI-3. Community and bottom-type maps of South Sound, Grand Cayman (modified after Rigby and Roberts, 1976). Area in square is considered in this study. The broken lines represent the traverses of 1988 investigation.

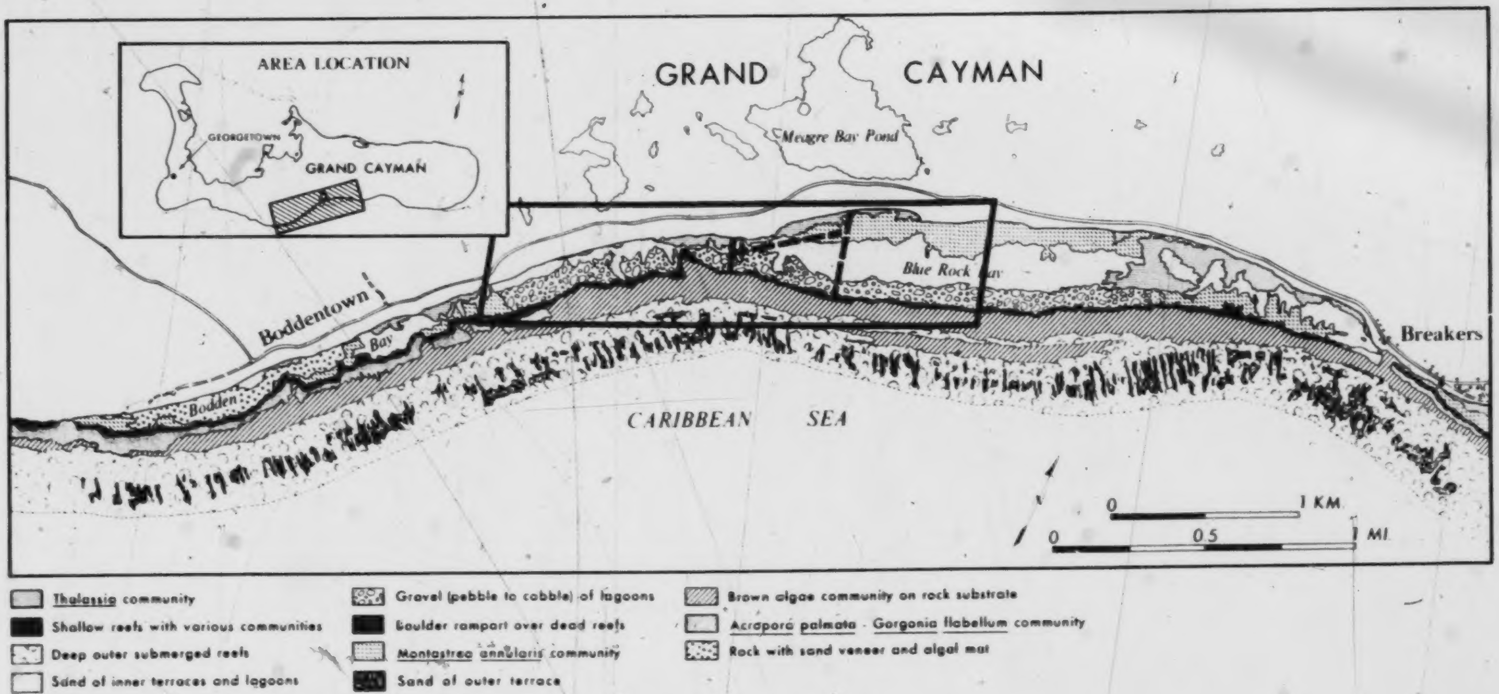
AREA LOCATION
GEORGETOWN
GRAND CAYMAN
GRAND CAYMAN
Meagre Bay Pond
Boddentown
Bay
Bodden
Blue Rock Bay
Breakers
CARIBBEAN SEA
0
1 KM
0
0.5
1 MI
Thalassia community
Shallow reefs with various communities
Deep outer submerged reefs
Sand of inner terraces and lagoons
Gravel (pebble to cobble) of lagoons
Boulder rampart over dead reefs
Montastrea annularis community
Sand of outer terrace
Brown algae community on rock substrate
Acropora palmata - Gorgonia flabellum community
Rock with sand veneer and algal mat

Figure VI-4. Community and bottom-type maps of Blue Rock Bay, Grand Cayman (modified after Rigby and Roberts, 1976). Area in square is considered in this study. The broken lines represent the traverses of 1988 investigation.

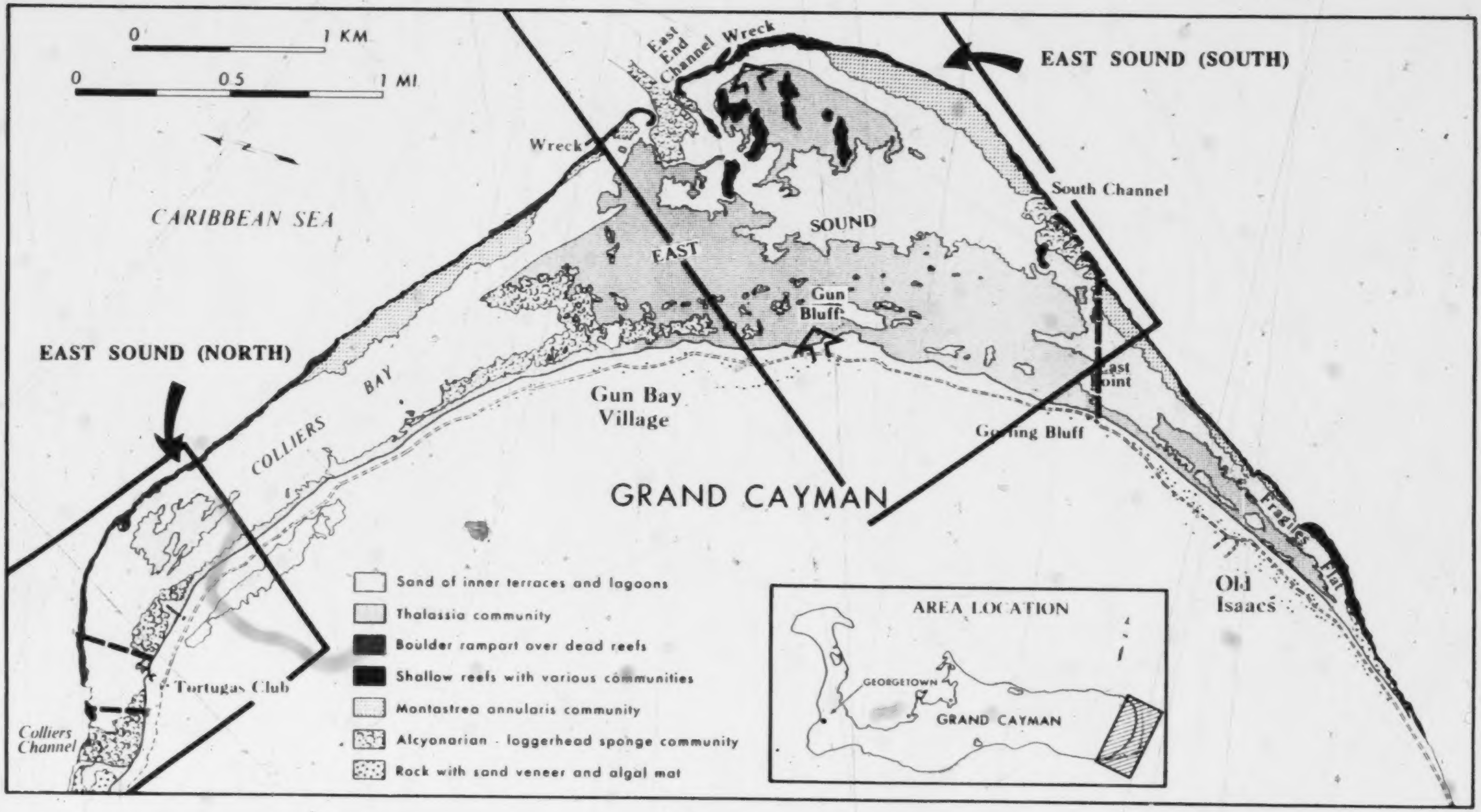
0 1 KM
0 0.5 1 MI
CARIBBEAN SEA
EAST SOUND (NORTH)
EAST SOUND (SOUTH)
Wreck
East End Channel
Wreck
South Channel
EAST
SOUND
Gun Bluff
East Point
Gun Bay Village
Gorling Bluff
COLLIERS
BAY
GRAND CAYMAN
Frazies Flat
Old Isaacs
Tortugas Club
Colliers Channel
Sand of inner terraces and lagoons
Thalassia community
Boulder rampart over dead reefs
Shallow reefs with various communities
Montastrea annularis community
Alcyonarian - loggerhead sponge community
Rock with sand veneer and algal mat
AREA LOCATION
GEORGETOWN
GRAND CAYMAN

Figure VI-5. Community and bottom-type maps of East Sound, Grand Cayman (modified after Rigby and Roberts, 1976). Area in square is considered in this study. The broken lines and arrows represent the traverses of 1988 investigations and spot investigations in 1987, respectively.

sand veneer with algal mat. The characteristics of each community are fully described by Rigby and Roberts (1976).

The grey-level histogram of the aerial photograph map is the plot of the density level versus the area corresponding to each density level. Generally, grey-level histograms of the aerial photograph map show four distinct peaks and a high density tail (Fig. VI-6). However, there are cases where the second peak does not exist because it merges with the third peak.

Based on information on spatial distribution of communities on the published maps and grey-level histogram, the *Thalassia* community can be easily delineated on the aerial photograph maps. This community is represented by areas with shades of yellow and cyan (density levels 1 to 8) which form the first peak of grey-level histogram. Most of the areal distribution of sand, shown on the published map, corresponds to areas with shades of orange and magenta, and violet (density levels 13 to 24) which form the third and fourth peaks of grey-level histogram.

The areas with shades of green (density levels 9 to 12) on the aerial photograph maps correspond to the distribution of various communities on the published maps. The areas of density level 9 corresponds to part of the sand. The areas of density level 10 corresponds to the *Montastrea annularis* and alcyonarian communities. Difficulty was encountered in delineating the areas of dark green (density levels 11 and 12) which correspond to part of the sand and gravel beds. The minor components, e.g. rock and sand veneer with algal mat, cannot be delineated on the aerial photograph map.

Verification of primary classification of aerial photograph map

Additional ground data obtained from field investigations were used to verify the primary classification of aerial photograph maps. Relative tonal differences between communities can be delineated from studying the water surfaces. Generally, *Thalassia* gives rise to dark grey-green colours while barren sand has a distinctive light cream colour.

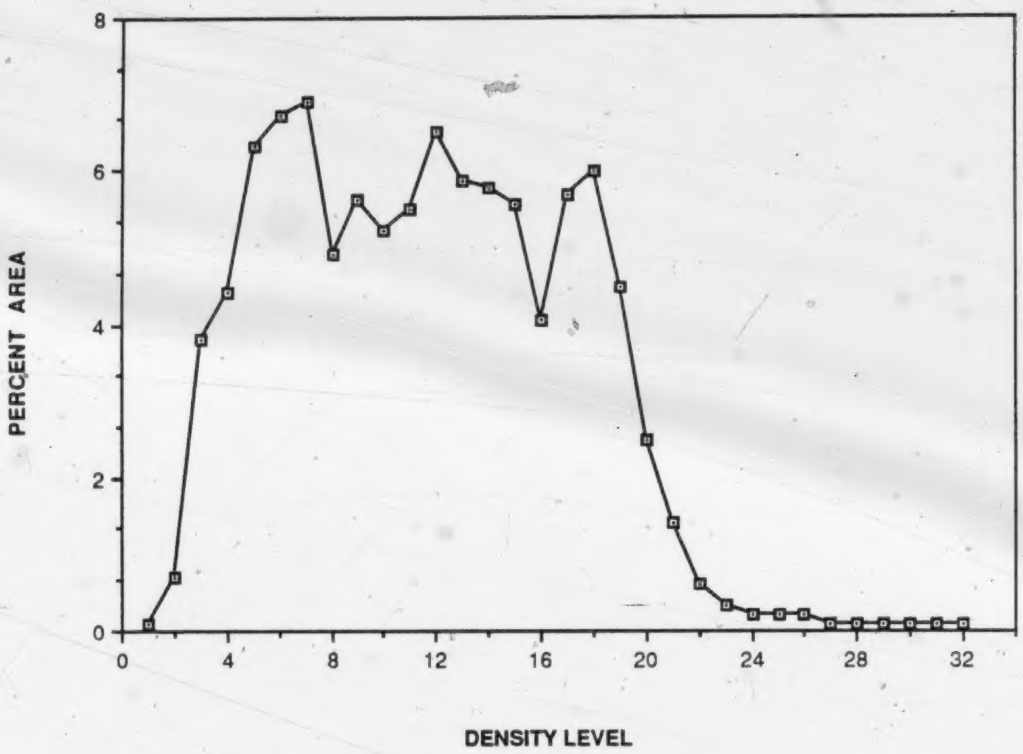

Figure VI-6. Grey level histogram of aerial photograph map of East Sound (South).

The areas covered with dense brown algae show as light brown, in contrast to the dark grey-green of *Thalassia* and the light colour of sand. The variation in tone exhibited by the variety of corals, including gorgonians, is subtle; colours vary from shades of greenish brown to yellowish brown. Water depth has an effect on the tone of substrate communities because both the intensity and spectral quality of the transmitted light vary with depth as a result of scattering and absorption by water molecules and by dissolved and suspended material (Holmes, 1957; Jerlov, 1966; Prieur and Sathyendranath, 1981; Sathyendranath and Morel, 1983). The same community occurring in deep water seems to have a darker tone than in shallow water. In reality, the tone of each community is far more complex. For example, although an area of *Thalassia* may be dark overall it is not of uniform tone. The variation in the tone of the *Thalassia* community reflects variation in the density of plant cover, the amount of epibionts on the leaves and sediment mounds created by marine organisms, such as the burrowing shrimp, *Callianassa* (Plate VI-4). Despite this, the overall signature of each community can be identified and the information used to distinguish one community from another. Based on the appearance and changes in relative tone observed from the water surface, bottom communities were categorized into: (1) *Thalassia* community, (2) coral community, (3) brown algae community, (4) sand, and (5) transition zone.

Thalassia community: The *Thalassia* community is dominated by the flat-bladed grass, *Thalassia testudinum*, associated algae such as *Penicillus*, *Avrainvillea*, *Halimeda*, *Udotea*, *Caulerpa*, and the manatee grass, *Syringodium filiformi*. The *Thalassia* community can be subdivided into: (1) areas with a dense cover of grass and relatively few algae (Plate VI-4A), and (2) areas having a less dense cover of grass but with more numerous algae and manatee grass (Plate VI-4C).

Coral community: The coral community (Plate VI-5) consists of various corals such as *Acropora palmata*, *A. cervicornis*, *Montastrea annularis*, *Diploria strigosa*, *D. clivosa*, *Agaricia agaricites*, *Porites porites*, and *P. astreoides*. This community also includes the soft coral gorgonians.

Brown algae community: The brown algae community represents two different surface areas, namely rubble flat and rock floor. The rubble flat area (Plate VI-6, VI-7) consists of sand, boulder- and cobble-sized pieces of corals (e.g. *Diploria strigosa*, *Montastrea annularis*, *M.cavernosa*, and *Acropora palmata*) which are loose or bound by encrusting algae into a solid structure. Corals fragments have been bored and encrusted by calcareous red algae, the foraminifera, *Homotrema rubrum*, serpulids, and bryozoa. Brown algae, e.g. *Padina*, are common, but green algae are sparse. The abundance of brown algae gives the rubble zone an overall brown appearance. Topographically, the rubble flat slopes gently shoreward from the reef crest in shallow water areas.

Inside the lagoons, the brown algae community represents the exposed rock floor and/or a thin veneer of sand (Plates. VI-8A, B). In general, the rock floor is covered with abundant short-brown algae with rare green algae and *Thalassia*. Corals, such as *Siderastrea* and *Diploria*, also occur, but only as small heads, a few centimetres in diameter (Plate VI-8A).

Sand: The sand flat is composed mainly of skeletal debris resulting from biological and mechanical destruction of the reef community and the disintegration of calcareous algae such as *Halimeda*. In general, the loose, moving, ripple-marked sand seems to be barren (Plate VI-8C, D).

Transition zone: This is the area of sand with calcareous green algae and a sparse growth of seagrasses along with green algae (Plate VI-9B, C, D, and E).

The tone of the bottom communities observed in the field may be ranked in decreasing darkness as follows: *Thalassia*, transition zone, corals, brown algae communities and barren sand. The changes of relative tone on the negative of aerial photograph are the inverse of those observed in the field. Therefore, the lightest area on

PLATE VI-4

(A) Dense growth of *Thalassia* community with epibionts on leaves in East Sound (North). Field of view is approximately 60 cm. Photo by I. G. Hunter.

(B) Typical growth of *Thalassia* community in shallow water (less than 30 cm deep), short leaves with brownish green colour with less epibionts on leaves. The photograph was taken from Blue Rock Bay. Field of view is approximately 2 m. Photo by B. Jones.

(C) Intergrowth of *Thalassia* and various algae (e.g. *Halimeda* (h)), in East Sound (South). Field of view is approximately 50 cm. Photo by B. Jones.

(D) Less dense growth of *Thalassia* in shallow water in Blue Rock Bay. Field of view is approximately 1 m. Photo by B. Jones.

(E) *Callianassa* mounded sand (c) associated with *Thalassia* beds from East Sound. Field of view is approximately 60 cm. Photo by R. W. MacDonald.

(F) *Acropora palmata* (a) associated with *Thalassia* beds in Blue Rock Bay. Field of view is approximately 2 m. Photo by I. G. Hunter.

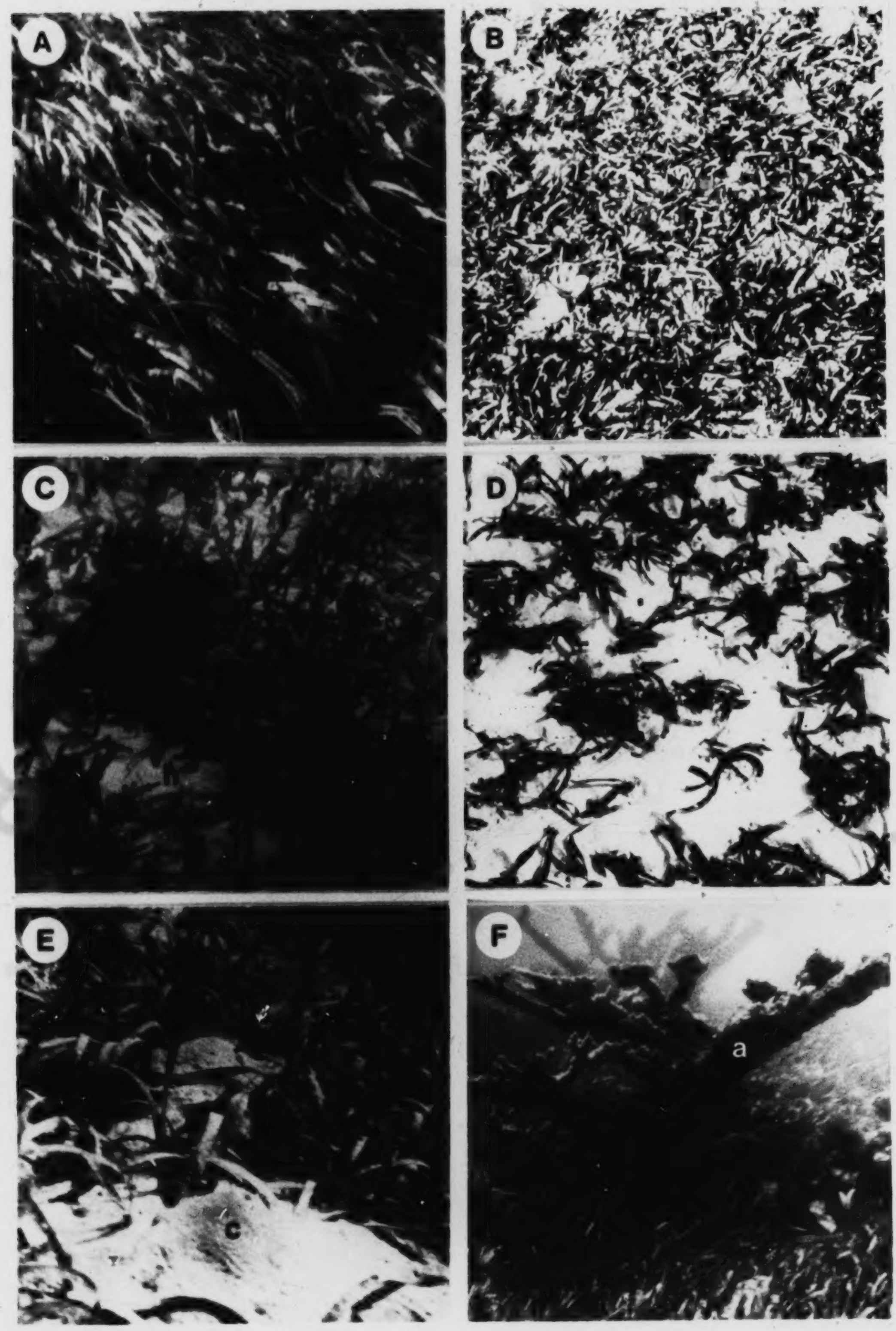
A
B
C
D
E
c
F
a

PLATE VI-5

(A) Isolated head of *Montastrea annularis* in sandy area in East Sound (South). Field of view is approximately 3 m. Photo by B. Jones.

(B) Patch reefs consisting of *Montastrea annularis* and gorgonians in South Sound. Field of view is approximately 2 m. Photo by B. Jones.

(C) Patch reefs of dense growth of gorgonians and seafans in shallow water in Frank Sound. Gorgonians are the dominant and most visible elements. Field of view is approximately 2 m. Photo by B. Jones.

(D) Gorgonians and seafans in the rocky floor in Frank Sound. Field of view is approximately 2 m. Photo by B. Jones.

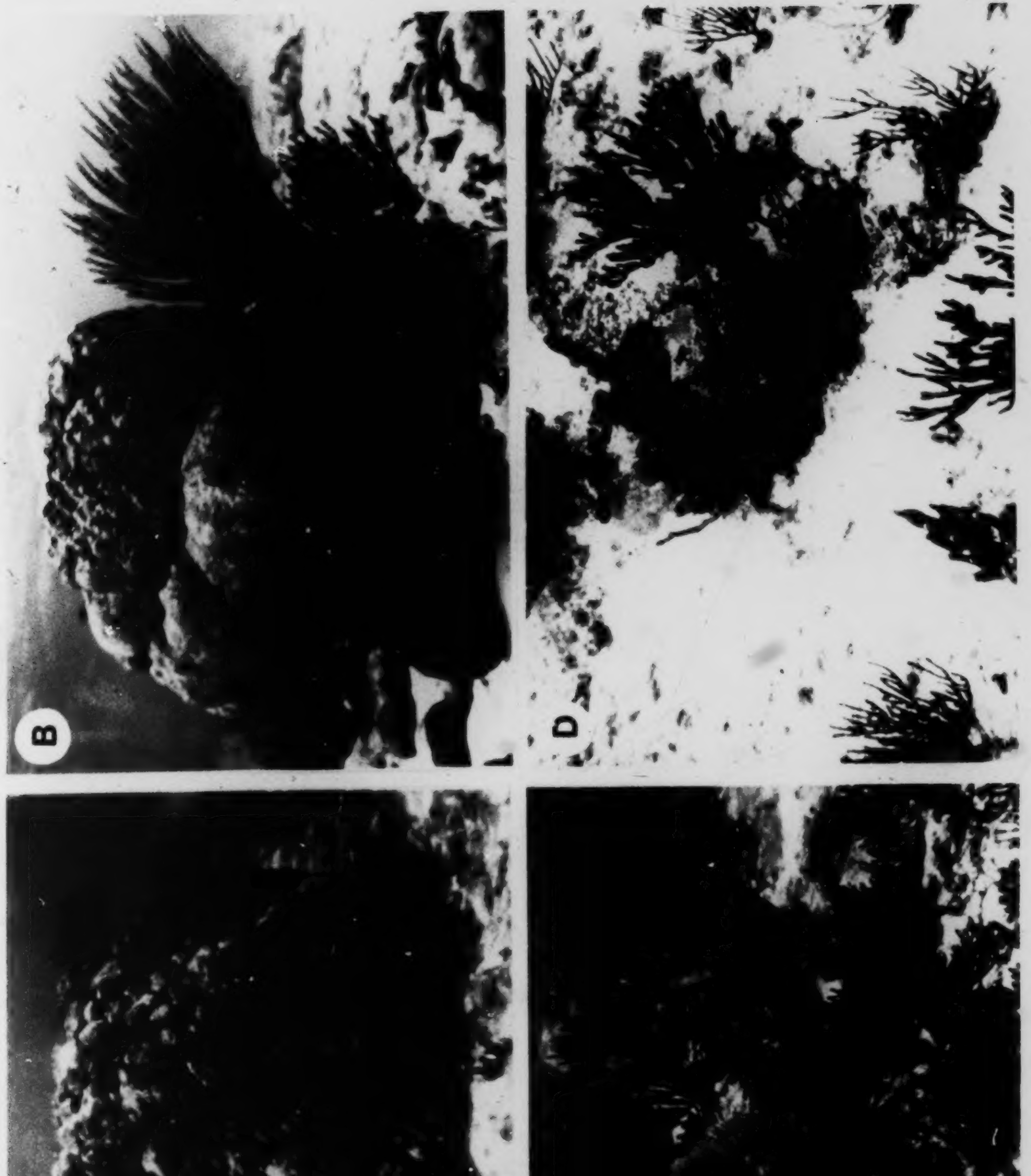
A
B
C
D

PLATE VI-6

(A) Rubble flat behind reef crest in East Sound (South) comprised of boulder- and cobble-sized coral fragments covered with brown algae. Field of view is approximately 3 m. Photo by B. Jones.

(B) Rubble flat and sand behind reef crest in East Sound (South). Field of view is approximately 3 m. Photo by B. Jones.

(C) Rocky floor with thin sand veneer covered with brown algae, *Montastrea annularis* (m) and gorgonians. Field of view is approximately 2.5 m. Photo by B. Jones.

(D) Rocky floor with brown algae at Tortuga Club, East Sound (North). Field of view is approximately 1.5 m. Photo by B. Jones.

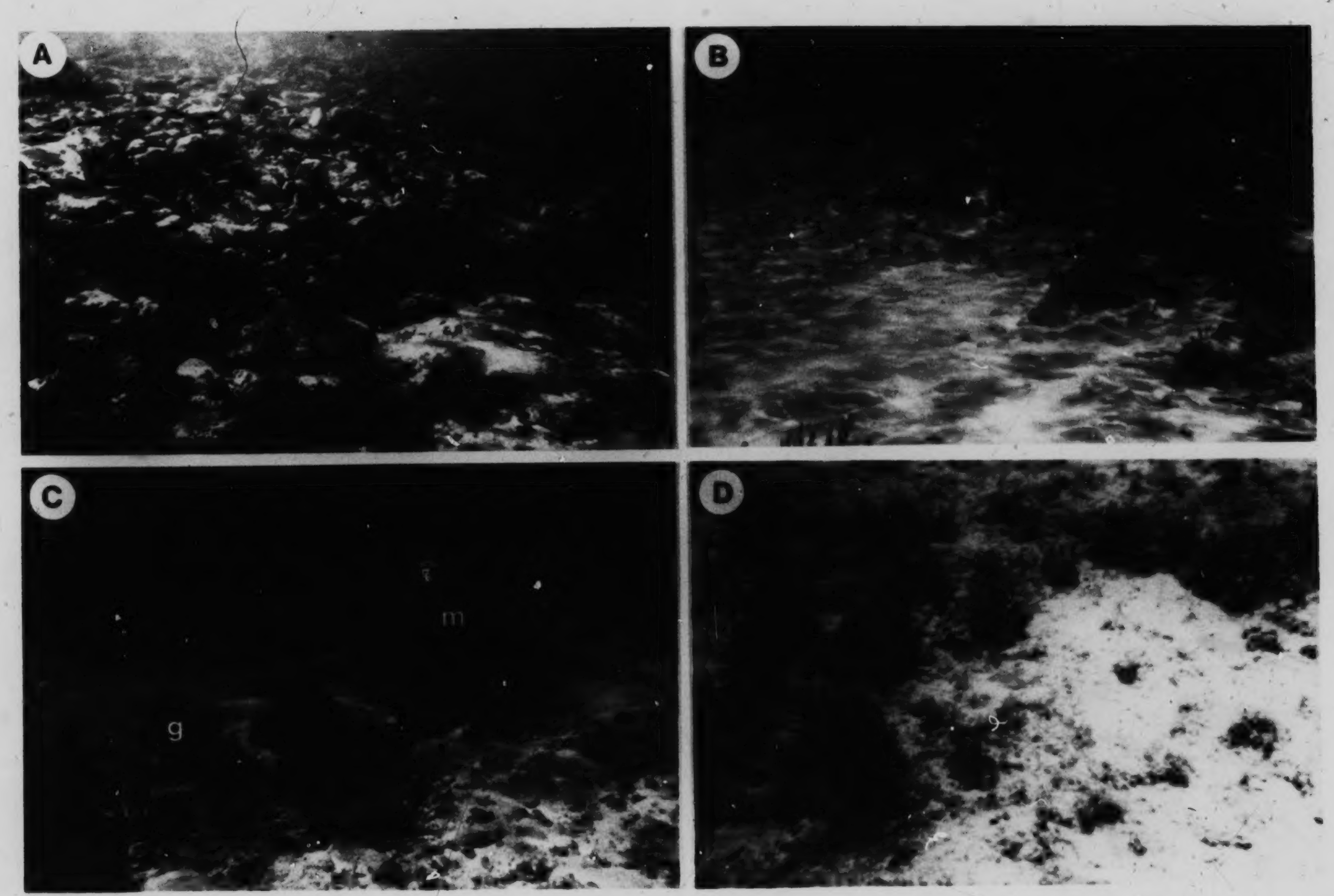
A
B
C
D
m
g

PLATE VI-7

(A) Gravel beds behind boulder-based barrier consisting of coral fragments encrusted by calcareous red algae, foraminifera, serpulids. Brown algae are abundant. Field of view is approximately 1.5 m. The photograph was taken from Blue Rock Bay by B. Jones.

(B) Sheet of coarse sand with brown algae behind reef crest in East Sound (South). Field of view is approximately 1 m. Photo by B. Jones.

(C) Sand and coral fragments (cf) with variety of algae, e.g. *Halimeda* (h) and brown algae in Blue Rock Bay. Small heads of coral are also present, e.g. *Siderastrea radians* (s). Field of view is approximately 3 m. Photo by I. G. Hunter.

(D) Rocky floor with algae, *Halimeda* (h), *Padina* (pa), in Blue Rock Bay. Field of view is approximately 3 m. Photo by B. Jones.

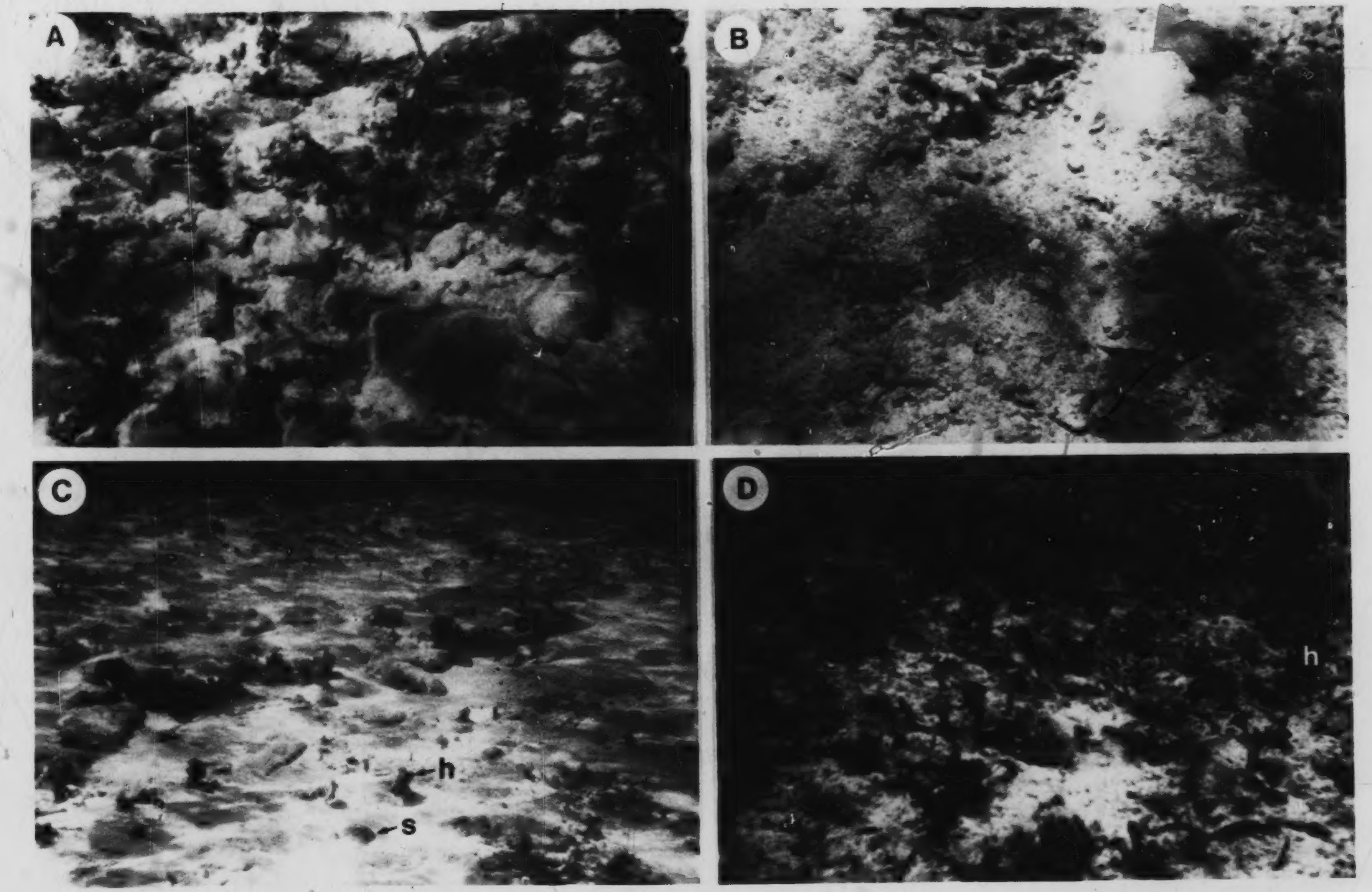
A
B
C
h
s
D
h

PLATE VI-8

(A) Exposed rock floor and thin veneer of sand covered with short brown algae and small coral heads, *Siderastrea* (s), east of Tortuga Club, East Sound (North). Field of view is approximately 1 m. Photo by I. G. Hunter.

(B) Brown algae on sand from East Sound (North). Field of view is approximately 1.5 m. Photo by I. G. Hunter.

(C) Rippled barren sand in Blue Rock Bay. Field of view is approximately 1.5 m. Photo by I. G. Hunter.

(D) Sand with a few algae, *Udotea* (u), and sea urchin, *Tripneustes ventricosus*, in Blue Rock Bay. Field of view is approximately 1 m. Photo by I. G. Hunter.

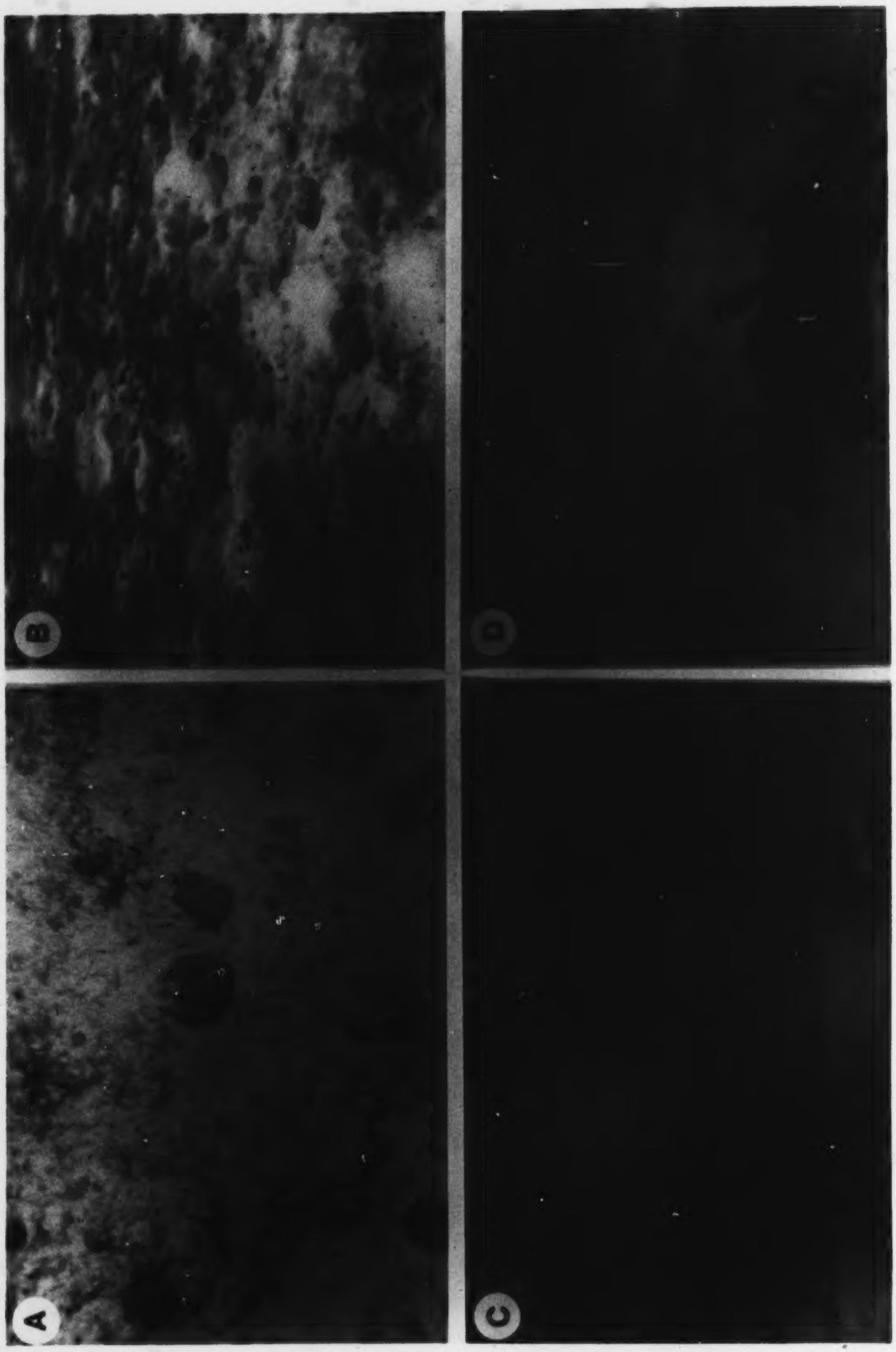
A
B
C
D

PLATE VI-9

(A) Sharp boundary between *Thalassia* community and sand. This is a typical boundary seen in East Sound (North) where the wave energy is relatively strong. Field of view is approximately 1 m. Photo by I. G. Hunter.

(B) Manatee grass, *Syringodium filiformi,* represent pioneer colonization on the rippled sand substrate. Field of view is approximately 50 cm. The photograph was taken from east of Tortuga Club, East Sound (North). Photo by I. G. Hunter.

(C) Sparse growth of *Thalassia* with oncolite (o) in Blue Rock Bay. White colour on *Thalassia* leaves are epibionts. Field of view is approximately 30 cm. Photo by B. Jones.

(D) Variety of algae, e.g. *Halimeda* (h), brown algae (b), grow in sandy area in front of *Thalassia* beds in Blue Rock Bay. Field of view is approximately 30 cm. Photo by B. Jones.

(E) *Caulerpa* (c) algae in sandy area of transition zone in East Sound (South). Field of view is approximately 1 m. Photo by I. G. Hunter.

(F) Typical view of sediments and organisms in blowout. Sediments are sand and cobble-sized coral fragments. Brown algae, *Padina* (pa), are abundant along with some *Penicillus* (p). Field of view is approximately 40 cm. Photo by B. Jones.

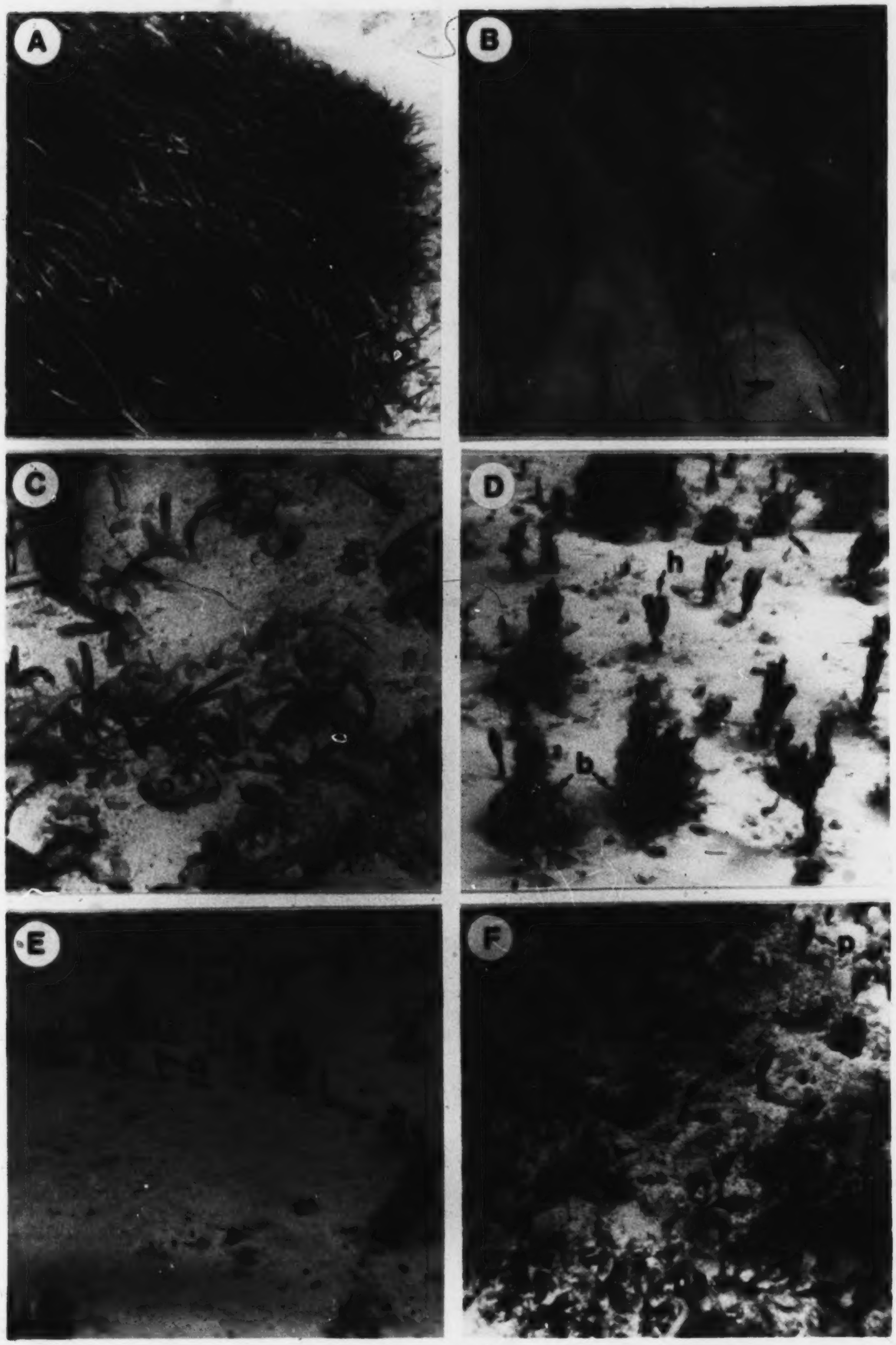
A
B
C
D
h
b
E
F
p

the aerial photograph map represents the *Thalassia*; and then, the transition zone, the corals, the brown algae, and the barren sand, in increasing darkness.

Based on the study of all information obtained from spatial distribution of communities on published maps, interpreted aerial photographs, and field investigations, the appropriate colours were assigned to the corresponding community. Of those 32 levels, levels 1-4 were assigned to the dense *Thalassia* community, 5 to 8 to the less dense *Thalassia*, 9 to the area of transition zone, 10 to the corals, 11 to 12 to the brown algae covered surfaces, 13 to 24 to the barren sand, 25-32 (in some cases 22-32) to the edge artifact caused by halo error (Table VI-2).

H. ACCURACY ASSESSMENT

The accuracy of aerial photograph maps is commonly assessed by selecting a sample of points from the map and comparing the map classification with some verification data, e.g. ground truth or a published map. In this study, the published maps of Rigby and Roberts (1976) were used as reference data. The 1979 aerial photograph map (Plate VI-1A) of East Sound (North) was selected for testing mapping accuracy for a number of reasons.

First, there was a time lapse between the published map (representing data from 1967) and the aerial photograph maps (representing data from 1971, 1979, and 1985) so it was necessary to select the area in which minimal changes in community distribution had occurred. The *Thalassia* community was used as the indicator of change because: (1) *Thalassia* community is the most distinct and easiest community to identify, and (2) this community seems to be more sensitive to changes in environment than other communities. For example, Moore and Robert (*in* Moore, 1963) could not find any trace of *Thalassia* at a number of localities along the East Coast of Florida as recorded in 1960. The consistent presence of *Thalassia* in East Sound (North) through time (1967 to 1985) suggests that there were only minimal environmental changes in that area (Tables VI-3 and VI-4).

Table VI-2. Summary of the detection of community categories from aerial photograph maps by means of density-slicing technique.

Category	Tone	Density level	Colour density
dense *Thalassia*	light	1 to 4	1Y, 2Y, 3Y, 4Y
less dense *Thalassia*	light	5 to 8	1C, 2C, 3C, 4C
Transition zone	light	9	1G
Corals	medium	10	2G
Brown algae	medium	11 to 12	3G, 4G
Sand	dark	13 to 24	1O, 2O, 3O, 4O 1M, 2M, 3M, 4M 1V, 2V, 3V, 4V
Halo error	-	25 to 36	1R, 2R, 3R, 4R 1B, 2B, 3B, 4B

Note: Y = yellow, C = cyan, G = green, O = orange, M = magenta, V = violet R = red, B = blue. Numbers indicate relative shades of colour; 1 = very light, 2 = light, 3 = medium, 4 = dark. (see also Plate VI-1).

Table VI-3. Summary of the distribution of biologic communities and substrate in term of percent area with respect to the total area of each locality and the actual area (in hectare, ha).

Location	Community	1971		1979		1985	
		Area (%)	Area (ha)	Area %	Area (ha)	Area (%)	Area (ha)
South Sound (Total area = 24 000 ha)	Dense *Thalassia*	8.3	199	8.7	209	12.5	300
	Less dense *Thalassia*	29.9	717	30.3	727	32.6	782
	Transition zone	6.9	166	4.4	106	5.0	120
	Sand	36.0	864	38.1	914	30.3	727
	Corals	7.0	168	5.7	137	5.7	137
	Brown algae	11.9	286	12.8	307	13.9	334
Blue Rock Bay (Total area = 9000 ha)	Dense *Thalassia*	2.9	26	2.5	23	3.5	31
	Less Dense *Thalassia*	8.6	77	11.9	107	12.3	111
	Transition zone	6.4	58	5.6	50	5.0	45
	Sand	48.3	435	51.7	465	46.5	418
	Corals	9.7	87	5.2	47	7.3	66
	Brown algae	24.1	217	23.1	208	25.4	229
East Sound (South) (Total area = 32 000 ha)	Dense *Thalassia*	15.9	509	17.3	554	no data	no data
	Less dense *Thalassia*	18.7	598	21.0	672	no data	no data
	Transition zone	4.9	157	5.4	173	no data	no data
	Sand	42.7	1366	39.3	1258	no data	no data
	Corals	5.6	179	6.6	211	no data	no data
	Brown algae	12.2	390	10.4	333	no data	no data
East Sound (North) (Total area = 8000 ha)	Dense *Thalassia*	5.2	42	5.6	45	5.6	45
	Less dense *Thalassia*	8.4	67	10.1	81	9.3	74
	Transition zone	2.4	19	4.2	34	2.7	22
	Sand	70.5	564	66.4	531	66.2	530
	Corals	3.7	30	4.1	33	4.1	33
	Brown algae	9.8	78	9.6	77	12.1	97

Table VI-4. Summary of the distribution of various communities (in percent) in East Sound (North) as shown in published map (Figs. VI-3, VI-4, and VI-5) by Rigby and Roberts (1976). The area of each community was obtained via the digitized-graphic-tablet technique.

Community	South Sound	Blue Rock Bay	East Sound (South)	East Sound (North)	Frank Sound
Thalassia	35.1	7.7	50.4	14.1	no data
Sand	47.8	34.0	35.9	67.5	no data
Montastrea	2.6	20.1	6.7	-	no data
Alcyonarian	-	-	4.4	15.8	no data
Gravel	8.1	38.2	-	-	no data
Reefs*	-	-	2.6	-	no data
Brown algae	5.6	-	-	-	no data
Rock with sand veneer	0.8	-	-	2.6	no data

*Shallow reefs with various communities

Table VI-5. Summary of modified data on the percent of biologic communities and substrate of East Sound (North).

Community	Data from this study (1979 aerial photograph map)	Data from Rigby and Roberts (1976)
Thalassia	15.7	14.1
Sand	70.6	67.5
Corals	4.1	15.8
Brown algae	9.6	2.6

Second, it has been suggested that the scale of aerial photographs affects the resolution of the image (e.g. Avery, 1977; Paine, 1981). The smaller the scale, the more difficult and less certain is the interpretation. The 1979 aerial photograph map (Plate VI-2A) was compared with the published map (Fig. VI-5) in order to determine if small scale aerial photograph could give reasonable results.

The major communities that have been delineated on published map (Fig. VI-5) can be differentiated on aerial photograph maps (Plate VI-2A). Since the data on the published maps and those obtained in this study were collected under different basis, those data were rearranged in the similar manner (Table VI-5). For data obtained in this study, the transition zone was grouped with the sand. For data obtained by Rigby and Roberts (1976), the coral and alcyonarian communities were grouped together. Rock and sand veneer and the algal mat of Rigby and Roberts (1976) is equivalent to the brown algae community in this study.

Sampling techniques

Generally, simple random and stratified random sampling (see Chapter 5) have been considered as the appropriate technique of sampling ground data (Rudd, 1971; Zonneveld, 1974; van Genderen and Lock, 1976, 1977; Hathout and Forrest, 1980; Fitzpatrick-Lins, 1981; Paine, 1981). In this study, the systematic sampling technique was used for convenience. This sampling technique can be expected to be about as precise as the stratified random sampling with one unit per stratum (Cochran, 1963).

Since the binomial distribution has been considered the most appropriate mathematical model for map accuracy estimation (Ginevan, 1979; Rosenfield, 1982) the required sample size for a desired error was calculated, in this study, using the formula for the normal distribution approximation to the binomial distribution

$$n = \frac{pq}{E^2} z^2_{(1-\alpha/2)}$$

(also see Chapter 5).

In order to compute the sample size (n), the values of p, q, E, and $z_{(1-\alpha/2)}$ must be specified. The percentage area of *Thalassia* was used to specify p, and q represents the percentage area of communities other than *Thalassia*. If the maximum allowable error in estimating the area of *Thalassia* is ±5% of the total area and the 95% confidence interval was used, then, E is 5 and $z_{(1-\alpha/2)} = 1.96$. Based on these figures ($p = 15$, $q = 85$, $E = 5$, $z_{(1-\alpha/2)} = 1.96$), the number of sampling points for East Sound (North) should be at least 196. In this study, 251 sample points were selected on a grid spacing of 60 m. The grid system was placed identically on the aerial photograph map and the published map. The sample points were taken at the grid intersection, and the substrate at each point was identified.

Results

The accuracy of aerial photograph maps is normally expressed by the statement of the percentage of the map area that has been correctly classified when compared with reference data. The accuracy test results are presented in tabular form (Table VI-6) which shows the number of points correctly and incorrectly identified. The major diagonal indicates the agreements between the reference data (represented by the columns of the matrix) and the classified data (represented by the rows of the matrix). The overall accuracy for an aerial photograph map is calculated by dividing the sum of the entries that form the major diagonal (i.e. the number of correct classification) by the total number of samples taken. The overall accuracy, however, does not indicate how the accuracy is distributed across the individual category. Two major concerns about aerial photograph maps are: (1) how well the area can be mapped, and (2) the accuracy of information the map can provide. Several researchers (e.g. Ginevan, 1979; Aronoff, 1982; Story and

Table VI-6. A map accuracy error matrix.

		Number of sample points by community category identified from published map (Rigby and Roberts, 1976)				
		Thalassia	Sand	Coral	Sand and algal mat	Row total
Number of sample points by community category identified from aerial photograph map (1979)	*Thalassia*	49	3	2	-	54
	Sand	3	154	5	1	163
	Coral	-	-	18	-	18
	Sand and algal mat	-	-	10	6	16
	Column total	52	157	35	7	251

Note: Sum of the major diagonal = 227
Overall accuracy = (227/251) x 100 = 90%

Producer's accuracy
Thalassia = (49/52) x 100 = 94%
Sand = (154/157) x 100 = 98%
Coral = (18/35) x 100 = 51%
Sand & algal mat = (6/7) x 100 = 86%

User's accuracy
Thalassia = 49/54 = 91%
Sand = (154/163) x 100 = 94%
Coral = (18/18) x 100 = 100%
Sand & algal mat = (6/16) x 100 = 38%

Congalton, 1986) refer to the accuracy which describes how well the area can be mapped as "producer's accuracy" and the accuracy which describes the accuracy of information the map can provide as a "user's accuracy".

The producer's accuracy is determined by dividing the number of correctly classified samples of category X by the total number of samples classified as category X in the reference data, i.e. column total for category X. The resulting percentage of producer's accuracy obtained by this method indicates the probability that a reference sample will be correctly classified on the aerial photograph map.

The user's accuracy is determined by dividing the number of correctly classified samples in category X by the total number of samples classified as category X in the classified aerial photograph map (row total for category X). The resulting percentage accuracy is indicative of the probability that a sample from the classified aerial photograph map actually represents that category on the ground.

The overall map accuracy (Table VI-6) is 90% (24 out of 251 or approximately 10% of classified data were incorrectly identified). If the producer's accuracy is considered, the accuracies of classification of *Thalassia*, sand, coral, and brown algae are 94, 98, 51, and 86 percent, respectively. On the other hand, if the user's accuracy is considered, the accuracies of classification of *Thalassia*, sand, coral, and brown algae are 91, 94, 100, and 38 percent, respectively.

Both types of accuracies need to be considered because each set of figures represents an accuracy in different senses. The producer's accuracy indicates only the errors caused by omission of samples that have not been correctly classified as category X. On the other hand, the user's accuracy indicates errors caused by omission from the correct category and commission into another category. The user's accuracy may be referred as the reliability of the map (Congalton and Rekas, 1985). For example, the producer's accuracy for the coral classification is relatively low, 45 percent. Conversely, the probability that coral, which was identified on the aerial photograph as coral, actually is coral is 100 percent (as indicated by user's accuracy).

The overall accuracy fall within the limit of the permissible error rate in image interpretations, 85 to 90 percent, recommended by the U.S. Geological Survey Circular 671 (Anderson, 1971; Anderson *et al.*, 1972). This suggests that the classification of aerial photograph maps is acceptable and the small-scale aerial photograph (in this case 1: 50,000) can give relatively good results.

I. FACTORS AFFECTING CLASSIFICATION

Although the accuracy of classification (or mapping accuracy) is acceptable based on U. S. Geological Survey Circular 671, it is useful to consider the causes of discrepancy between the aerial photograph maps and the published maps. Based on the data obtained from field observations and from aerial photographs, there is evidence suggesting that the incorrect classification is subjected to a persistent bias. A number of reasons may account for the misclassification: (1) the limitation of conventional mapping techniques, (2) lack of contrast in tone between features on aerial photograph maps thus they cannot be distinguished , and (3) the difference in basic assumptions of the mapping techniques.

Limitation of conventional mapping technique

Rigby and Roberts (1976) noted that communities which are less than 20 m wide cannot be mapped using conventional techniques. This limitation may be used to explain the misclassification of corals to either sand or brown algae communities. Locally, the sandy area with coral heads and patch reefs were mapped as the *Montastrea* community by Rigby and Roberts (1976). This is because small features such as coral heads and patch reefs are not shown on the published map. On the other hand, the aerial photograph map permits detailed information which reveal the spatial characteristics of biologic communities and substrate. The smallest feature which can be shown is limited by the resolution of the aerial photograph used. For the scales of aerial photograph used in this study, more subtle differentiations can be discerned than is possible with conventional mapping techniques.

Lack of contrast in tone between different features

There is evidence in a few areas that part of the misclassification may stem from a reflection of the substrates. For example, the misclassification of brown algae on sandy area to *Thalassia* at the northeast corner of South Sound (Fig. VI-3, Plate VI-3) is due to lack of contrast in tone of those surfaces. From field observations, the sediments in this area, where mangrove swamp water from the interior of the island bathes the shore, comprise largely organic debris. It is the high organic content that makes the darker tone, making it impossible to distinguish from *Thalassia*. However, this is an exception since such areas cannot be located in other lagoons.

The misclassification of corals to *Thalassia* seems to occur in the area where corals are flourishing, e.g. immediately in front the channel. In such area, the tone of corals is dark and very similar to the tone created by *Thalassia*. Although these two communities can be distinguished on aerial photograph based on the texture, they are difficult to separate on the aerial photograph maps. This phenomena, however, occurs in only a few small areas. Familiarity with the area will enhance the qualitative interpretation.

The presence of suspension particles can also have an effect on the reflection of the substrate. For example, in the eastern portion of Frank Sound, where the amount of suspension particles is relatively high compared to the other lagoons, the reflection of the *Thalassia* community is the same as the one of the transition zone. This is because suspended sediments increase the reflectance of visible light from water (Robinson, 1985; Drury, 1987).

Basic assumption in mapping techniques

The basic assumption of aerial photograph maps is different from conventional maps. The aerial photograph map is constructed on the basis of reflectance of the surface material. For example, gravel beds as shown on published maps cannot be differentiated on the aerial photograph map. Those areas are identified as coral, sand, and brown algae communities on aerial photograph map. This is because the gravel bed consists of broken corals, which have been encrusted by encrusting organisms, e.g. calcareous red algae, foraminifera and others, with sand in the spaces between. In such areas, small clumps of brown algae are common. The abundance of these algae give the gravel bed on overall light brown appearance. Another example is the case where coral heads and patch reefs are covered by sand veneer. Those corals will be recorded as sand on aerial photograph maps.

J. DETECTION OF BOTTOM FEATURES

Several bottom features, which could not be shown on conventional maps, can be identified on aerial photograph maps. For example, the series of *Thalassia* banks and crescentic grass-free areas (called blowouts by Scoffin, 1970) can be distinguished. The general characteristics of *Thalassia* banks in the lagoons around Grand Cayman are similar to those described in other areas, e.g. in Florida (Wanless, 1981) and Barbados (Patriquin, 1975). That is, the landward edge is steep, with exposed rhizomes of *Thalassia* (Plate VI-10), while the seaward edge slopes gently (Fig. VI-7). Two or more blowouts are normally joined together, developing a cusp-like structure oriented parallel to shore (Plate VI-3). Jones (1988b) suggested that the origin of the *Thalassia* banks and the grass-free cusps is probably due to their occurrence close to shore in a shallow water environment that is dominated by wave activity. As waves encroach on the shoreline and break, they produce back eddies which serve to erode the front of the bank.

The blowout structure has been recognized on aerial photographs by several authors (e.g. Ball *et al*, 1967; Kelly and Conrod, 1969). However, with the aid of the density

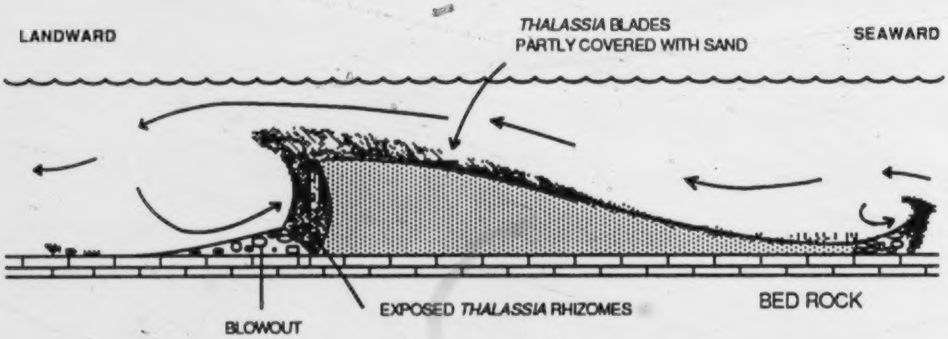
LANDWARD
THALASSIA BLADES PARTLY COVERED WITH SAND
SEAWARD
BLOWOUT
EXPOSED THALASSIA RHIZOMES
BED ROCK

Figure VI-8. Schematic diagram showing cross-section of *Thalassia* bank (modified after Scoffin, 1970).

PLATE VI-10

General view of *Thalassia* bank which is about 30 cm high and eroded rhizome mat of *Thalassia* on seaward side of a blowout (A). Note the characteristics of sediment in a blowout (B). Photo by B. Jones.

A

slicer, the zonation of organisms on the blowout can be delineated. The sediments found in blowouts are sand and cobble-sized coral fragments associated with dense brown algae and some green algae (Plates VI-9F, VI-10). The zone of brown algae (Plate VI-3A) is representd by dark green (3G and 4G), while the sediments are represented by light green (1G). The density of seagrasses in the *Thalassia* banks is represented by shades of cyan (1C to 4C, from dense to sparse density). The series of colours (cyan and green) in Plate VI-3A represent a series of blowout.

Another feature seen in the aerial photograph maps is the distribution of seagrasses patches (Plates VI-2 and VI-3A). Usually the patches are round to elongate, and grow in the back-reef area. These grass distributions are probably related in some way to the patterns of the currents in the area since the seagrasses normally colonize in the protected area.

The most remarkable features found on the aerial photograph map obtained by density slicing technique are the patterns and positions of biologic communities and substrate. For example, the distribution of the *Thalassia* beds and the exact positions of the beds in relation to the plant density can be determined. Although some of the dense *Thalassia* beds (represented by shades of yellow, 1Y to 4Y) are located in the middle portion of the lagoons, most of them are located close to shore. The pattern of distribution of communities and substrate, in turn, indicates the patterns of wave and current energies in the lagoons. The locations of blowouts seem to indicate the area of maximum wave action and erosion. The positions of brown algae and corals indicate the area of hard substrate. It appears that the aerial photograph map showed the distribution patterns and bottom features of biologic communities and substrate which may be difficult to delineate in the field.

K. DETECTION OF CHANGES IN COMMUNITIES THROUGH TIME

The changes in communities through time, 1971 to 1985, in South Sound, Blue Rock Bay, East Sound (South), and East Sound (North) were considered, based on the data in Table VI-3. Since the accuracy of the map is relatively high and the misclassification probably stemmed from a persistent bias, it is assumed that the percent of communities in Table VI-3 is not subject to error.

Generally, occurrences of minor communities such as brown algae, corals (except for 1979), and transition zones are relatively consistent in every lagoon during 1971 to 1985. The percentage of corals in Blue Rock Bay area decreased from approximately 10% in 1971 to approximately 5% in 1979. This observation is consistent with Rigby and Roberts (1976, p. 62), who noted that

> The small patch reefs in both Blue Rock Bay and Pease Bay appear unhealthy and not expanding, but merely surviving or slowly dying. Many heads are nearly sediment-covered from the turbid water, which is also warmer than that at the outer margin of the lagoon.

Changes of *Thalassia* community

Thalassia is the major community in the lagoons around Grand Cayman. In order to understand the distribution of *Thalassia* in the lagoons around Grand Cayman the conditions required for the establishment of *Thalassia* must be considered. The ecology and distribution of *Thalassia* is determined by factors such as water temperature, light penetration, turbidity, salinity, wave action, and thickness of soft sediment (Moore, 1963; Scoffin, 1970). *Thalassia* is widespread in shallow, clear, well-illuminated marine environments in tropical and subtropical climates. *Thalassia* can survive a wide range variation in temperature and salinity. Although *Thalassia* can tolerate temperatures from 20° to 36°C, there is a definite temperature optimum in the range of 28 to 30°C (Zieman, 1975a, 1975b). Roessler (1971) demonstrated that the production rate of *Thalassia* was affected, e.g. the leaves were killed off, where water temperatures were 3°C above the natural ambient. The salinity tolerances are between 25 to 40‰ (Moore, 1963). McRoy and McMillan (1977) tested the tolerance of seagrasses to salinity and found that *Thalassia* survived in salinities of up to 60‰.

Although *Thalassia* can grow on a variety of sediments, textural characteristics may partly control the density of growth. Bernatowicz (1952) showed that *Thalassia* in Bermuda grows in continuous meadows on muddy bottoms, but in patches on coarse sediment. While *Thalassia* in South Biscayne Bay, Florida was able to grow in sediment less than 1 cm deep, maximum growth density required a sediment in excess of 50 cm deep (Zieman, 1972). In Bimini Lagoon, Scoffin (1970) recorded no *Thalassia* growth in sediment less than 7 cm thick.

In general, the distribution of *Thalassia* in the lagoons along the south coast of Grand Cayman increased during 1971 to 1985 (Table VI-3). In East Sound (South) the percent of *Thalassia* increased from approximately 35% in 1971 to 38% in 1979. In Blue Rock Bay the percent of *Thalassia* increased from approximately 12% in 1971 to 14% in 1979, and 16% in 1985. This is consistent with Rigby and Roberts (1976) who recorded the expansion of *Thalassia* in this lagoon. In South Sound the percent of *Thalassia* increased from approximately 32% in 1971 to 39% in 1979, and to 45% in 1985. The results obtained from comparing aerial photograph maps (1971, 1979, and 1985) of South Sound, using systematic sampling techniques, indicated that the growth of *Thalassia* was evident in the northeastern portion of the lagoon, a low-energy area with thick sediment accumulations (Roberts *et al.*, 1975). The areas where *Thalassia* expanded are located along the marginal loose sand. In such areas, a sparse growth of *Thalassia* and manatee grass, associated with a variety of algae (Plate VI-9B to E), are observed. Some *Thalassia* has been removed in the western portion of the lagoon where the energy was high (Roberts *et al.*, 1975).

The physical conditions in the lagoons around Grand Cayman, e.g. temperature, salinity, water depth, seem to be favourable for *Thalassia* colonization and growth. Seasonal variation in the productivity of *Thalassia* in this area can be expected since the water temperature varies throughout the year (Table VI-1). The *Thalassia* community in lagoons around Grand Cayman grow in rather protected environments. The rocky zones and the shifting sand sheets do not support substantial *Thalassia* communities. The rocky areas do not have a sediment cover thick enough for the plants to take root. In areas where the sediment is thick, wave action seems to be the major factor that prevents wide-spread *Thalassia*. Tidal currents and wave action causes sediment shifting and creates an environment which is not conducive to *Thalassia* colonization and growth. These conditions are demonstrated in East Sound (North) where the boundary between *Thalassia* and sand is sharp (Plate VI-9A). However, a narrow transition zone is also present.

It has been suggested that circulation of water and sediment distribution in a fringing reef lagoon are determined by lagoon geometry and the input of water across the reef crest (Kohn and Helfrich, 1957; Inman *et al.*, 1963; Roberts *et al.*, 1975). East Sound (North) is relatively narrow and subjected to high energy whereas the wave energy in lagoons along the south shore are considerably lesser (Rigby and Roberts, 1976, Text-Figure 9). This may explain why the area of *Thalassia* increased in the lagoons along the south shore.

The increase of *Thalassia*, in particular between 1979-1985, may be partly due to the mass mortality of the sea urchin, *Diadema antillarum*, which was formerly abundant in lagoons around Grand Cayman (Rigby and Roberts, 1976; B. Jones, 1988 pers. comm.). The number of sea urchins has drastically decreased in the Caribbean Sea in 1983 (Lessios *et al.*, 1984; Bak, 1985; Hughes *et al.*, 1985; Carpenter, 1985, 1988; Hunte *et al.*, 1986). The *Diadema antillarum* were found to be responsible for the formation of bare halos in *Thalassia* beds around coral reefs (Ogden *et al.*, 1973).

Thalassia beds may not be affected by the tropical hurricanes. It has been reported that *Thalassia* beds were not noticeably damaged in several areas (Thomas *et al.*, 1961; Stoddart, 1963; Ball, 1967).

L. INTERRELATIONSHIP BETWEEN COMMUNITIES

Ecologically, there is a limited interrelationship between communities which grown on the hard substrate (e.g. brown algae and corals) and those which grow on soft substrate. Hartog (1977) showed that communities on soft mud, sand, coral rubble and solid rock all develop through a number of stages towards the final stage in the succession, the *Thalassia testudinum* community (Fig. VI-8). The relationship between communities present in lagoons around Grand Cayman was determined statistically using regression analysis (see Chapter 5). The results of linear regression analysis (Table VI-7, Fig. VI-9) indicated a strong negative relationship between sand and transition zone, sand and *Thalassia*, and sand and the combination of *Thalassia* and transition zone with correlation coefficients (r) of -0.70, -0.82, and -0.86, respectively. The correlation coefficients of *Thalassia* and transition zone (r = 0.32), brown algae and transition zone (r = 0.44), and *Thalassia* and brown algae (r = -0.44) are relatively low. Although the actual interrelationship between communities are far more complex, the statistical results support the idea of progressive development from sandy substrate to transition zone (or coralline algae in Fig. VI-7) to *Thalassia*. As the areas of transition zone and *Thalassia* increase the areas of sand decrease.

M. IMPLICATIONS OF CHANGES IN DISTRIBUTION OF *THALASSIA* COMMUNITY

The influence of *Thalassia* on sedimentation processes has been extensively documented by Ginsburg (1956), Ginsburg and Lowenstam (1958), Humm (1964), Scoffin (1970), Wanless (1981), and Almasi *et al.*, (1987). *Thalassia* alters the prevailing sedimentation processes in a variety of ways, but the major effects are to increase sedimentation rates, to preferentially concentrate finer particle sizes, and to stabilize deposited sediments. The efficiency of *Thalassia* in baffling the flow and promoting deposition of the fine suspended particles depends primarily upon the density of plant

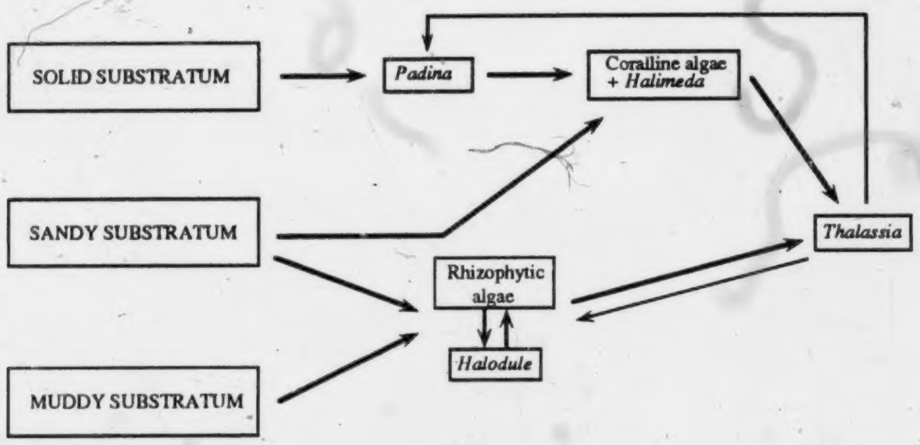
SOLID SUBSTRATUM
Padina
Coralline algae + Halimeda
SANDY SUBSTRATUM
Thalassia
Rhizophytic algae
Halodule
MUDDY SUBSTRATUM

Figure VI-8. Schematic diagram showing the succession series leading to the *Thalassia testudinum* community. Thick arrows indicate progressive developments; thin arrows indicate regressive developments (modified after Hartog, 1973 *in* Hartog, 1977).

Table VI-7. Summary of the results of regression analysis.

Variables	Correlation coefficient (r)
Thalassia and transition zone	0.32
Thalassia and brown algae	- 0.44
Transition zone and brown algae	0.44
Thalassia and sand	-0.82
Transition zone and sand	-0.70
Combination of *Thalassia* and transition zone and sand	-0.86

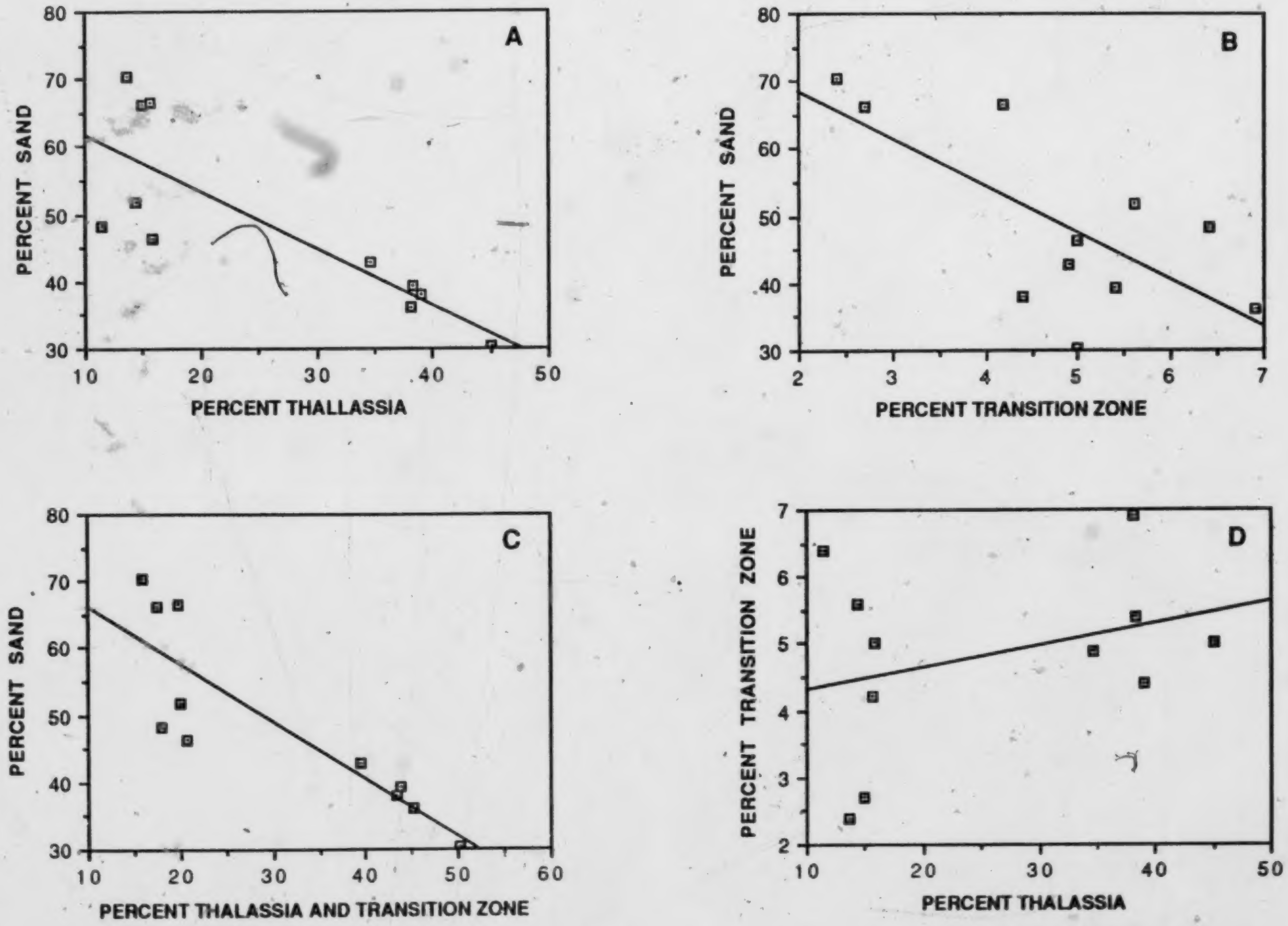

Figure VI-9. Graphs showing cross-plots between *Thalassia* and sand (A), transition zone and sand (B), combined *Thalassia* and transition zone and sand (C), and *Thalassia* and transition zone (D). The lines represent the linear regression. See Table VI-7 for correlation coefficients for each of the linear regressions.

growth (Wayne, 1974; Ward *et al.*, 1984). Lynts (1966) and Scoffin (1970) showed that the density of *Thalassia* growth has a significant effect on the ability of *Thalassia* beds to retain fine (< 62 µm) sediments. This increase in fine-grained sediment with increasing density of plant cover is related both to the increased efficiency of a bed to remove and retain fine sediments transported into it from surrounding areas by current flow and to the increase in the local production of fine sedimentary particles within the grass beds. Swinchatt (1965) and Lynts (1966) observed that changes in the texture of the sediments in a reef tract off Florida correlated well with the distribution of seagrasses. The building and binding of sediments by seagrasses may affect areas from a few square metres in area to mega-ripples to banks with areas of hundreds or even thousands of square metres (Ginsburg and Lowenstam, 1958) and thus result in reduction of water depth over the *Thalassia* banks.

The fining-upwards sedimentary sequences caused by the lateral seaward migration of blowouts (in other words the migration of *Thalassia* banks) has been recognized (Patriquin, 1975; Wanless, 1981). Wanless (1981) noted that the fining-upwards sequence is not a gradual shift in the grain size but rather a decrease in a coarse mode and increase in a fine mode.

Many workers (e.g. Humm, 1964; Stockman *et al.*, 1967) have noted that the emergent portions of *Thalassia* serve as an ideal substrate for carbonate secreting, encrusting coralline algae, and that this carbonate material is eventually added to the sediment. The first attempt to quantify the rate of production of mud-sized carbonate from epibionts on *Thalassia* blades was made by Land (1970), in Jamaica. He estimated rates of production of 180 g/m^2/yr. In Barbados, Patriquin (1972) estimated a production rate of 2800 g/m^2/yr. Neither study considered aerial variations nor seasonal variations in the growth rates of the seagrasses and epibionts. Nelsen and Ginsburg (1986) conducted a study in Florida Bay. They included aerial and seasonal variations in the abundance of grass and epibionts into consideration. The weighted average rate of accumulation from epibionts was estimated at 118 ± 44 g/m^2/yr. However, they stated that averaging the variations of standing crop at each station and the variations among all 58 stations could have produced an overestimate of abundance.

That type of study has never been conducted in the lagoons around Grand Cayman. It is obvious that further field observations are needed in order to pursue the study. The mapping technique described in this study can be used to construct the base map, thus improving the accuracy of the analysis.

L. SYNOPSIS

From the analysis of aerial photographs of lagoons around Grand Cayman, it may be concluded that:

(1) the analysis of colour and black-and-white aerial photographs, using density-slicing technique and field investigations, is useful for identifying the biologic communities and substrate in the lagoons,

(2) these aerial photograph maps permit detailed qualitative and quantitative information which reveal the spatial and temporal characteristics of biologic communities and substrate with the overall accuracy of 90%,

(3) the misclassification of aerial photograph maps (compared to published maps) stems from limitations in mapping techniques, lack of contrast in tone between different features, and differences in assumptions of mapping techniques,

(4) several bottom features such as *Thalassia* banks and blowouts can be identified on aerial photograph maps,

(5) the results of the study of changes in the distribution of biological communities and substrate through time suggest that there was a noticeable increase in *Thalassia* and a decrease in sand in the lagoons along the south coast during 1971 to 1985,

(6) the results from statistical analysis of interrelationships between communities support the succession development patterns of biologic communities and substrate proposed by Hartog (1977), and

(7) the mapping technique described in this study can be used to improve the accuracy of the quantitative analysis on the rate of carbonate sedimentation in the lagoons.

VII. APPLICATION OF IMAGE ANALYSIS TO SIZE MEASUREMENT

A. INTRODUCTION

Size is one of the basic descriptive measures of a particle. Size, defined by the American Society for Testing Materials, is the dimension which best characterizes the state of subdivision (ASTM designation E-20-51T, 1952). Size analysis usually involves considerations of: (1) the technique for measuring size, and (2) the analysis of data. Particle size can be measured by several techniques and expressed in various ways. Pettijohn (1975) stated that size may be expressed as volume, weight, surface area, cross-sectional area, setting velocity, and intercepts through particles or projections. The choice of technique is governed by many factors, such as the purpose of the study, the range of size of particle to be measured, and the nature of the sample (for example, the degree of consolidation). In order to analyse data statistically a large sample size is needed. Time and operator fatigue usually limits the number of particles that can be measured. However, if certain levels of accuracy are to be achieved size measurement must be continued until those requirements are satisfied.

The use of image analysis in size analysis is described by reference to two specific applications, each representing a particular problem. The first application is the analysis of the size of borings in Devonian stromatoporoid heads and the second application is the analysis of the size of vermetid gastropods. The aim of the experiment is to investigate the most appropriate method for measuring the size of features composed of nonuniform tones.

B. APPLICATION - I: SIZE ANALYSIS OF *TRYPANITES WEISEI* IN THE DEVONIAN STROMATOPOROIDS

As an example of how the image analysis may be applied to size analysis of features with nonuniform tones, the borings, *Trypanites weisei*, in Devonian stromatoporoid heads are considered. For each thin section there was: (1) an assessment of boring size, (2) an estimate of the percent of the area that is bored, (3) determination of the orientation of the borings, and (4) determination of the orientation of the geopetal structures in the borings. In order to evaluate the validity of image-analysis techniques in size analysis, results obtained in this study were compared with analyses done by conventional techniques (Pemberton *et al.*, 1988).

Materials

Three stromatoporoid heads (X, Y and Z) with *Trypanites weisei* from the Late Devonian Waterways Formation were serially sectioned into vertical slices at approximately 1 cm intervals. Five thin sections, A, F, G, H, and D, were cut from head X, started from the periphery towards the center of the head. Thin sections B, I, J, K, L, and E were cut from head Y in the same manner as those thin sections from head X. Only one thin section (C) came from head Z. In total, twelve oversized thin sections (7.5 x 5 cm) and their negative photographs, printed in a 20 x 25 cm format, were made. These were used for measuring the size of the borings and the orientation of the geopetal structures in the boring.

The stromatoporoids contain well preserved *Trypanites weisei* (Plate. VII-1) which are elongate, narrow, parallel-sided, straight to gently curved, and circular to semi-circular in cross-section (Pemberton *et al.*, 1988). The borings are filled with light-coloured micrite, dark-coloured micrite, skeletal fragments, dolomite, non-ferroan calcite, and ferroan calcite (Pemberton *et al.*, 1988). The complex spatial distribution of the material in the borings cause variation of tone in each boring. There is a lack of contrast in tone between the material filling the borings and the host stromatoporoids. A detailed study of the stromatoporoid heads and their borings has been published by Pemberton *et al.* (1988).

PLATE VII-1

Negative photograph of thin section A showing the distribution of *Trypanites weisei* in the stage I growth of *Clathrocoilona inconstans* (Cl) and the stage II growth of *Trupetostroma papulosum* (Tp). The borings were truncated along the erosion surface (es). The orientation of the laminated micrite (m), which filled depressions that developed following growth increments of *C. inconstans*, is used as a datum line for measuring orientation of geopetal structures (from Pemberton *et al.*, 1988, Figure 1).

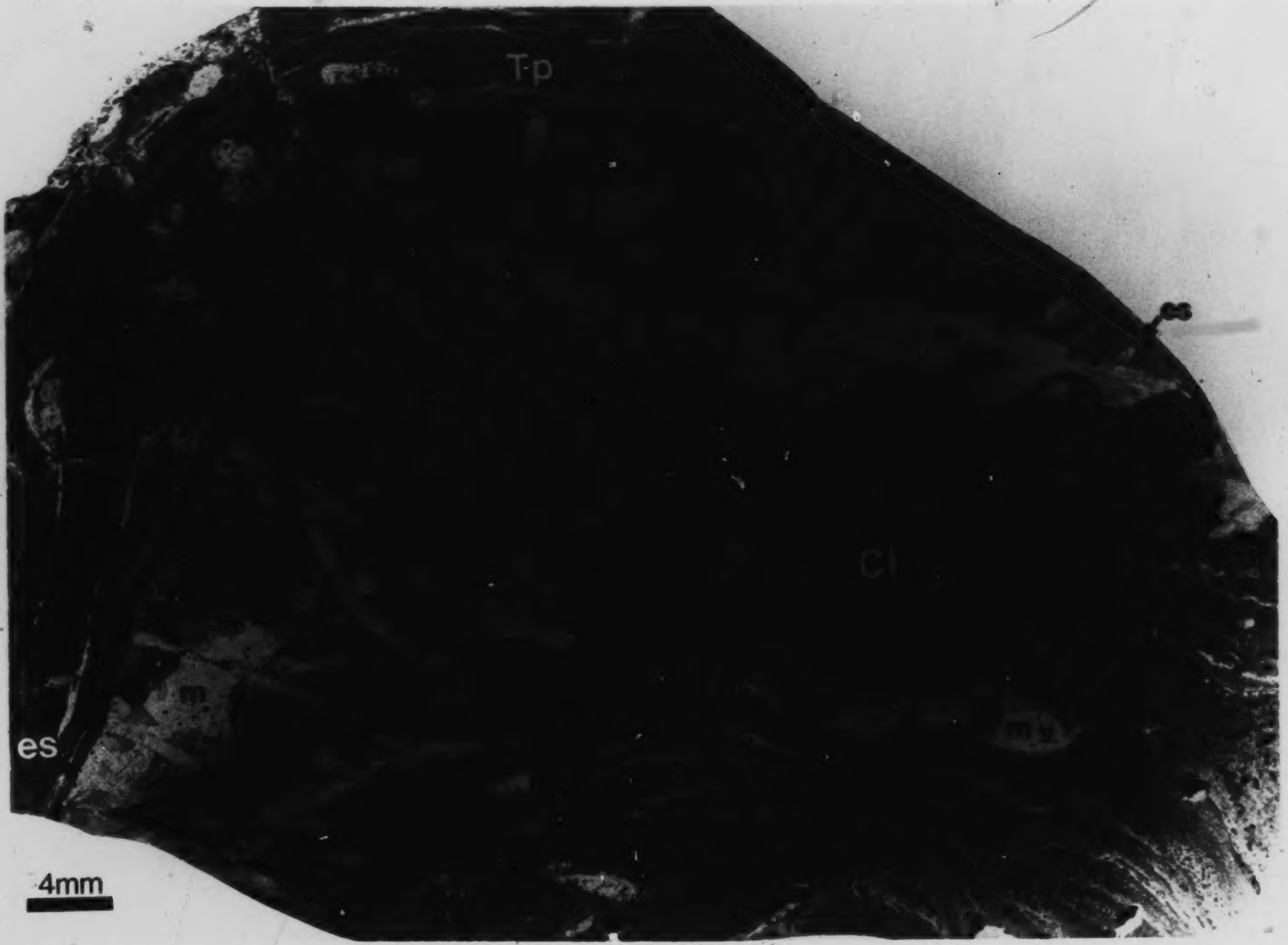
Tp
Cl
my
m
es
4mm

Geometry of borings

In longitudinal section, the borings generally taper towards the base (Plate. VII-1). For simplicity, it is assumed, following Pemberton *et al.* (1980, 1988), that the boring is essentially a cylinder with a hemispherical cap at one end.

In thin section, the cross-sectional profiles of the borings range from circular to elliptical, dependent on the angle of the section plane (Fig. VII-1). The length of the boring cannot be determined from the cross-sectional profiles unless the profile of boring was cut parallel to the axis of the cylinder (Fig.VII-1F).

The diameter (*d*) of the boring is, however, preserved in all cross-sectional views which cut through the axis of the cylinder (e.g. section A to D), except for sections which are entirely from the cap region (e.g. section E). Section E gives diameter, *d'*, which is smaller than *d*. However, the cap region is relatively small compared to the whole boring. Therefore, providing the sample size is large, the distribution of *d* should represent the distribution of the diameters of boring.

Methods used in study of trace fossils

Laboratory techniques for studying trace fossils in lithified and unlithified sediments, as summarized by Ekdale *et al.* (1984), include X-ray radiography, infrared photography, ultraviolet photography, staining, modified Bushinsky oil technique, and casting techniques. Each technique, which has its own advantages and disadvantages (Table VII-1), is useful for a particular type of material and task. Most of the techniques, however, are mainly used for enhancing the biogenic structure while some techniques provide three-dimensional structures of trace fossils.

Measurements of the size and shape of the borings are made in order to quantitatively describe the morphology. The size of trace fossil is usually obtained by simple manual measurement methods (using caliper, micrometer, or ruler) and it is usually recorded in terms of length and width (e.g. Kobluk and Nemcsok, 1982; Nield, 1984;

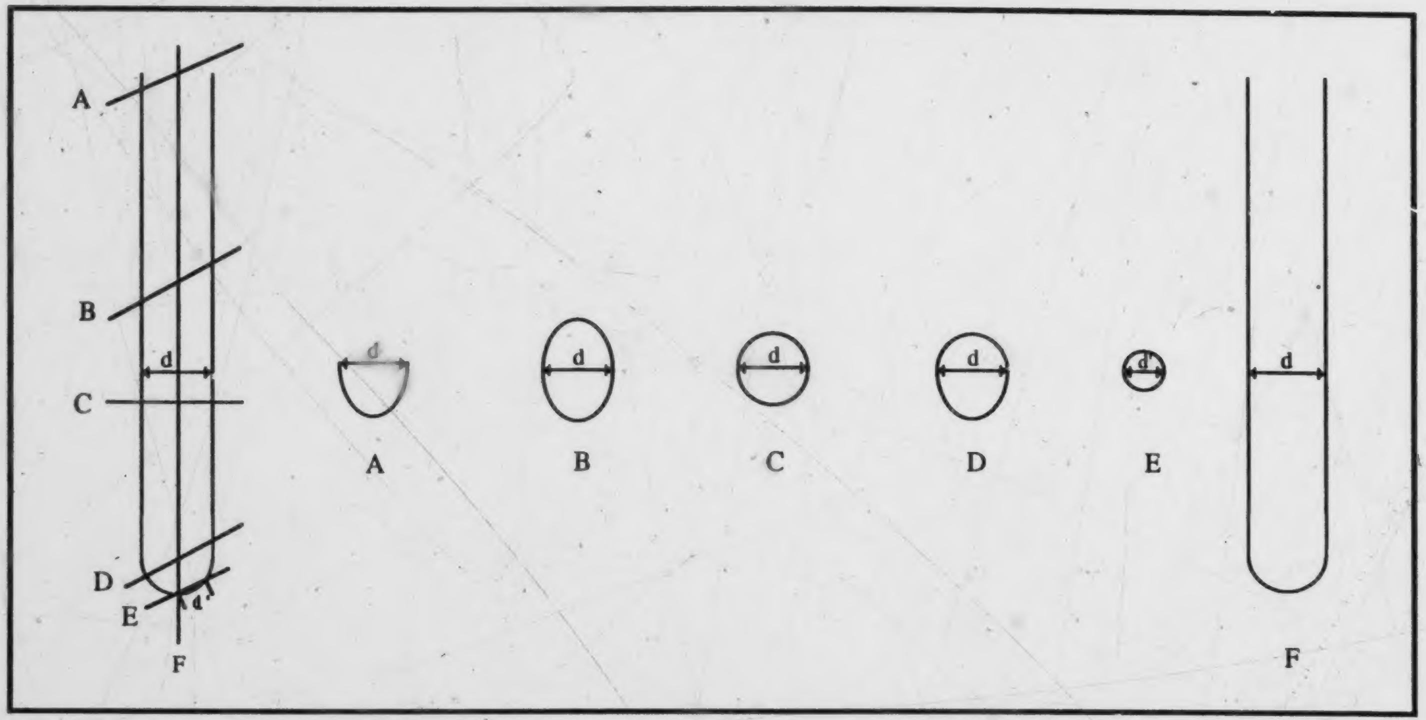
A
B
C
D
E
F
d
d'
A
B
C
D
E
F
d
d
d
d
d
d

Figure VII-1. Schematic diagram showing cross-sectional views of cylindrical boring with hemispherical cap cut at various angles and positions.

Table VII-1. Laboratory techniques for studying trace fossils (modified after Ekdale *et al.*, 1984).

Technique	Application	Advantages	Disadvantages	References
X-ray radiography	Unmasks diagenetic effects	Suitable for lithified and unlithified sediments	Basic equipment costly; thin slab must be cut	Hamblin, 1962a; Bouma, 1969
Infrared photography	Variation in texture of sediment rich in organics	Straight-forward, inexpensive	Poor on well-sorted sediments	Rhoads and Stanley, 1966
Ultraviolet photography	Enhances obscure structures in pure carbonates	Inexpensive, simple methodology	Poor on sandy and iron-rich sediments	Farrow, 1975
Staining	Heightens contrasts of porosity and mineralogy	Inexpensive	Porous strata only	Hamblin, 1962b; Risk and Szczuczko, 1977
Modified Bushinsky oil technique	Enhances obscure structures in chalk	Inexpensive, spectacular results	Time-consuming	Bromley, 1981
Casting technique	Analyses of endolithic microorganisms	Three-dimensional structure	Time-consuming; most agents applied to remove the rock or skeletal substrate cause structural damage to trace fossils	Golubic *et al.*, 1975; Pemberton *et al.*, 1980

Pemberton *et al.*, 1980, 1988). The area of each boring is calculated by assuming the boring shape to be a simple geometric figure, such as a rectangle or circle (Pemberton *et al.*, 1988). The total bored area can then be calculated. Kobluk and Kozelj (1985), using the digitized pad, reported the size of macroborers in terms of cross-sectional area. Hein and Risk (1975), MacGeachy (1975), and MacGeachy and Stearn (1976) used X-ray radiography methods to estimate the percentage of the volume of each coral which had been bored.

Techniques used in this study

Three different instruments were used to obtain quantitative data of the borings, namely density slicer, automatic image analyser, and digitized graphic tablet. Thin section A (Plate. VII-1) was used to test the applicability of each instrument.

Density-slicing technique

The size analysis of the borings was done in essentially the same way as for aerial photographs (see Chapter 6). The small size and numerous borings, however, prevented the use of thin sections and the masking techniques used for the aerial photograph. The negative photographs cannot be used directly as an input image since only transparent materials can be used with the density slicer. Thus, additional sample preparation was necessary because the profiles of all borings had to be traced on overlay transparencies. Following masking, only the bored areas were exposed to the Vidicon camera (Plate VII-2A). The small size of boring, however, introduced significant halo error (Plate VII-2B). Instrument limitations prevented size measurements; the planimeter attached to the density slicer can only measure the vertical or horizontal distances. In order to measure the dimension of the oriented borings it was necessary to rotate the borings to either the vertical or horizontal position. This is not practical when numerous borings need to be measured.

PLATE VII-2

Images of thin section A obtained from density slicing technique (A), and the halo error (B).

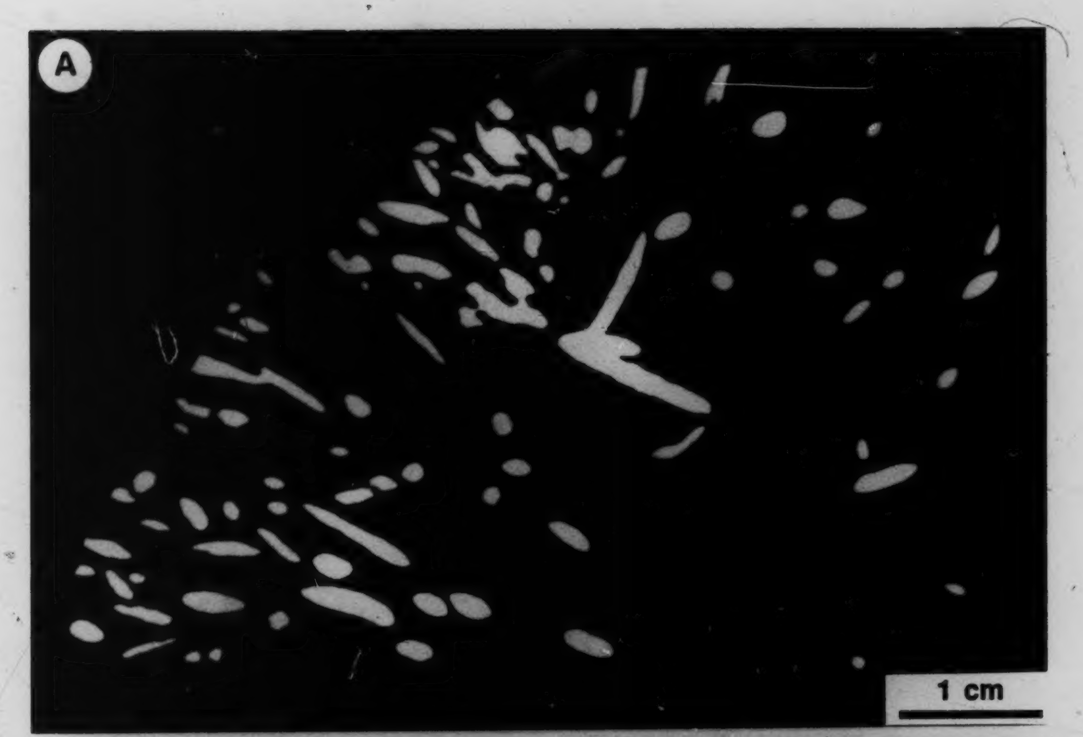
A
1 cm

B
1 cm

Likewise, the orientation of geopetal fabric cannot be measured with the density slicing technique.

Automatic-image-analysis technique

The lack of contrast between the material filling the borings and the host stromatoporoids means that additional sample preparation is needed if the automatic image analyser is to be used. The masking procedures employed in sample preparation for the density-slicing technique are applicable. However, sample preparation can only be done by tracing and filling the outlines of the borings onto overlay transparencies. The outlines to be filled must have a closed contour (Plate VII-3A). Thus, additional manual editing is usually needed. After the outlines have been filled (Plate VII-3B), the total bored area can be measured by calculating the sum of the area of all pixels composing the image of the borings. The percent of bored area can be calculated with respect to the total area of the thin section (Plate VII-3C).

The size of individual boring can be measured using Feret's diameter. With the instrument used, Feret's diameter can be measured at any angle because the X-Y coordinates can be rotated 180 degree around the feature. The length and width of the borings are represented by the maximum and minimum Feret's diameters, respectively. The size measurement of an individual boring is difficult, however, because many of the borings lie close to one another, touch each other or, sometimes cross-cut each other (Plate VII-1). In the automatic image analyser, the touching and cross-cutting borings are treated as a single feature. Erosion and dilatation techniques cannot be used effectively in this case because: (1) the cross-cutting profiles cannot be separated, and (2) small-size profiles are removed after erosion. The only option available is to interact with the image itself and separate touching features before performing the measurements (Plate VII-3D). This is a time consuming process when dealing with a large number of features.

PLATE VII-3

Image of thin section A obtained at each step when using automatic image analysis system.

(A) The binary image of an outlines of *Trypanites*.

(B) The binary image of an outlines of *Trypanites* in (A) being filled by black pixel.

(C) The binary image of total area of stage I growth of *Clathrocoilona inconstans*.

(D) The binary image of *Trypanites* after the separation of touching borings.

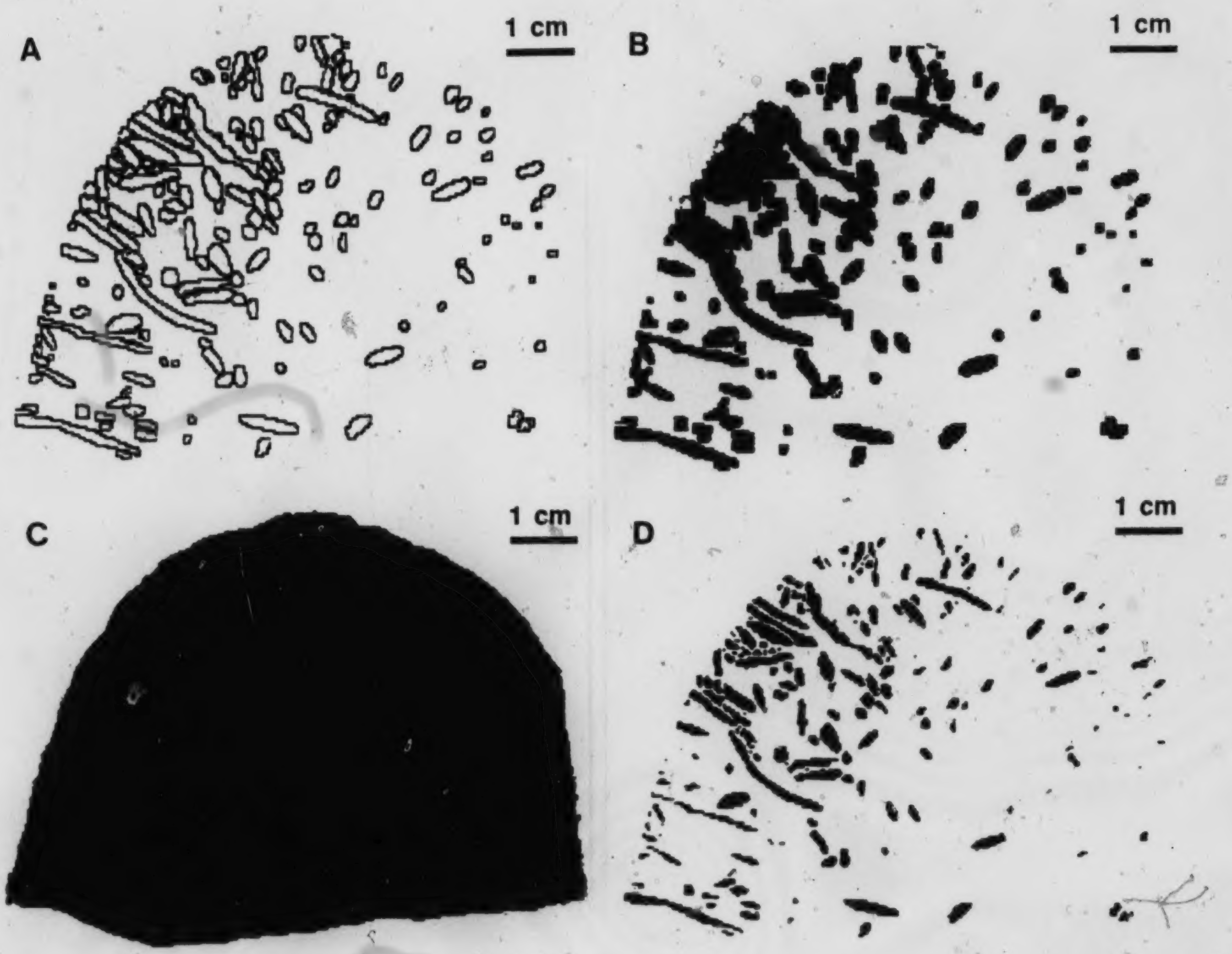
A
1 cm
B
1 cm
C
1 cm
D
1 cm

Digitized-graphic-tablet technique

When using the digitized-graphic-tablet technique, the data is entered manually by tracing the profile of the boring to be measured. Both thin sections and negative photographs can be used as input images. Thin sections, however, are not suitable because some of the borings are too large to fit in a field of view under the microscope, even with the lowest magnification available (x2.5). Also, it is very difficult to trace small and irregularly shaped features on the graphic tablet while viewing the microscope image simultaneously. It is more convenient to work with the negative photograph because the borings can be traced directly. An enlarged photograph (x3.58) provides better accuracy since the basic scale of the instrument is in millimetres.

There are various basic size measurements provided in the Kontron program. These parameters include AREA, AREA DIF, FERET XY, DMAX, and DELL AB (Table VII-2). The parameter AREA (Table VII-2A) can be used to measure an area within the perimeter by tracing the perimeter continuously before returning to the starting point in order to terminate measurement. This parameter was used to measure the area of each boring and the area of the thin section.

The AREA DIF can be used to measure the area of objects which require more than one area measurement. The clockwise rotation of the pen results in additive value, while counter-clockwise rotation results in subtractive values (Table. VII-2B). This parameter is useful in measuring the area of cross-cutting to prevent duplication of measurements of cross-cut areas.

The FERET XY (Table VII-2C) determines the maximum dimensions in X and Y directions. The error involved in using FERET XY for the size measurement of borings is extreme because the borings are long and thin. The measured length is equal to the cosine of the angle of the alignment of boring multiplied by the true longest dimension. The maximum error of 29% can be encountered when only vertical and horizontal Feret

Table VII-2. Basic measurements made by the digitized graphic tablet applicable to size analysis of boring.

Display	Measurement	Application
A 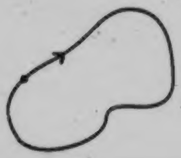	AREA	measure cross-sectional area; percentage of bored area
B 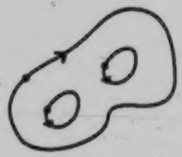	AREA DIF	area measurement of cross-cut boring
C 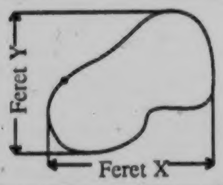	FERET XY	determine the maximum dimensions of the projected profile in X and Y directions
D 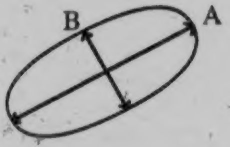	DELL AB	an approximation of the dimensions of borings
E 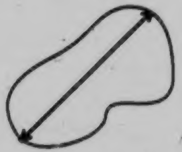	D MAX	maximum dimension
F 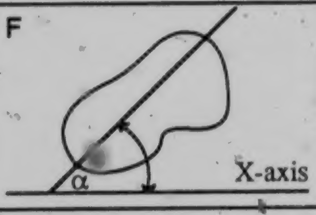	ANGLE	orientation of geopetal structures

diameters are measured and the object is aligned in a 45° direction (Fig. VII-2). The measured width is much greater than the true dimension.

The DELL AB is the measurement of the major and minor axes of an elliptical-type structure. For irregular structures (i.e. not circles or ellipses), the axes A and B (Table VII-2D) may approximate the length and width. Since the cross section of the borings are either elliptical or semi-circular, the function DELL AB is selected to measure the major (or length) and minor (width or diameter) axes of boring profiles.

The parameter DMAX (Table VII-2E) gives the maximum dimension of the feature. The maximum dimension can be derived by placing the start of the continuous perimeter trace at one end of the structure and returning to the starting point to terminate measurement. This parameter is not useful in this study because the size of the boring is described by the diameter (minor axis) of the cross-sectional profile.

The angle of the geopetal structure was measured using the function ANGLE which determines the angle between DMAX and the X axis of the tablet (Table VII-2F). In order to obtain information on the orientation of the geopetal structures, the datum line (an internal lamination) was placed parallel to the X axis of the tablet. The geopetal fabrics were measured, with reference to the datum line, by tracing the line representing the orientation of geopetal on the upper surface of boring, starting from the lowest point of the profile and returning to the start to terminate measurements.

The digitized graphic tablet appears to be the most suitable technique for measuring the size and orientation of feature with nonuniform tone. Although the data is entered manually and, therefore, requires more operating time, the digitized- graphic-tablet technique still provides an easy method of acquiring data. It took approximately seven hours to obtain data on length, width, cross-sectional area and the orientation of the geopetal structure of total 928 borings contained in five thin sections (A, B, C, D and E). Manual measurement required approximately 40 hours to measure length and width of 697 borings (B. Jones, 1987, pers. comm.). Based on the average number of features

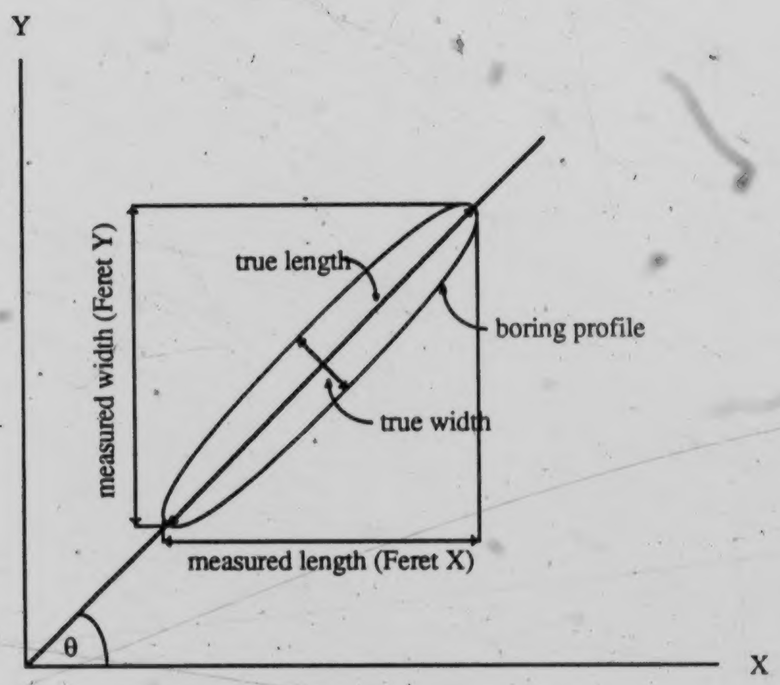
Y
X
θ
true length
boring profile
true width
measured width (Feret Y)
measured length (Feret X)

Figure VII-2. Schematic diagram showing Feret's diameter. The error associated in length measurement is equal to cosine θ x true length. If θ is 45°, the error involve is approximately 29%.

measured in one hour, the digitized-graphic-tablet technique is approximately 8 times faster than the conventional method. The results reported in this study were obtained with the digitized graphic tablet. The degree of instrument and operator error likely to be involved is less than 5%, as suggested by the coefficient of variation (see Chapter 4).

Comparison of the results obtained via digitized graphic tablet with those obtained via conventional method

Because the size measurement of boring were obtained based on the assumption that the major and minor axes of ellipsoidal structure represented the length and the width of cross-sectional profile of the borings, it is necessary to verify this assumption before discussing results. The verification was done by comparing the measurements of borings on thin sections A, B, C, D and E with the measurements of the same thin sections obtained by Pemberton *et al.* (1988) using manual methods (Table VII-3).

Visually, the mean values of the width obtained from two measurement techniques are close whereas the mean values for cross-sectional area and length show some differences. The differences between mean values of cross-sectional area, length, and width were analysed statistically to see if the differences are significant.

Statistical tests

The *t* test was used to test whether the differences between mean values of cross-sectional area, length, and width obtained via two methods are significant (see Chapter 5). Given that the thin sections provide random slices through the borings, the assumption on randomness required for the *t* test is satisfied. The requirement that the sample came from a normally distributed population was checked using the stabilized probability plot (see Chapter 5). The results of stabilized probability plot of the width of the borings in thin sections A to E (Figs. V-2 and VII-3) suggest that all groups of data came from populations with a normal distribution at the 95% confidence interval. The equality of

Table VII-3. Summary of data on size measurement on *Trypanites* (in mm) in thin sections A to E. Bold figures are referred to data obtained in this study while plain figures are referred to data obtained by Pemberton *et al.* (1988).

Thin section	No. of boring	Area*			Length			Width		
		minimum	mean	maximum	minimum	mean	maximum	minimum	mean	maximum
A	**199** 142	**0.18** 0.25	**2.35** 3.28	**13.59** 19.51	**0.53** 0.56	**2.65** 3.17	**15.73** 13.97	**0.36** 0.28	**1.10** 1.05	**2.34** 1.68
B	**355** 268	**0.10** 0.25	**1.51** 2.19	**15.38** 18.73	**0.58** 0.56	**1.90** 2.14	**18.43** 16.76	**0.32** 0.28	**1.03** 1.02	**2.23** 1.96
C	**204** 137	**0.16** 0.25	**1.91** 3.09	**14.24** 22.16	**0.53** 0.84	**2.48** 2.90	**23.14** 19.83	**0.43** 0.28	**1.00** 1.05	**1.94** 1.96
D	**106** 94	**0.43** 0.47	**2.23** 3.36	**14.56** 16.78	**0.80** 0.84	**2.65** 3.15	**11.87** 12.01	**0.50** 0.56	**1.02** 1.05	**1.66** 1.96
E	**64** 56	**0.36** 0.55	**1.90** 2.39	**6.74** 9.05	**0.78** 0.84	**2.52** 2.52	**9.25** 9.50	**0.56** 0.56	**0.99** 0.98	**1.62** 1.68

* calculated from data in Pemberton *et al.* (1988).

variances of two samples was checked using *F* test (see Chapter 5). The results of *F* test will be discussed together with the results of *t* test for each parameter.

Statistical test of width measurement: The values of *F* calculation of width of all samples are less than *F* critical (Table VII-4). This suggests that the variances of the width measurement obtained by methods are not significantly different at the 95% confidence interval. The values of *t* calculation of width for all samples are less than values of the *t* critical (Table VII-4). This indicates that the mean values obtained in this study are not significantly different from those obtained by Pemberton *et al.* (1988). In other words, the width of borings obtained via digitized graphic tablet is comparable to measurements obtained by Pemberton *et al.*(1988).

Statistical test of length measurement: The *F* calculation for the length of all samples but those from thin section B are less than *F* critical (Table VII-5). This suggests that all samples but thin section B have an equal variance. The *t* calculation for length measurement of thin sections C and E are less than *t* critical while the *t* calculation of thin sections A and D are higher than *t* critical (Table VII-5). This suggests that only the mean values of length measurement from thin sections C and E obtained in this study and those obtained by Pemberton *et al.* (1988) are not significantly different at the 95% confidence interval. The possible courses which may be used to explain the differences in mean values of length measurement from thin sections A and D will be discussed later.

Statistical test of cross-sectional area measurement: The results of the *F* test for cross-sectional area of borings indicates that samples used in this study and the ones used by Pemberton *et al.* (1988) come from populations which have different variances at the 95% confidence interval. This is because all *F* calculation for cross-sectional areas are greater than *F* critical (Table VII-6). Therefore, the *t* test for cross-sectional area cannot be performed.

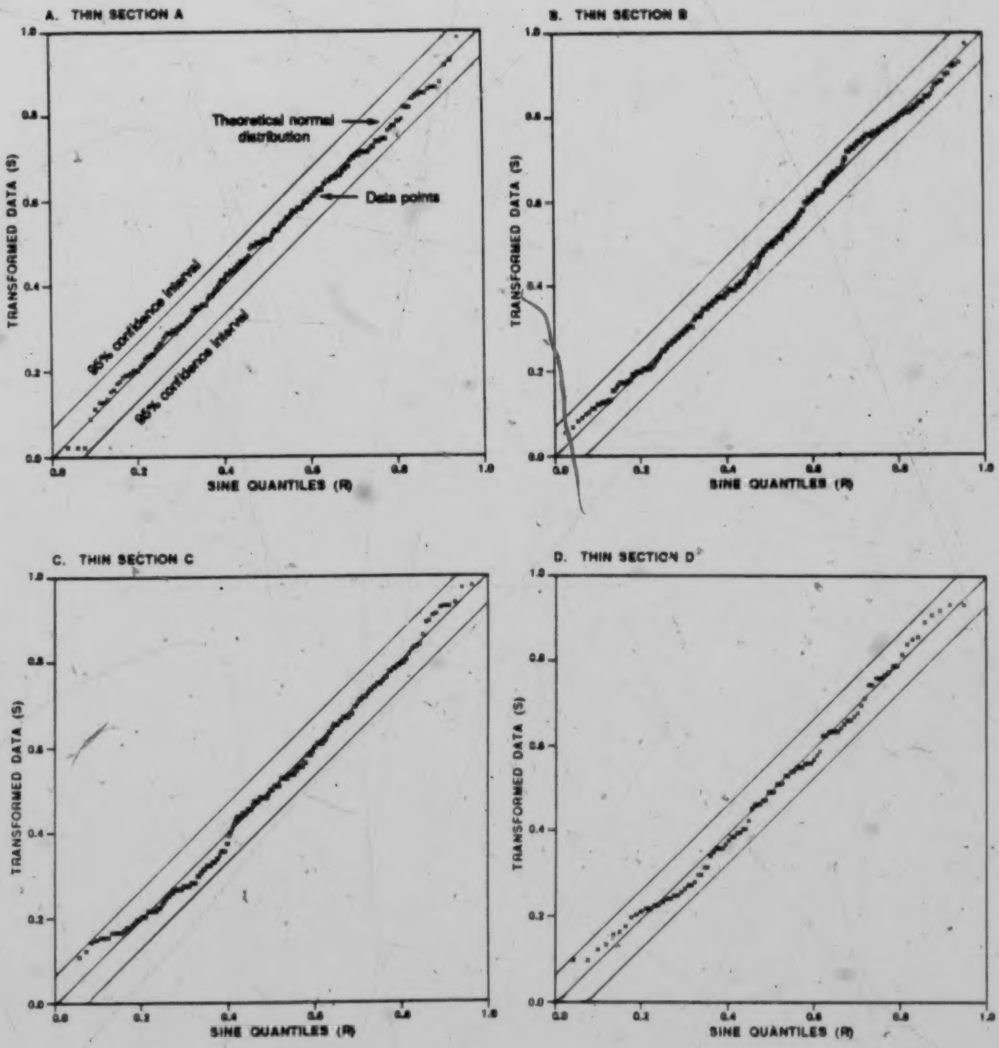

Figure VII-3. The graphs showing the results of normality test of width measurement of borings in thin sections A, B, C, and D at 95% confidence interval.

Table VII-4. Summary of the results of *F* test and *t* test of width (diameter) of *Trypanites* in thin sections A to E.

Thin section	Data set # 1 (this study)			Data set # 2 (Pemberton *et al.*, 1988)			F- test		t - test	
	Count	Mean n_1	Variance $\bar{x}_1$	Count s_1^2	Mean n_2	Variance $\bar{x}_2$	F-calc. s_2^2	Critical value of F ($\alpha = 0.05$)	t-calc.	Critical value of t ($\alpha = 0.05$)
A	199	1.10	0.10	142	1.05	0.07	1.43	1.55	1.33	1.652
B	355	1.03	0.08	268	1.02	0.08	1.01	1.55	0.69	1.648
C	204	1.00	0.09	137	1.05	0.09	1.04	1.55	1.43	1.652
D	106	1.02	0.07	94	1.05	0.10	1.43	1.55	0.77	1.660
E	64	0.99	0.04	56	0.98	0.06	1.50	1.65	0.35	1.660

Table VII-5. Summary of the results of F test and t test of length data of *Trypanites* in thin sections A to E.

Thin section	Data set # 1 (this study)			Data set # 2 (Pemberton *et al.*, 1988)			F- test		t - test	
	Count n_1	Mean $\bar{x}_1$	Variance s_1^2	Count n_2	Mean $\bar{x}_2$	Variance s_2^2	F-calc.	Critical value of F ($\alpha = 0.05$)	t-calc.	Critical value of t ($\alpha = 0.05$)
A	199	2.65	5.13	142	3.17	7.94	1.54	1.55	1.81	1.652
B	355	1.90	2.4	268	2.14	4.84	2.02	1.55	-	-
C	204	2.48	5.96	137	2.90	6.99	1.17	1.55	1.47	1.652
D	106	2.65	2.98	94	3.15	3.49	1.17	1.55	1.94	1.660
E	64	2.52	2.61	56	2.52	2.86	1.10	1.65	0.01	1.660

Table VII-6. Summary of the results of *F* test and *t* test on the cross-sectional area data of *Trypanites* in thin sections A to E.

Thin section	Data set # 1 (this study)			Data set # 2 (Pemberton *et al.*, 1988)			F- test		t - test	
	Count n_1	Mean $\bar{x}_1$	Variance s_1^2	Count n_2	Mean $\bar{x}_2$	Variance s_2^2	F-calc.	Critical value of F ($\alpha = 0.05$)	t-calc.	Critical value of t ($\alpha = 0.05$)
A	199	2.35	4.86	142	3.28	9.95	2.05	1.55	-	-
B	355	1.51	2.13	268	2.19	7.96	3.74	1.55	-	-
C	204	1.91	4.27	137	3.09	11.10	2.60	1.55	-	-
D	106	2.23	4.09	94	3.36	6.70	1.64	1.55	-	-
E	64	1.90	1.67	56	2.39	2.80	1.68	1.55	-	-

Discussion

Since size of boring is best described by its diameter, it can be concluded that the digitized graphic tablet can be used as a tool in size analysis of boring. The causes of the differences in variances of measurement on cross-sectional area and length, however, will be discussed.

The differences in variances of measurements on cross-sectional area and length may arise from bias in sampling. The sample size used in this study is much larger than that used by Pemberton *et al.* (1988). Considering the distribution of length, cross-sectional area, and width (Figs. VII-4, VII-5, VII-6), it can be seen that the excess samples (samples that were not used by Pemberton *et al.*, 1988) are the small borings. The difference in sampling has an effect on the mean and variance values of cross-sectional area and length, i.e. it reduces the mean value (Table VII-3). This is because the range (maximum - minimum) of those two types of measurements is large (approximately 20 mm and 15 mm^2 for length and cross-sectional area, respectively). The difference in sampling does not have much effect on mean and variance of width because the range of width is small (approximately 2 mm).

The another possible error introduced in cross-sectional area measurement is the method used to obtain the data. Pemberton *et al.* (1988) obtained data on cross-sectional area by assuming the borings to have a simple geometric figure, e.g. rectangle, and then calculated the area using the formula for that figure. Thus, the differences in area measurements obtained via the digitized graphic-tablet technique and by assuming the borings are rectangular are investigated.

In order to investigate the error involved, the cross-sectional areas of the test sample (Fig. IV-5) were measured using three different methods: (1) by digitized graphic tablet, (2) by assuming the borings to have rectangular shape, and (3) by assuming the borings to have an elliptical shape. The mean values of major and minor axes obtained via digitized graphic tablet were used as length and width of those borings. It was assumed that the

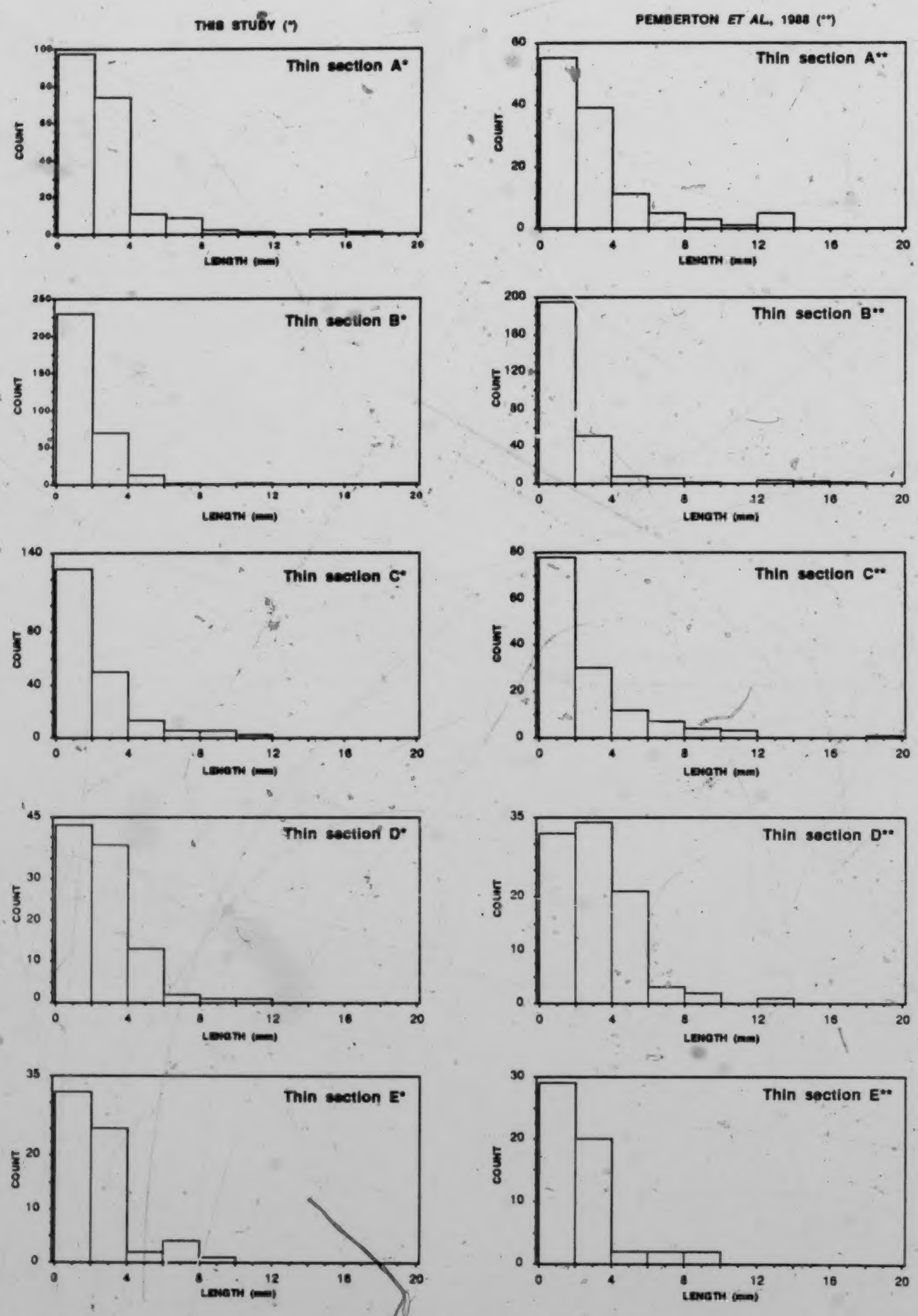

Figure VII-4. Frequency histogram for the length of the borings from thin sections A, B, C, D, and E.

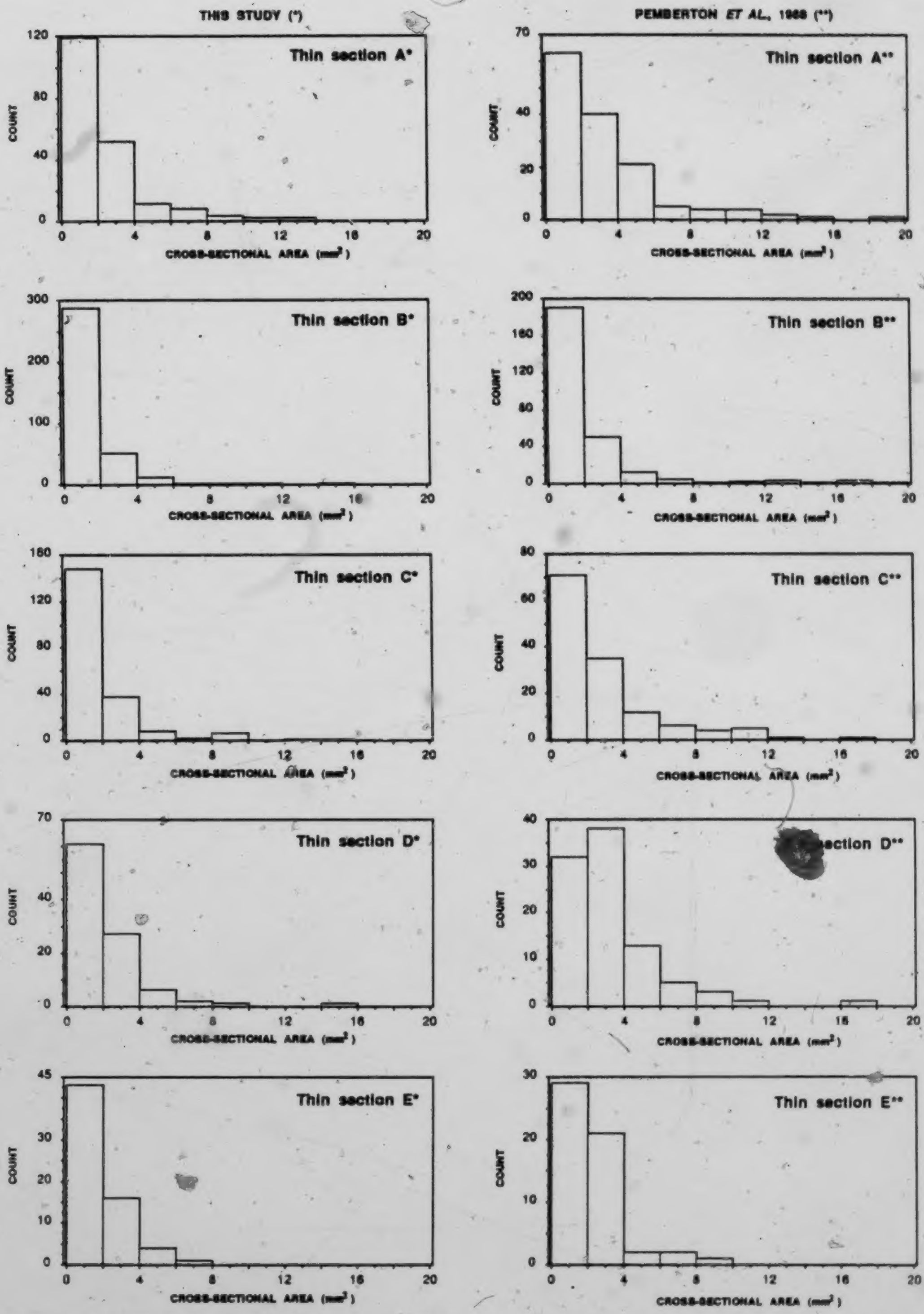

Figure VII-5. Frequency histogram for the cross-sectional area of the borings from thin sections A, B, C, D, and E.

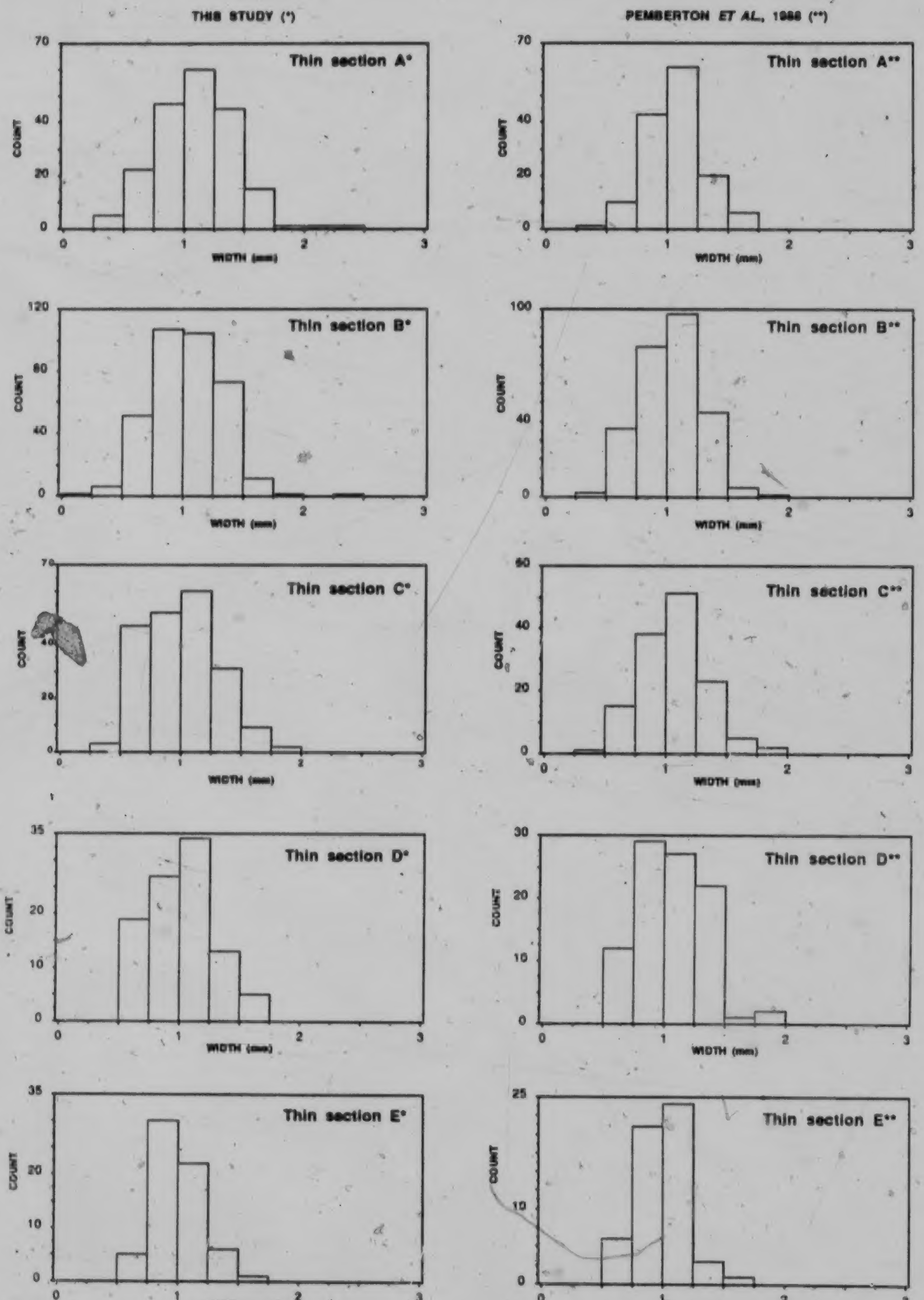

Figure VII-6. Frequency histogram for the width of the borings from thin sections A, B, C, D, and E.

areas of the borings obtained via graphic tablet are not subject to error and were used as a basis for comparison.

The error involved when assuming the borings to be rectangular ranges from 28 to 31% while the error involved when assuming the boring to be elliptical ranges from 1 to 4% (Table VII-7). From these results, it is suggested that the basic geometric assumption on area calculation is important. A large error can be introduced when the assumed shape and the actual shape are significantly different.

Since the cross-sectional profile of boring is only the approximation of an ellipse, it would be interesting to investigate whether the percent error involved in area calculation (when using the rectangle formula) depends upon the shape of the cross-sectional profile. To investigate the shape effect, sets of measurements selected from the size measurement of borings were used. A boring's diameter is fixed at 1 mm while length varies from 1.14 to 4.37 mm (Table VII-8). The calculated areas (in Table VII-8) were obtained by assuming that the borings' profile is rectangular. The measured areas were obtained using the digitized graphic tablet. The percent difference of the calculated and measured areas is then determined, using the measured area as the basis of comparison. It can be seen that, from the cross-plots of length and percent error, as length increases the percent error decreases slightly (Fig. VII-7). This suggests that the shape of the cross-section of borings has an effect on the amount of error involved in area calculation. However, the range of percent error (27.43 to 28.88) is relatively small.

The error on area measurement affects the calculation of percent of bored area as shown in Table VII-9. In general the percent of bored area obtained by Pemberton *et al.* (1988) is greater than that obtained in this study. This is partly due to the fact that the error introduced when assuming the boring to have a simple geometric figure is a cumulative error while the error occurred in the digitized-graphic-tablet technique is random.

Table VII-7. Assessment of error measured area by digitized graphic tablet versus calculated area using rectangle (calculated area-1) and ellipse (calculated area-2).

Unit code	mean major axis	mean minor axis	measured area	calculated area-1	% difference of measured area vs area-1	calculated area-2	% difference of measured area vs area-2
1	6.89	1.45	7.76	10.02	29.11	7.87	1.39
2	4.15	1.62	5.19	6.71	29.23	5.57	1.50
3	2.43	1.22	2.26	2.96	31.02	2.32	2.79
4	4.21	1.53	5.08	6.43	26.00	5.05	0.57
5	4.23	1.37	4.50	5.78	28.54	4.54	0.95
6	3.10	1.33	3.18	4.12	29.52	3.24	1.73
7	4.20	1.26	4.14	5.30	28.10	4.17	0.62
8	2.04	1.15	1.83	2.35	28.42	1.84	0.86
9	2.09	1.24	1.97	2.59	31.42	2.03	3.20
10	3.93	1.39	4.22	5.46	29.26	4.29	1.60
11	10.08	1.26	9.54	12.65	32.56	9.94	4.12
12	4.82	1.45	5.41	6.99	29.23	5.49	1.50

Table VII-8. Data on size measurement used to evaluate the effect of shape of cross-sectional profile on percent error.

Width (mm)	Length (mm)	Calculated* area	Measured** area	% difference
1.00	1.14	1.16	0.90	28.88
1.00	1.55	1.58	1.23	28.45
1.00	2.16	2.20	1.72	27.91
1.00	3.13	3.19	2.50	27.60
1.00	4.37	4.46	3.50	27.43

$$\% \text{ difference} = \frac{(\text{calculated area - measured area}) \times 100}{\text{measured area}}$$

* area of rectangle
** area obtained via graphic tablet

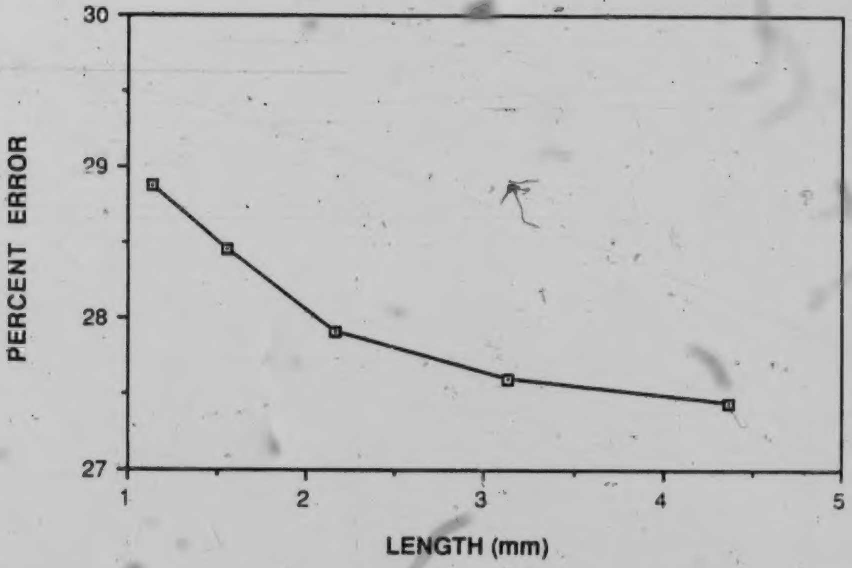

Figure VII-7. Cross-plot of length of boring and the percent error involved in area calculation, data from Table VII-8.

Table VII-9. Summary of data on the percent boring of *Trypanites* in thin sections A to E. Bold figures refer to data obtained in this study. Plain figures refer to data from Pemberton *et al.* (1988).

Thin section	Total stage I & II		Total stage I		Total stage II	
	# of boring	% of boring	# of boring	% of boring	# of boring	% of boring
A	**199*** 142*	**17.46** 19.50	**162** 118	**19.34** 22.72	**35** 24	**10.54** 10.65
B	**355** 268	**19.55** 24.24	**348** 262	**22.55** 27.64	**7** 6	**2.50** 3.25
C	**204** 137	**12.82** 16.91	**204** 137	**12.82** 16.91	**0** 0	**0** 0
D	**106*** 94*	**8.18** 12.73	**98** 86	**9.44** 14.87	**6** 6	**1.96** 5.12
E	**64** 56	**5.18** 6.06	**64** 56	**5.18** 6.06	**0** 0	**0** 0
Total	**928** 697		**876** 659		**48** 35	

* included boring that cut both stage I and II.

Size distribution

The diameter of borings measured from twelve thin sections show that the mean ranges from 0.99 to 1.10 mm (Table VII-10). The variation of diameter in each thin section is less than one standard deviation. If all of the borings are considered together the average diameter is 1.03 mm. The mode of size distribution occurs at the size-classes 1.0 to 1.2 mm or at 0.8 to 1.2 mm where the mode is not unique.

An attempt was made to investigate the possibility that size analysis performed on one thin section can represent the size analysis of the whole community. One-way analysis of variance was used to test if the mean diameter of borings obtained from each thin section shows any significant difference from one another. The results of one-way analysis of variance indicates that the variation within samples is greater than the variation among samples (Table VII-11). The *F* calculation values are less than the *F* critical values for both heads X and Y (Table VII-11). This suggests that there is no significant difference in means between thin sections. It also suggests that no matter how the stromatoporoid head was cut, the size distribution obtained from one thin section can be used to represent the distribution of population, providing a large sample size is used from that thin section.

Effect of orientation of boring on percent bored area

It has been suggested that *Trypanites* penetrates approximately normal to the substrate (Kobluk *et al.*, 1978; Kershaw, 1980; Kobluk and Nemcsok, 1982). This behaviour has an effect on the distribution of the cross-sectional profiles of borings obtained from various portions of the stromatoporoid heads. For example, most of the cross sections of boring in thin section obtained from the periphery region of the head have circular or semi-circular cross-sectional profiles. On the other hand, the longitudinal section as shown in thin section came from the center portion of the head (Fig. VII-8).

If the *Trypanites* used in this study penetrate approximately normal to the substrate, the distribution of the orientation of the borings obtained from thin sections from the

Table VII-10. Summary of data on width measurement of *Trypanites* (in mm) from twelve thin sections.

Thin section	No. of boring	Minimum	Maximum	Mean	Mode	Standard deviation
Head X						
A	199	0.36	2.34	1.10	1.0 - 1.2	0.32
F	137	0.54	1.95	1.05	1.0 - 1.2	0.22
G	130	0.54	1.64	1.05	0.8 - 1.0	0.23
H	96	0.52	1.63	1.02	0.8 - 1.2	0.28
D	106	0.50	1.66	1.02	1.0 - 1.2	0.27
Head Y						
B	355	0.32	2.23	1.03	0.8 - 1.0	0.28
I	348	0.36	2.19	1.01	0.8 - 1.0	0.28
J	277	0.45	2.08	1.07	1.0 - 1.2	0.28
K	153	0.50	1.73	1.01	1.0 - 1.2	0.25
L	155	0.55	1.59	1.03	1.0 - 1.2	0.25
E	64	0.56	1.62	0.99	0.8 - 1.0	0.20
Head C						
C	204	0.43	1.8	1.00	0.8 - 1.0	0.30

Table VII-11. Results of analysis of variance of diameter of *Trypanites*.

A. Analysis of variance of diameter of *Trypanites* from thin sections cut from stromatoporoid head X.

Source of variation:	Sum squares:	Degree of freedom	Mean square:	F-test
Among groups	0.59	4	0.15	1.89
Within groups	50.95	664	0.07	
Total	51.54	668		

B. Analysis of variance of diameter of *Trypanites* from thin sections cut from stromatoporoid head Y.

Source of variation:	Sum squares:	Degree of freedom	Mean square:	F-test:
Among groups	0.67	5	0.13	1.81
Within groups	99.22	1347	0.07	
Total	99.88	1352		

periphery and the center regions of the heads should be different. The orientation of boring, with respect to the axis of the boring, was estimated by using the length of the major and minor axes (Fig. VII-9). The orientation of the borings cut at the periphery of the head show the angle distribution ranges from 0 to 90° when observed in thin section (Fig. VII-10). However, the changes in the distribution of the orientation of borings from the periphery of the head (thin section B) towards the center of the head (thin sections I, J, K, and L) are evident (Fig. VII-10). The distribution of orientation of the borings in thin section E is relatively similar to that obtained from thin section K, which came from approximately the same distance from the center of the head but in the opposite direction. The range of angle of orientation decreases in thin sections obtained from the center portion of the head (Fig. VII-10). The results on the analysis of orientation of boring in this study support the observation made by several authors (Kobluk *et al.*, 1978; Kershaw, 1980; Kobluk and Nemcsok, 1982) that *Trypanites* penetrate approximately normal to the substrate.

The number of borings per thin section of stromatoporoid heads X and Y decreases from the periphery to the center of the head (Table. VII-12). This is probably due to the fact that the outer layer of the stromatoporoids were exposed for longer periods, allowing the *Trypanites* to colonize. The percent bored area, however, does not always show a similar trend to the number of borings in thin section. For example, the percent bored area of thin sections B, I, J of head Y increases while the number of borings decreases (Table VII-12). This is due to the fact that at the center of the head the borings show longitudinal sections. The volume of bored area would be best described if a three-dimensional structure could be constructed. In practice this is difficult, especially when dealing with small borings. Therefore, the percent bored area may be best represented by averaging the percent bored areas obtained from various sections of the specimen.

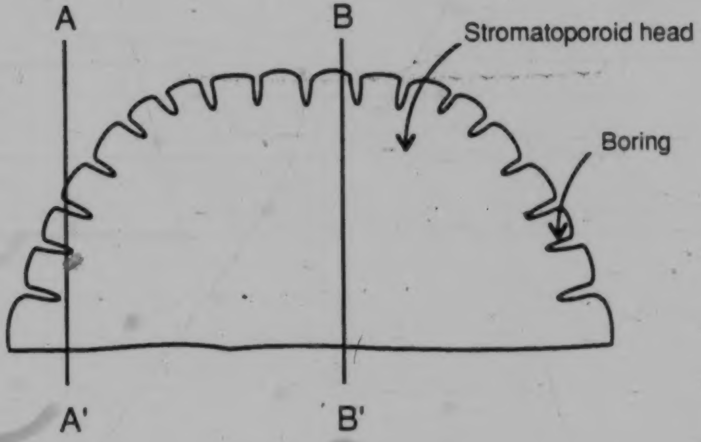
A
B
Stromatoporoid head
Boring
A'
B'

Figure VII-8. Schematic diagram of stromatoporoid head showing differential distribution of borings. Most of the cross sections of boring in section A-A' have circular and semi-circular profiles while the profiles in section B-B' are longitudinal sections.

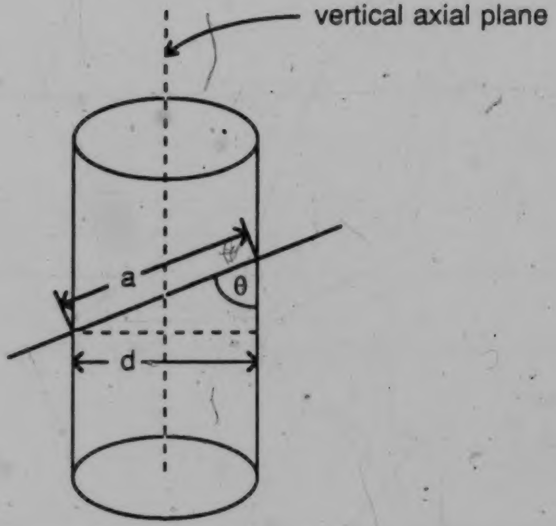

The orientation of the cylinder (with respect to vertical axial plane) can be estimated as follows:

$$\theta = \sin^{-1} d/a$$

where a = major axis or length of cross-sectional area
d = minor axis or diameter of cross-sectional area

Figure VII-9. Schematic diagram showing the orientation of boring with respect to the vertical axis.

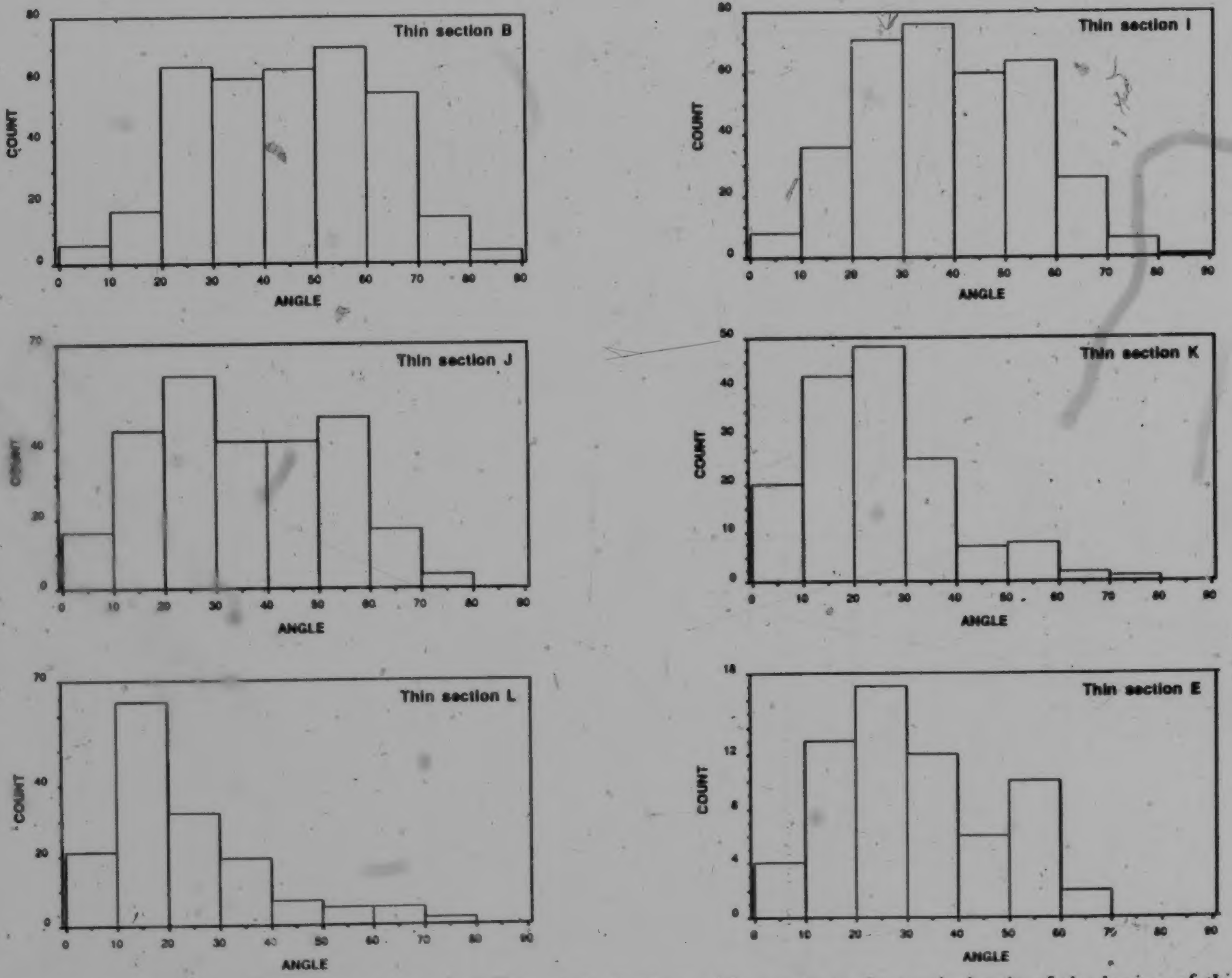

Figure VII-10. Frequency histogram of the orientation of the borings with respect to the vertical axis of the boring of thin sections B, I, J, K, L, and E.

Table VII-12. Summary of number of borings and percent bored area per thin section.

Thin section	Thin section area (mm^2)	No. of boring	Total bored area	% bored area
Head X				
A	2626.90	199	454.44	19.34
F	1903.89	137	306.14	16.08
G	2077.58	130	348.72	16.78
H	3059.18	96	220.83	7.22
D	2571.86	106	213.97	9.44
Head Y				
B	2702.47	355	511.83	22.55
I	2168.23	348	614.36	28.33
J	2113.20	277	661.51	31.30
K	1414.18	153	416.38	29.44
L	1633.98	155	494.56	30.26
E	2417.37	64	117.74	5.18

A. HEAD X

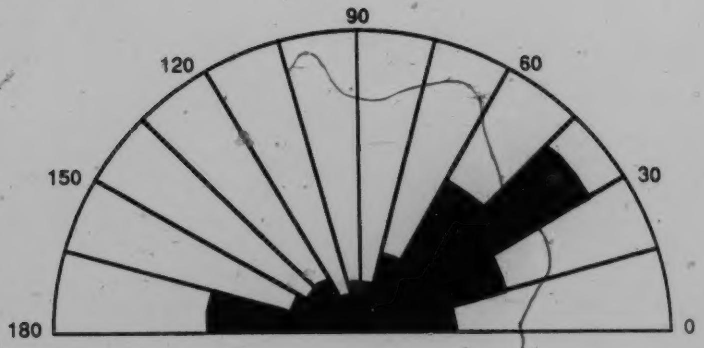

B. HEAD Y

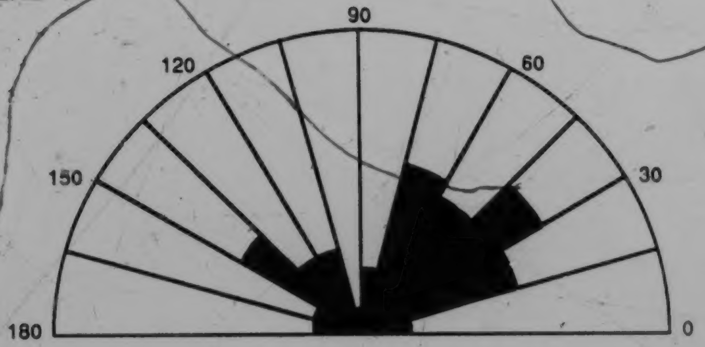

C. HEAD Z

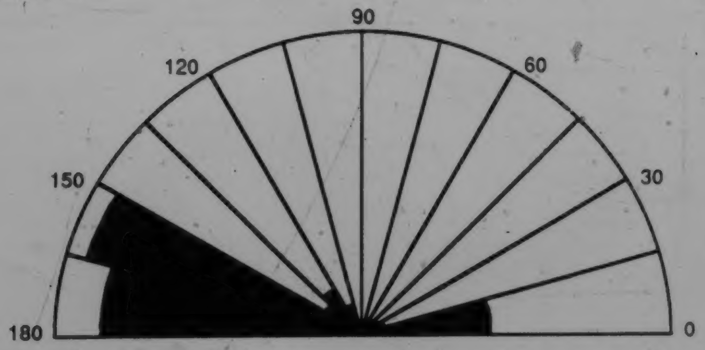

Figure VII-11. Diagrams showing the orientation of the geopetal structures in stromatoporoid heads X, Y, and Z.

Orientation of geopetal structure

The results of the measurement of orientation of geopetal structure in the borings showed that the direction of the geopetal structure is highly variable. Major trends, however, can still be recognized. Kershaw (1980) and Pemberton *et al.* (1988) suggested that change in the direction of the geopetal structure may be caused by periodic movement, e.g. storm activity. Kershaw and Riding (1978) suggested that if the domical-shaped stromatoporoids were susceptible to water movement, they would have been returned to the most stable position. This might also be the case for the stromatoporoids used in this study (as indicated by the major trends).

Synopsis

From the study of size analysis of *Trypanites weisei* from the Late Devonian Waterways Formation, it may be concluded that:

(1) the digitized graphic tablet is considered the most appropriate technique for size measurement of features with nonuniform grey tones in terms of time consumption and reliability of the results. On the other hand, the density-slicing and automatic-image-analysis techniques have limitations in the size analysis of aggregated particles exhibiting nonuniform grey tones,

(2) in addition to size measurements, the orientation of geopetal structure can be obtained via digitized-graphic-tablet technique,

(3) the deviations in the measurements obtained from the digitized graphic tablet and from those obtained by conventional techniques stem from the bias in sampling and the basic geometric assumption,

(4) the results of statistical tests on the mean diameter of borings suggest that size distribution obtained from one thin section can be used to represent the distribution of the whole community, providing large numbers of borings are contained in thin section, and

(5) the percent bored area, however, depends on which portion of the specimen was cut for the thin section. Therefore, the percent bored area averaged from several sections of the specimen may be the most representative.

C. APPLICATION - II: SIZE ANALYSIS OF VERMETID GASTROPODS

The image analysis technique described for measuring the size of borings is equally applicable for measuring the size and thickness of shells. In order to demonstrate this application, samples of the vermetid gastropods *Dendropoma (Novastoa) irregulare*? from Grand Cayman were measured.

Materials

Samples of vermetid gastropods used in this study were collected from Boddentown and Great Bluff Estates on Grand Cayman (Fig. VII-12A). At Boddentown, the samples were obtained from encrustations on beachrock (Fig. VII-12B). At Great Bluff Estates, samples were collected from a loose block (2 x 1.5 x 0.75 m) on the beach and from a lower ledge submerged in water about 1 m deep (Fig. VII-12C). The samples (Plate. VII-4) have a core formed of densely packed, tightly coiled to loosely sinuous to almost straight *Dendropoma* (*Novastoa*) *irregulare*?, with sediment and encrusting organisms present between the shells (Jones and Hunter, 1989b). In hand specimen, the amber colour shells contrast sharply with the white-to-cream coloured sediment and red coloured encrusting foraminifera, *Homotrema rubrum*.

Method of study

Three samples from the loose block collected from the beach of Great Bluff Estates were slabbed to approximately 1 cm thickness. One slab from each sample was used for the study. The slabs were photographed and prints were made with approximately 6.5x magnification. Negative photographs with approximately 4x magnification were made

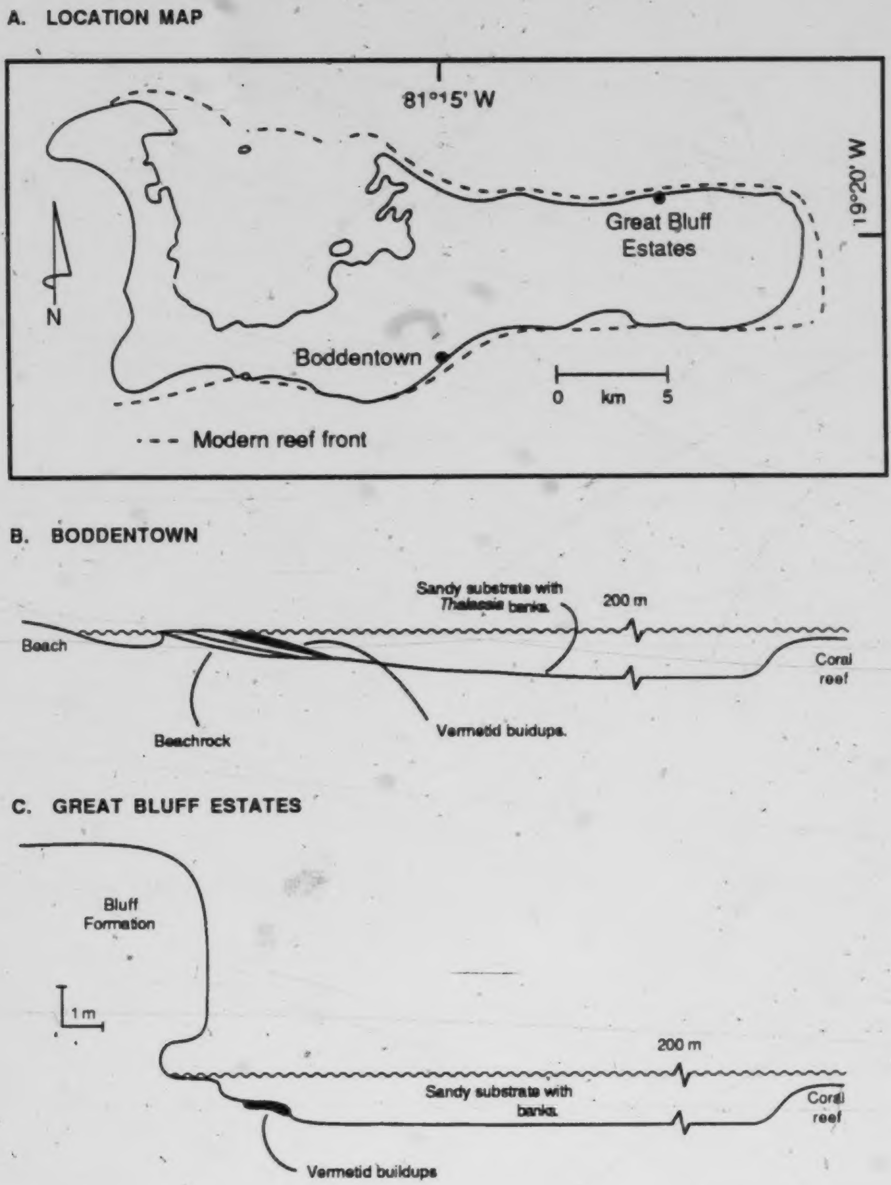

A. LOCATION MAP

B. BODDENTOWN

C. GREAT BLUFF ESTATES

81°15' W
19°20' N
N
Great Bluff
Estates
Boddentown
0 km 5
- - - Modern reef front
Sandy substrate with
Thalassia banks
200 m
Beach
Coral
reef
Beachrock
Vermetid buidups
Bluff
Formation
1 m
200 m
Sandy substrate with
banks
Coral
reef
Vermetid buildups

Figure VII-12. Location map of Grand Cayman (A), and schematic cross-sections of the coastal areas at Boddentown (B) and at Great Bluff Estates (C) showing the general setting of the vermetid buildups (modified after Jones and Hunter, 1989b).

PLATE VII-4

Photograph of hand specimen of vermetid gastropods, collected from the loose block on beach at Great Bluff Estates, Grand Cayman.

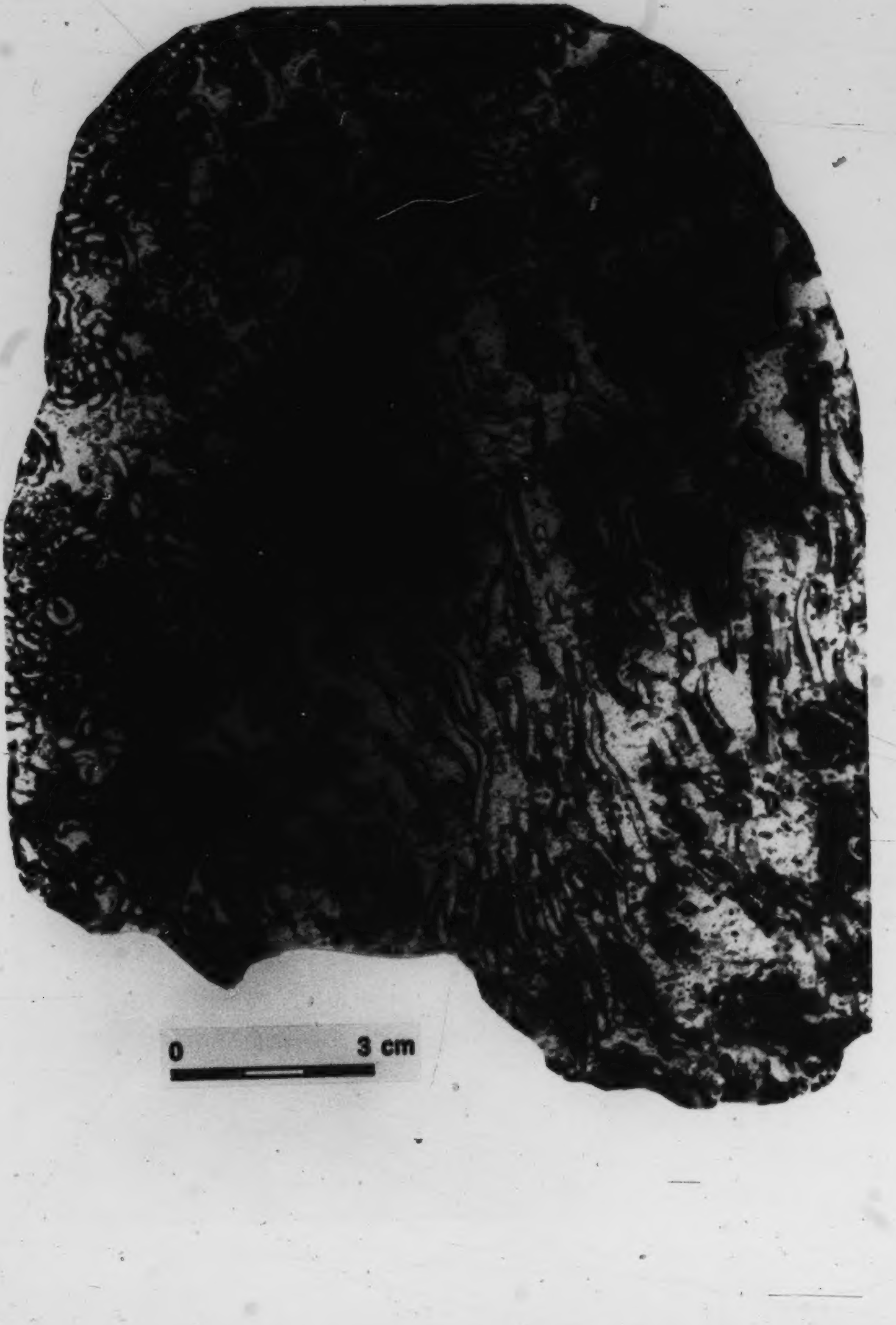
0
3 cm

from twelve thin sections obtained from samples collected from Boddentown and the lower ledge at Great Bluff Estates.

The negative photographs taken from thin sections show a sharp boundary between the body cavity and the shell while the photographs taken from the slabs show a blurred boundary. This is due partly to the shadow created by the uneven surface of the slab, and to the high magnification of the photographs. However, the boundary between the body cavity and the shell can be distinguished visually.

The length of vermetid gastropods is difficult to measure because of their sinuous nature. Therefore, shell size is best described by its diameter. In this study, it is assumed that the shell of vermetid gastropods are essentially cylindrical and have a constant shell thickness (Fig. VII-13). Thus, the diameter of the body cavity can be obtained by measuring the diameter of the inner cylinder. The thickness of the shell can be calculated from the difference between the outer and inner radii (Fig. VII-13).

The small size of vermetid gastropods and the complex spatial distribution of grey tone on the image prevents the use of the automatic image analyzer and the density slicer. The size and thickness of the shell were measured from the photographs, using the digitized-graphic-tablet technique. The parameter DELL AB was used. The diameter of the shell is represented by the minor axis of the cross-sectional profiles. Only the cross-sections which have approximately circular or elliptical profiles were measured. The coiled cross-sectional profiles were excluded from the analysis since the size measurements obtained using DELL AB do not represent the approximate dimensions of those profiles.

Results of size measurements

Data on size measurements of *Dendropoma (Novastoa)* obtained from all photographs were grouped together according to the location from which the samples were collected. Therefore, three groups of data were considered: (1) samples from Boddentown, (2) samples from the lower ledge at Great Bluff Estates, and (3) samples

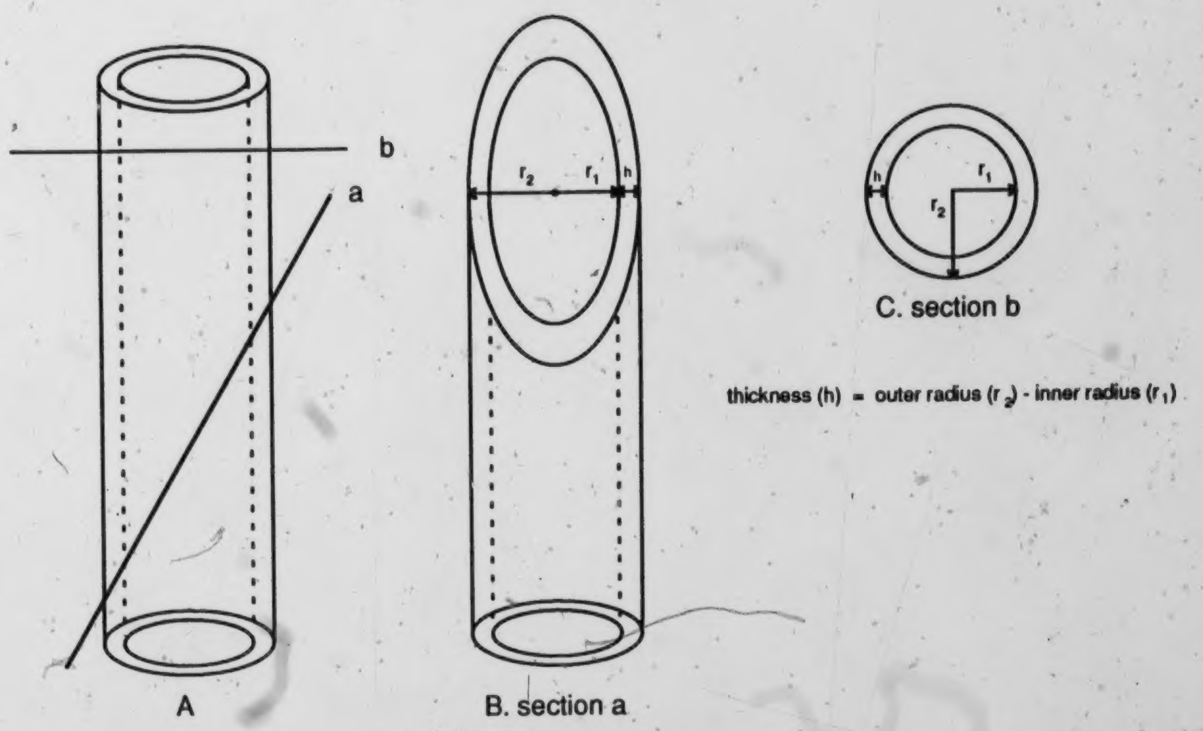
b
a
A
r_2
r_1
h
B. section a
h
r_1
r_2
C. section b
thickness (h) = outer radius (r_2) - inner radius (r_1)

Figure VII-13. Schematic diagram showing cross section of vermetid gastropod (A). For a section either making an angle (B) or perpendicular (C) with the axis of the cylinder, the body cavity of vermetid gastropod is represented by the inner diameter of the cylinder and the thickness of the shell (h) can be calculated.

Table VII-13. Summary of data on shell diameter (mm) and thickness (mm) of vermetid gastropods from Grand Cayman. (min. = minimum, max. = maximum, S.D. = standard deviation).

Location	No. of shell	Diameter (mm)				Thickness (mm)			
		min.	mean	max.	S.D.	min.	mean	max.	S.D.
Boddentown	723	0.19	1.18	2.84	0.51	0.02	0.26	0.85	0.15
Great Bluff Estates (loose block)	694	0.30	1.41	2.55	0.34	0.08	0.30	0.59	0.08
Great Bluff Estates (lower ledge)	269	0.28	1.24	2.65	0.51	0.06	0.31	0.87	0.15
All localities (Boddentown & Great Bluff Estates)	1686	0.19	1.28	2.84	0.46	0.02	0.28	0.87	0.13

from the loose block from the beach at Great Bluff Estates. The number of shells measured ranged from 269 to 723 (Table VII-13). The mean diameter of the shells from each locality ranges from 1.18 to 1.41 mm with a standard deviation of 0.34 to 0.51 (Table VII-13). The mean thickness of the shell ranges from 0.26 to 0.31 mm with a standard deviation of 0.08 to 0.15 (Table VII-13). If the vermetid gastropods from all the localities (1686 measurements) are considered together, the shell diameter ranges from 0.19 to 2.84 mm with a mean of 1.28 mm and a standard deviation of 0.46. The thickness of the shells ranges from 0.02 to 0.87 mm, with a mean of 0.28 mm and a standard deviation of 0.13 (Table VII-13).

The size-frequency histograms as well as the frequency histograms of shell thickness of vermetid gastropods show a unimodal distribution (Figs. VII-14 and VII-15). The size-frequency distributions of samples from Boddentown and from the lower ledge at Great Bluff Estates are both show slight positive skew (Fig. VII-14A and B). The frequency histogram of the shells from the loose block at Great Bluff Estates is close to a normal distribution (Fig.VII-14C). However, the results from the normality testing, using the stabilized probability plot (see Chapter 5), suggests that the size distribution from all localities does not follow a normal distribution at the 95% confidence level (Fig. VII-15). The shape of the frequency histograms for shell thickness at a particular locality follows the shape of the size-frequency histograms. The distribution curves of shell thickness from Boddentown and the lower ledge at Great Bluff Estates are positively skewed (Fig. VII-16A & B) while the one from loose block at Great Bluff Estates show approximately normal distribution (Fig. VII-16C).

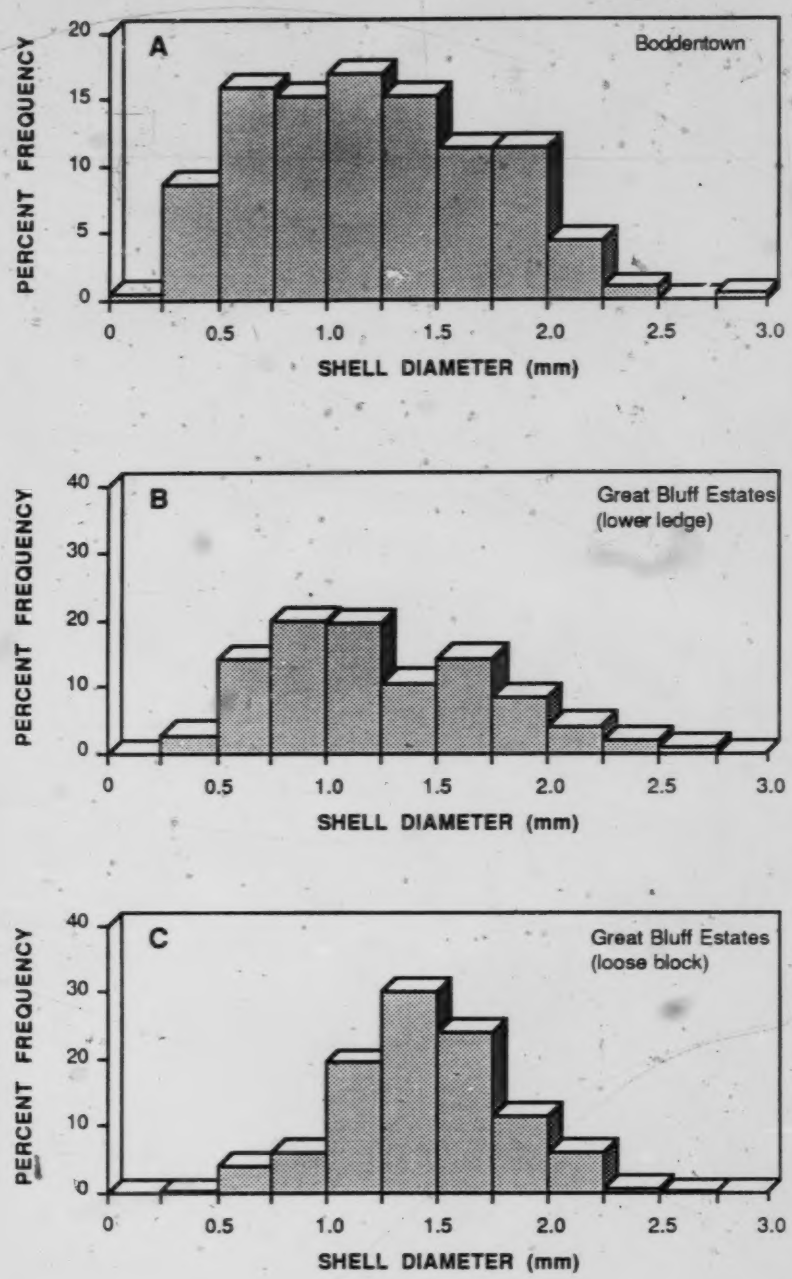

Figure VII-14. Size-frequency histograms of vermetid gastropods from Boddentown (A), lower ledge at Great Bluff Estates (B), and loose block at Great Bluff Estates (C).

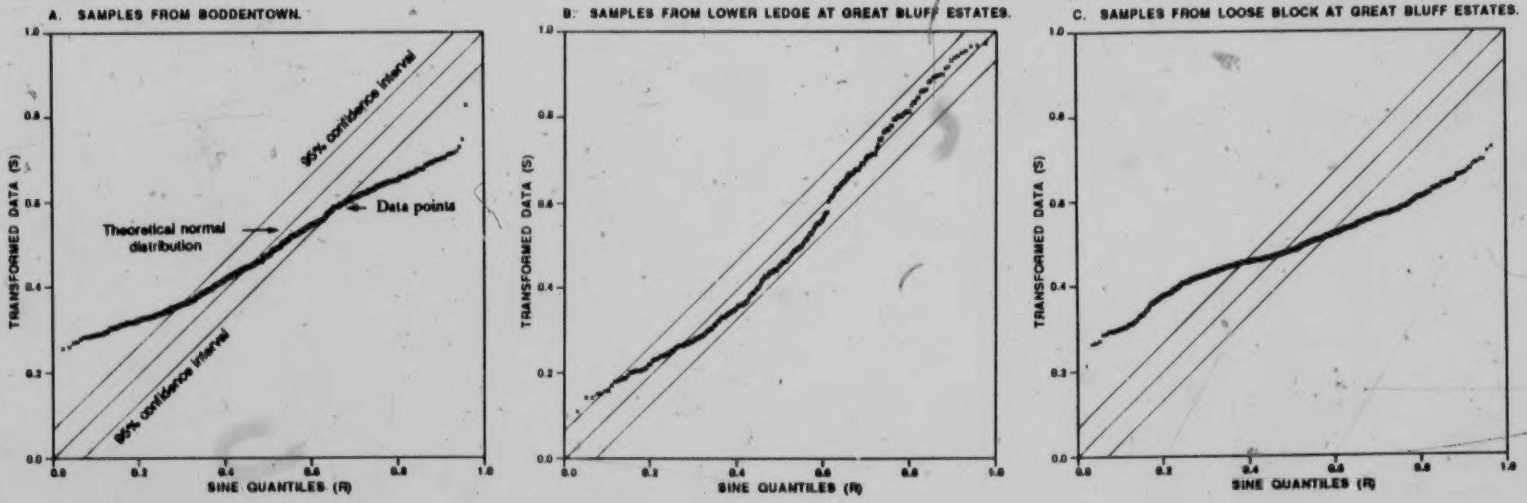

Figure VII-15. The graphs showing the results of normality test of samples from Boddentown (A), lower ledge at Great Bluff Estates (B), and loose block at Great Bluff Estates (C).

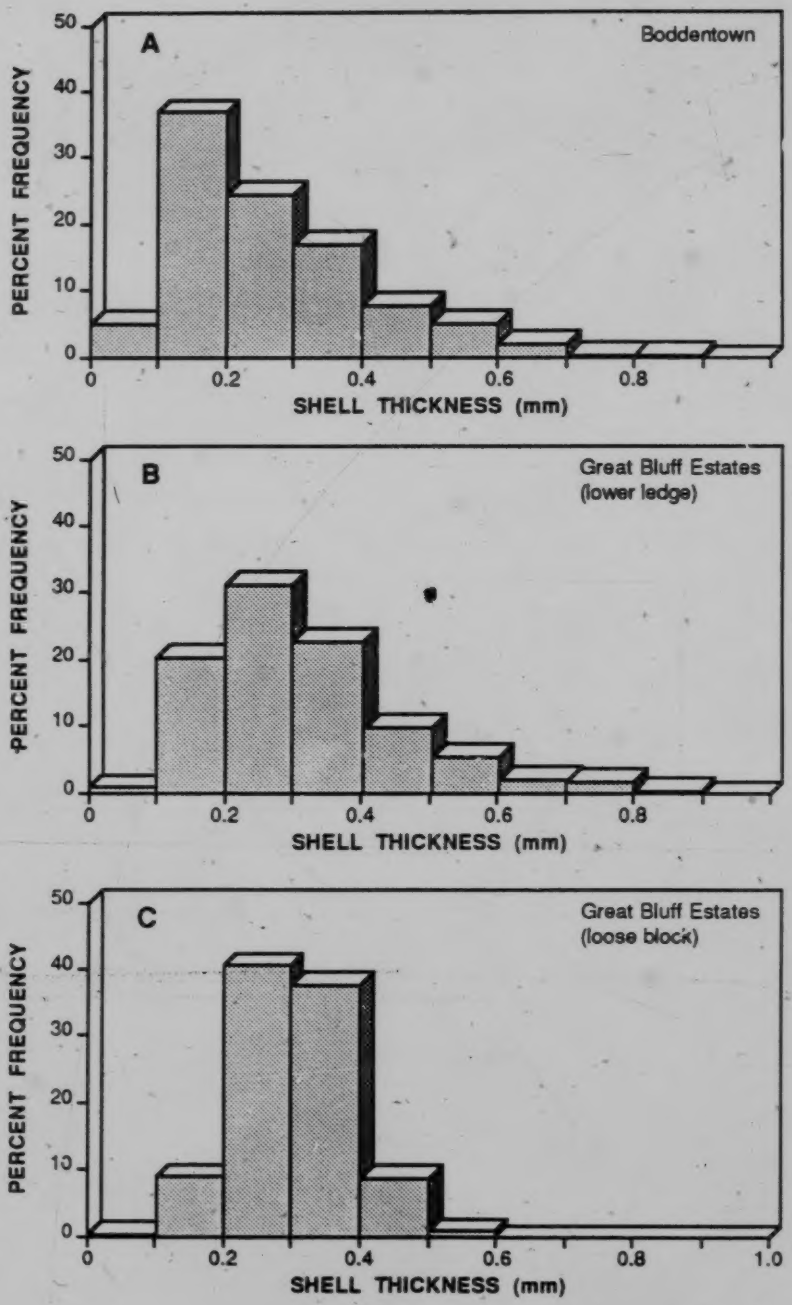

Figure VII-16. Frequency histograms of shell thickness from Boddentown (A), lower ledge at Great Bluff Estates (B), and loose block at Great Bluff Estates (C).

Discussion

Ontogenetic variation

The change of form of vermetid gastropod with ontogeny can be observed in samples from Grand Cayman. Jones and Hunter (1989b) stated that shells from Great Bluff Estates (beach block) were initially tightly coiled but later changed to an almost straight shell. Another change of form of vermetid gastropods, observed in this study, is the relationship in increment of size and thickness of shell with time. Although the absolute time involved is not known for the various growth stages of the same species, the shells of juveniles obviously have a smaller diameter than the shell of mature individuals.

The cross-plots between diameter and thickness of shells from the three localities show a similar trend (Fig. VII-17). In the early stage, both diameter and thickness increase rapidly as shown by the linear trend (the first portion of the curves in Fig. VII-17). This suggests that the growth of vermetid gastropods is the result of the combination of skeletal growth and accretion of shell thickness. The linear trend which would pass through the origin, if extended, suggests isometric growth (Raup and Stanley, 1978). This implies that the ratio of increment in diameter and thickness is relatively constant during the early stages of growth of vermetid gastropods.

In the later stage, the growth curves level off (the second portion of the curve). The increment of the diameter has nearly stopped as the shell diameter approaches 2 mm. The period after completion of growth is commonly referred to as maturity or the true adult stage (Raup and Stanley, 1978). This suggests that shells with diameters of approximately 2 mm represented the adult stage of *Dendropoma (Novastoa)*. The increase in thickness of the shell continued throughout life. This suggests that in the later stage (or the true adult stage) the growth of vermetid gastropods is anisotropic.

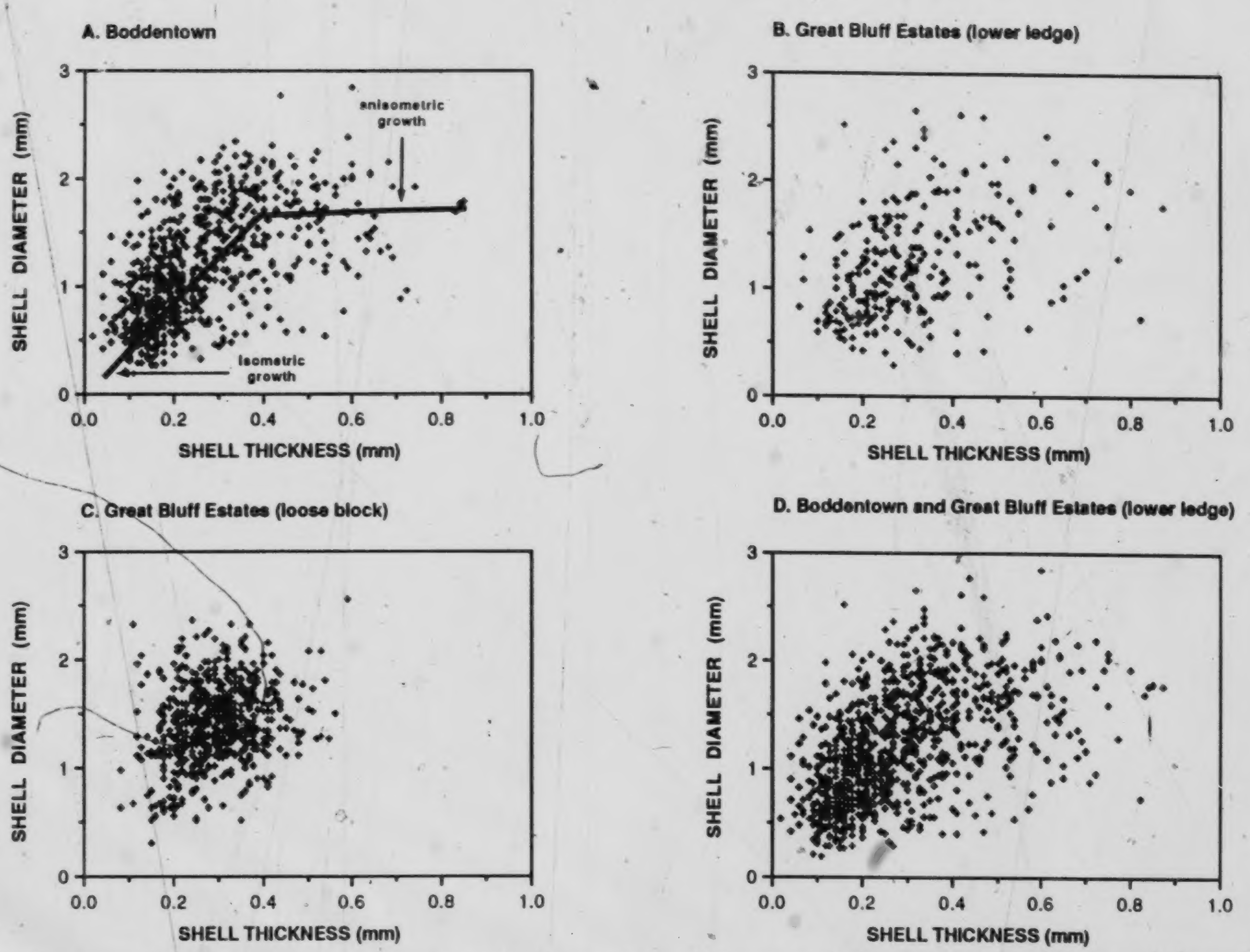

Figure VII-17. The cross-plots between shell diameter and its thickness of vermetid gastropods from Boddentown (A), lower ledge at Great Bluff Estates (B), loose block at Great Bluff Estates (C), and combined Boddentown and lower ledge at Great Bluff Estates (D).

Size-frequency distribution

The formation of the unimodal size-frequency distribution is normally taken to be indicative of a single species (e.g. Kobluk and Nemcsok, 1982; Nield, 1984). In similar manner, the size-frequency histograms of the shells from Grand Cayman suggest the presence of one species.

The mean diameter and size frequency histogram of the shells from the loose block from Great Bluff Estates and those from Boddentown and the lower ledge at Great Bluff Estates are visually different. The range of shell diameter and standard deviation from the loose block at Great Bluff Estates are narrower than those from the other two localities (Table VII-13). In order to test for differences in shell diameter from different localities, the Mann-Whitney *U* test (see Chapter 5) was used. The results of the test (Table VII-14) show that there is no significant difference in the diameter of shells from Boddentown and from the lower ledge at Great Bluff Estates at the 95% confidence level. In other words, it may be concluded that these samples were drawn from identical populations. The diameter of the shells from the loose block at Great Bluff Estates (1.41 mm) are significantly different from those from Boddentown (1.18 mm) and from the lower ledge at Great Bluff Estates (1.24 mm) at the 95% confidence level (Table VII-13 and VII-14). This implies that samples from the loose block at Great Bluff Estates were drawn from different populations. The results of C^{14} dating support this implication. C^{14} dating suggests that the vermetid gastropods from Boddentown and the lower ledge at Great Bluff Estates were approximately the same age, 208 ± 80 years B. P. and 318 ± 90 years B. P., respectively, while the samples of vermetid gastropods from the loose block at Great Bluff Estates were older, 678 ± 90 years B. P. (Jones and Hunter, 1989b).

When data from various sources (e.g. data on C^{14} dating, the results of the Mann-Whitney *U* test) are considered in conjunction with size-frequency distribution, the difference in the appearance size-frequency histograms of *Dendropoma (Novastoa)* may reflect differences in environmental conditions at the time these vermetid buildups were

Table VII-14. Summary of the results of the Mann - Whitney *U* test on diameter of vermetid gastropods. (GBE(BB) = Great Bluff Estates (beach block), GBE(LL) = Great Bluff Estates (lower ledge), and BT = Boddentown).

Location	No. of sample		Z calculated (corrected for ties)	Z for normal distribution (at $\alpha = 0.05$)
	n_1	n_2		
GBE(BB) vs BT	694	723	-9.317	±1.96
GBE(BB) vs GBE(LL)	694	269	-6.429	±1.96
BT vs GBE(LL)	723	269	-1.267	±1.96

formed. A size-frequency distribution depends upon growth rate and survivorship in a particular population or species (Craig and Hallam, 1963). Raup and Stanley (1978) stated that environmental conditions are the most important factors causing variation in survivorship curves (a graph on which the number of survivors is plotted against their age) within species. These environmental factors, in turn, cause the variation in the size-frequency histogram.

Dendropoma (Novastoa) is attached to rocky substrate approximately at the mean sea level where they are exposed to strong wave energy (Sanlaville, 1972; Safriel, 1975; Hughes, 1979; Barash and Zenziper, 1985). The food supply is limited by wave currents. The reproduction of *Dendropoma (Novastoa)* is also dependent on water currents since sperm must be shed into the water before being taken up by the inhalant current of females (Hughes, 1979; Barash and Zenziper, 1985). These shells are unable to move to a new location if local environmental conditions change. Sanlaville (1972) noted that vermetid gastropods cannot survive for long either in or out of water. Those observations indicate that the preservation of *Dendropoma (Novastoa)* is closely related to environmental conditions.

The difference in size-frequency distribution of vermetid buildups which formed approximately 600 and 200 years ago is likely due more to a difference in wave energy than to changes in sea level. During the past 6000 years, the mean sea level in the tropical western Atlantic approximates the present mean sea level (Curray, 1961; Fairbridge, 1961; Shepard, 1963; Lighty *et al.*, 1982). However, oscillations of short period and diminishing amplitude from over 6 m to less than 1 m may occur (Fairbridge, 1961).

The size-frequency distribution of the shells from Boddentown and the lower ledge at Great Bluff Estates may reflect various growth stages of the shells where both juveniles (smaller diameter) and adults (larger diameter) were present. The frequency histograms of shell thickness and the cross-plots of shell diameter and thickness also suggest a similar trend.

The approximately normal distribution of size-frequency of the shells from the loose block at Great Bluff Estates may be explained as being a result of most gastropods dying at an early stage and fewer individuals surviving to the mature stage. The positive skew size-frequency histograms of the shells from the lower ledge at Great Bluff Estates and Boddentown may represent the size distribution of various generations of vermetid gastropods. This suggests that the coastal environment around Grand Cayman was more suitable for vermetid buildups 200 years ago than 600 years ago.

Synopsis

From the study of vermetid gastropods from Grand Cayman, it may be concluded that:

(1) size-frequency histograms suggest that the vermetid buildups around Grand Cayman were formed by one species, *Dendropoma (Novastoa) irregulare*?,

(2) the results from size analysis suggest that coastal environmental conditions around Grand Cayman 600 and 200 years B.P. may not have been the same, and

(3) there is evidence which suggests that *Dendropoma (Novastoa) irregulare*?, changed form with ontogeny in at least 2 aspects: (i) from a tightly coiled shell in the early stage to an almost straight shell in the later stage (Jones and Hunter, 1988), and (ii) in the early stage the relationship between the increment in diameter and thickness of shell is isometric growth (represent by a linear trend) while in the later stage this relationship is anisometric (represent by a linear trend approximately parallel to the X axis).

VII. CONCLUSIONS

The main concerns of this study in the assessment of the use of image analysis in carbonate sedimentology were: (1) concerns about the image-processing techniques, (2) application of image analysis to mapping, and (3) application of image analysis to size analysis.

In order to assess the choice of image-processing techniques, three different image analysers (density slicer, automatic image analyser, and digitized graphic tablet) were used in three problems. It may be concluded that:

(1) there are no general procedures that specify how image analysis should be used in carrying out a given task, i.e. the choice of image-processing techniques are problem-dependent,

(2) the density-slicing technique is suitable for delineating boundaries between areas separated by subtle differences in image tone but it has a limitation in size measurement since only the vertical and horizontal directions can be measured effectively,

(3) the automatic image analyser is useful in analysis of images of a feature which is well-defined and homogeneous in tone, and

(4) the physical dimensions of features in a complex image can be measured with ease using the digitized graphic tablet.

The application of image analysis to mapping was demonstrated by identifying the biologic communities and substrate types in the lagoons around Grand Cayman from aerial photographs. From these experiments it may be concluded that:

(1) the biologic communities and substrate types in the lagoons can be identified on colour and black-and-white aerial photographs, using a density slicer in conjunction with field investigations, with an accuracy of 90%,

(2) misclassification on the aerial photograph maps (compared to the published maps) stems from limitations in the mapping techniques, lack of contrast in tone between different features, and difference in assumptions of mapping techniques,

(3) the aerial photograph maps, which reveal the spatial and temporal characteristics of biologic communities and substrate types, permit more accurate detailed qualitative and quantitative information than visual assessment on the ground, and

(4) quantitative study of changes in the distribution of biological communities and substrate through time suggest that there was an increase in *Thalassia* and decrease in sand in the lagoons along the south coast during 1971 to 1985.

The application of image analysis to size analysis was illustrated by: (1) analysing *Trypanites weisei* from the Late Devonian Waterways Formation, and (2) analysing vermetid gastropods, *Dendropoma (Novastoa) irregulare*? from Grand Cayman. The conclusions on the size analysis of *Trypanites weisei* from the Late Devonian Waterways Formation are as follows:

(1) the results of statistical analysis suggest that, in two dimensions, size of boring is best described by its diameter and size distribution obtained from one thin section can be used to represent the distribution of the whole community, providing there are enough borings in that thin section, and

(2) the percent bored area averaged from a number of sections of the specimen may be the best representative because the percent bored area varies with the portion of the specimen cut for thin section.

From the study of vermetid gastropods from Grand Cayman, it may be concluded that:

(1) based on size-frequency histograms, the vermetid buildups around Grand Cayman was formed by one species, *Dendropoma (Novastoa) irregulare*?,

(2) the cross-plots between the diameter and shell thickness suggested that in the early stage the relationship between the increment in diameter and thickness of shell is isometric growth while in the later stage this relationship is anisometric, and

(3) based on the size distribution of vermetid gastropods and results from radiometric dating, the coastal environmental conditions around Grand Cayman were probably more suitable for vermetid buildups 200 years ago than 600 years ago.

The image analysis described in this study can be easily extended to other applications. The techniques described are faster and provide more accurate results than conventional methods. The mapping technique described in this study can be used advantageously in the reconnaissance stage of a new area since it permits subdivision of the area into the main units. Field investigations, then, can be planned easily and effectively. Optimum results, however, will only be obtained in well exposed areas. Considering the capabilities and the limitations of both instrument and aerial photography, aerial photograph maps can be used to improve the accuracy of quantitative analysis on the rate of the carbonate sedimentation in the lagoons around Grand Cayman.

IX. REFERENCES

Agterberg, F. P., 1981. Application of image analysis and multivariate analysis to mineral resource appraisal. Economic Geology, v. 76, p. 1016-1031.

Agterberg, F. P., and Fabbri, A. G., 1978a. Spatial correlation of stratigraphic units quantified from geologic maps. Computers and Geosciences, v. 4, p. 285-294.

Agterberg, F. P., and Fabbri, A. G., 1978b. Statistical treatment of tectonic and mineral deposit data. Global Tectonics and Metallogeny, v. 1, p. 16-28.

Almasi, M. N., Hoskin, C. M., Reed, J. K., and Milo, J., 1987. Effects of natural and artificial *Thalassia* on rates of sedimentation. Journal of Sedimentary Petrology, v. 57, p. 901-906.

Anderson, J. R., 1971. Land use classification schemes used in selected recent geographic applications of remote sensing. Photogrammetric Engineering, v. 37, p. 379-387.

Anderson, J. R., Hardy, E. E., and Roach, J. T., 1972. A land-use classification system for use with remote sensor data. United States Geological Survey Circular No.671, 16 p.

Aronoff, S., 1982. Classification accuracy: a user approach. Photogrammetric Engineering and Remote Sensing, v. 48, p. 1299-1370.

ASTM designation E-20 51T, 1952. Analysis by microscopical methods for particle size distribution of particulate substances of subsieve sizes. Book of ASTM Standards, Part 3, p. 1574-1583.

Avery, T. E., 1977. Interpretation of aerial photographs, Third Edition. Burgess Publishing Company, Minneapolis, Minnesota, 392 p.

Bak, R. P. M., 1985. Recruitment patterns and mass mortalities in the sea urchin *Diadema antillarum*. Proceedings of the Fifth International Coral Reef Congress, Tahiti, v. 5, p.267-272.

Ball, M. M., Shinn, E. A., and Stockman, K. W., 1967. The geologic effects of Hurricane Donna in south Florida. Journal of Geology, v. 75, p. 583-597.

Barash, A., and Zenziper, Z., 1985. Structural and biological adaptations of Vermetidae (Gastropoda). Il Bollettino Malacologico, v. 21, p. 145-176.

Bartlife, D. J., 1983. An automatic procedure for image segmentation. Pattern Recognition Letters, v. 1, p. 435-442.

Bates, R. L., and Jackson, J. A. (eds.), 1987. Glossary of geology, Third Edition. American Geological Institute, Alexandria, Virginia, 788 p.

Bernatowicz, A. J., 1952. Marine monocotyledonous plants of Bermuda. Bulletin of Marine Science of the Gulf and Caribbean, v. 2, p. 338-345.

Blume, H., 1967. A transformation for extracting new descriptors of shape. *In* Wathen-Dunn, W. (ed.), Models of the perception of speech and visual form. MIT Press, Boston, p. 362-380.

Bouma, A., 1969. Methods for the study of sedimentary structures. John Wiley & Sons, New York, 458 p.

Bradbury, S., 1979. Microscopic image analysis: problem and approaches. Journal of Microscopy, v. 115, p. 137-150.

Brenner, J. F., Lester, J. M., and Selles, W. D., 1981. Scene segmentation in automated histopathology: techniques evolved from cytology automation. Pattern Recognition, v. 13, p. 65-77.

Bromley, R. G., 1981. Enhancement of visibility of structures in marly chalk: modification of the Bushinsky oil technique. Bulletin of Geological Society of Denmark, v. 29, p. 111-118.

Browning, J. D., and Tanimoto, S. L., 1982. Segmentation of pictures into regions with a tile-by-tile method. Pattern Recognition, v. 15, p. 1-10.

Brunt, M. A., Giglioli, M. E., Mather, J. D., Piper, D. J., and Richards, H. G., 1973. The Pleistocene rocks of the Cayman Islands. Geological Magazine, v. 110, p. 209-221.

Calabi, L., and Hartnett, W. E., 1968. Shape recognition, prairie fires, convex deficiencies and skeletons. American Mathematical Monthly, v. 75, p. 335-342.

Carpenter, R. C., 1985. Sea urchin mass-mortality: effects on reef algal abundances, species composition, and metabolism and other coral reef herbivores. Proceedings of the Fifth International Coral Reef Congress, Tahiti, v. 4, p. 53-60.

Carpenter, R. C., 1988. Mass mortality of a Caribbean sea urchin: immediate effects on community metabolism and other herbivores. Proceedings of the National Academy of Science, v. 85, p. 511-514.

Castleman, K. R., 1979. Digital image processing. Prentice-Hall, Englewood Cliffs, New Jersey, 429 p.

Chao, E. C. T., Minkin, J. A., and Thompson, C. L., 1982. Application petrographic characterization of coal lithology. Journal of Coal Petrology, v. 2, p. 113-150.

Chayes, F., 1949. A simple point counter for thin-section analysis. American Mineralogist, v. 34, p. 1-11.

Chayes, F., 1956. Petrographic modal analysis. John Wiley & Sons, New York, 113 p.

Cochran, W. G., 1963. Sampling techniques. John Wiley & Sons, New York, 413 p.

Cole, M., 1971. Instrument errors in quantitative image analysis. Microscope, v. 19, p. 87-103.

Collins, R. E., 1961. Flow of fluids through porous materials. Reinhold Publishing Corporation, New York, 270 p.

Colwell, R. N. (ed.), 1983. Manual of remote sensing, Second Edition. American Society of Photogrammetry, Fall Church, Virginia, 2440 p.

Congalton, R., and Rekas, A., 1985. COMPAR: A computerized technique for the in-depth comparison of remotely sensed data. Proceedings of the 51th Annual Meeting of the American Society of Photogrammetry, Washington, D. C., p. 98-106.

Craig, G. Y., and Hallam, A., 1963. Size-frequency and growth-ring analyses of *Mytilus edulis* and *Cardium edule*, and their paleoecological significance. Palaeontology, v. 6, p. 731-750.

Crelling, J. C., 1982. Automated petrographic characterization of coal lithology. Journal of Coal Geology, v. 1, p. 347-359.

Crutwell, I. A., 1974. Pattern recognition by automatic image analysis. Microscope, v. 22, p. 27-37.

Curray, J. R., 1961. Late Quaternary sea level: a discussion. Geological Society of America Bulletin, v. 72, p. 1707-1712.

Dalton, R., Garlick, J., Minshull, R., and Robinson, A., 1975. Sampling techniques in geography. George Phillip and Son Ltd., London, 95 p.

Davis, A., Kuehn, K. W., Maylotte, D. H., and Peters, R. L. St., 1983. Mapping of polished coal surfaces by automated reflectance microscopy. Journal of Microscopy, v. 132, p. 297-302.

Davis, J.C., 1986. Statistics and data analysis in geology, Second Edition. John Wiley & Sons, New York, 646 p.

Davis, L. S., 1975. A survey of edge detection techniques. Computer Graphics and Image Processing, v. 4, p. 248-270.

Deravi, F., and Pal, S. K., 1983. Grey level thresholding using second-order statistics. Pattern Recognition Letters, v. 1, p. 417-422.

Dietterich, R. J., and Full, W. E., 1986. Pore analysis of Mississippian carbonate reservoir in Southwest Kansas using Petrographic Image Analysis. American Association of Petroleum Geologists Bulletin, v. 70, p. 582.

Dilks, A., and Graham, S. C., 1985. Quantitative mineralogical characterization of sandstones by back-scattered electron image analysis. Journal of Sedimentary Petrology, v. 55, p. 347-355.

Dorobek, S. L., 1987. Petrography, geochemistry, and origin of burial diagenetic facies, Siluro-Devonian Helderberg Group (Carbonate Rocks), Central Appalachians. American Association of Petroleum Geologists Bulletin, v. 71, p. 492-514.

Dorobek, S. L., Read, J. F., Niemann, J. M., Pong, T. C., and Haralick, R. M., 1987. Image analysis of cathodoluminescent-zoned calcite cements. Journal of Sedimentary Petrology, v. 57, p. 766-770.

Drury, S. A., 1987. Image interpretation in geology. Allen & Unwin Ltd., London, 243 p.

Duda, R. O., and Hart, P. E., 1973. Pattern classification and scene analysis. John Wiley & Sons, New York, 482 p.

Ehrlich, R., Crabtree, S. J., Kennedy, S. K., and Cannon, R. L., 1984. Petrographic image analysis, I. Analysis of reservoir pore complexes. Journal of Sedimentary Petrology, v. 54, p. 1365-1378.

Ekdale, A. A., Bromley, R. G., and Pemberton, S. G., 1984. Ichnology: the use of trace fossil in sedimentology and stratigraphy. Society of Economic Paleontologists and Mineralogists Short Course No. 15, Tulsa, Oklahoma, 317 p.

Emery, K. O., 1981. Low marine terraces of Grand Cayman Island. Estuarine Coastal and Shelf Science, v. 12, p. 569-578.

England, B. M., Mikka, R. A., and Bagnall E. J., 1979. Petrographic characterization of coal using automatic image analysis. Journal of Microscopy, v. 116, p. 329-336.

Fabbri, A. G., 1980. GIAPP: Geological image-analysis program package for estimating geometrical probabilities. Computers & Geosciences, v. 6, p. 153-161.

Fabbri, A. G., 1981. Image processing of coincident binary patterns from geological and geophysical maps of mineralized area. Proceedings of the Canadian Man-Computer Communication Society, Seventh Conference, June 10-12, 1981, Waterloo, Ontario, p. 323-333.

Fabbri, A. G., 1984. Image processing of geological data. Van Nostrand Reinhold Company Inc., New York, 244 p.

Fabbri, A. G., and Kasvand, T., 1978. Picture processing of geological images. Geological Survey Canada Paper 78-1B, p. 169-174.

Fairbridge, R. W., 1961. Eustatic changes in sea level. *In* Ahrens, L. H., Press, F., Rankama, K., and Runcorn, S. K. (eds.), Physics and chemistry of the earth. Pergamon Press, New York, p. 99-185.

Farrow, G. E., 1975. Techniques for the study of fossil and recent traces. *In* Frey, R. W. (ed.), The study of trace fossils. Springer-Verlag, New York, p. 537-554.

Fitzpatrick-Lins, K., 1981. Comparison of sampling procedure and data analysis for a land-use and land cover map. Photogrammetric Engineering and Remote Sensing, v. 47, p. 343-351.

Folk, R. L., Roberts, H. H., and Moore, C. H., 1973. Black phytokarst from Hell, Cayman Islands, British West Indies. Bulletin of the Geological Society of America, v. 84, p. 2351-2360.

Foster, A. B., Kenneth, G. J., and Schultz, L. L., 1988. Allometric shape change and heterochrony in the freeliving coral *Trachyphyllia bilobata* (Duncan). Coral Reefs, v. 7, p. 37-44.

Freund, J. E., and Williams, F. J., 1977. Elementary business statistics the modern approach, Third Edition. Prentice-Hall, Englewood Cliffs, New Jersey, 560 p.

Fu, K. S., and Mui, J. K., 1981. A survey on image segmentation. Pattern Recognition, v. 13, p. 3-16.

Gadgil, P. D., 1963. Soil sections of grassland. *In* Doeksen, J., and van der Drift, J. (eds.), Soil organisms. North-Holland, Amsterdam, p. 327-332.

Ginevan, M. E., 1979. Testing land-use map accuracy: another look. Photogrammetric Engineering and Remote Sensing, v. 45, p. 1371-1377.

Ginsburg, R. N., 1956. Environmental relationships of grain size and constituent particles in some south Florida carbonate sediments. American Association of Petroleum Geologists Bulletin, v. 40, p. 2384-2427.

Ginsburg, R. N., and Lowenstam, H. A., 1958. The influence of marine bottom communities on the depositional environment of sediments. Journal of Geology, v. 66, p. 310-318.

Goetcherian, V., 1980. From binary to grey tone image processing using fuzzy logic concepts. Pattern Recognition, v. 12, p. 7-15.

Goldstein, D. J., 1970. Aspects of scanning microdensitometry. I. Stray light (glare). Journal of Microscopy, v. 92, p. 4-16.

Golubic, S., Perkins, R. D., and Lukas, K. J., 1975. Boring microorganisms and microborings in carbonate substrates. *In* Frey, R. W. (ed.), The study of trace fossils. Springer-Verlag, New York, p. 229-259.

Gonzalez, R. C., and Wintz, P., 1987. Digital image processing, Second Edition. Addison-Wesley, Reeding, Massachusetts, 503 p.

Grover, G. A., and Read J. F., 1983. Paleoaquifer and deep burial related cements defined by regional cathodoluminescent patterns, Middle Ordovician carbonates, Virginia. American Association of Petroleum Geologists Bulletin, v. 67, p. 1275-1303.

Haberäcker, P., 1983. Digital image processing. *In* Cracknell, A. P. (ed.), Remote sensing applications in marine science and technology. D. Reidel Publishing Company, Lancaster, p. 83-185.

Hageman, S. J., 1988. Image processing and analysis with microcomputers. Journal of Paleontology, v. 62, p. 474-477.

Hahn, G. J., and Shapiro, S. S., 1967. Statistical models in engineering. John Wiley & Sons, New York, 355 p.

Hamblin, W. K., 1962a. X-ray radiography in the study of structures in homogeneous sediments. Journal of Sedimentary Petrology, v. 32, p. 201-210.

Hamblin, W. K., 1962b. Staining and etching techniques for studying obscure structures in clastic rocks. Journal of Sedimentary Petrology, v. 32, p. 530-533.

Haralick, R. M., Shanmugam, K., and Dinstein, I., 1973. Textural features for image classification. IEEE Transactions on Systems, Man and Cybernetics, v. SMC-3, p. 610-621.

Harris, W. D., and Umbach, M. J., 1972. Underwater mapping. Photogrammetric Engineering, v. 38, p. 765-772.

Hartog, C. den., 1977. Structure, function, and classification in seagrass communities. *In* McRoy, C. P., and Helfferich, C. (eds.), Seagrass ecosystems. Marcel Dekker, Inc., New York, p. 89-121.

Hathout, S. A., and Forrest, D., 1980. Use of the multidata Landsat image enhancement method for mapping the proposed area for Atikaki National Park. Canadian Surveyor, v. 34, p. 196-200.

Hayward, A. T. J., 1977. Repeatability and accuracy. Mechanical Engineering Publication Ltd., London, 63 p.

Hein, F. J., and Risk, M. J., 1975. Bioerosion of coral heads: inner patch reefs, Florida reef tract. Bulletin of Marine Science, v. 25, p. 133-138.

Hoel, P. G., 1982. Basic statistics for business and economics, Third Edition. John Wiley & Sons, New York, 629 p.

Hoffer, R. M., and Johannsen, C. J., 1969. Ecological potentials in spectral signature analysis. *In* Johnson, P. L. (ed.), Remote sensing in ecology. University of Georgia Press, Athens, p. 1-16.

Holmes, R. W., 1957. Solar radiation, submarine daylight and photosynthesis. *In* Hedgepeth, J. W. (ed.), Treatise on marine ecology. Geological Society of America Memoir 67(i), p. 109-128.

Hopley, D., 1978. Aerial photography and other remote sensing techniques. *In* Stoddart, D. R., and Johannes, R. E. (eds.), Coral reefs: research methods. UNESCO, Paris, p. 23-44.

Hughes, R. N., 1979. Coloniality in Vermetidae (Gastropoda). *In* Larwood, G., and Rosen, B. R. (eds.), Biology and systematics of colonial organisms. Academic Press, London, p. 243-253.

Hughes, T. P., Keller, B. D., Jackson, J. B. C., and Boyle, M. J., 1985. Mass mortality of the echinoid *Diadema antillarum* Philippi in Jamaica. Bulletin of Marine Science, v. 36, p. 377-384.

Humm, H. J., 1964. Epiphytes of the seagrass *Thalassia testudinum*, in Florida. Bulletin of Marine Science of the Gulf and Caribbean, v. 14, p. 306-341.

Hunte, W., Côtè, I., and Tomascik, T., 1986. On the dynamics of the mass mortality of *Diadema antillarum* in Barbados. Coral Reefs, v. 4, p. 135-139.

Hunter, I. G., and Jones, B., (1989). Corals and paleogeography of the Pleistocene Ironshore Formation of Grand Cayman. Proceedings of the Sixth International Coral Reef Symposium, Townsville, Australia, in press.

Inman, D. L., Gayman, W. R., and Cox, D. C., 1963. Littoral sedimentary processes on Kauai, a subtropical high island. Pacific Science, v. 17, p. 106-130.

Jarvis, L. R., 1981. Microdensitometry with image analyser video scanners. Journal of Microscopy, v. 121, p. 337-346.

Jerlov, N. G., 1966. Aspects of light measurement in the sea. *In* Bainbridge, R., Evans, G. C., and Rackham, O. (eds.), Light as an ecological factor. Blackwell Scientific Publications, Oxford, p. 91-98.

Jones, B., 1988a. Biostatistics in paleontology. Geoscience Canada, v. 15, p. 3-21.

Jones, B., 1988b. A field guide to the geology of the Cayman Islands. University of Alberta, Edmonton, 75 p.

Jones, B., and Goodbody, Q. H., 1984. Biological factors in the formation of quiet-water ooids. Bulletin of Canadian Petroleum Geology, v. 32, p. 190-200.

Jones, B., and Hunter, I. G., (1989a). The Oligocene-Miocene Bluff Formation on Grand Cayman. Caribbean Journal of Science, in press.

Jones, B., and Hunter, I. G., (1989b). Vermetid gastropod buildups from Grand Cayman, British West Indies. Journal of Paleontology, in press.

Jones, B., and Pemberton, S. G., (1989). Anatomy of an unconformity bounded carbonate sequence: the Pleistocene Ironshore Formation, Salt Creek, Grand Cayman. Palaios, in press.

Jones, B., Lockhart, E. B., and Squair, C., 1984. Phreatic and vadose cements in the Tertiary Bluff Formation of Grand Cayman Island, British West Indies. Bulletin of Canadian Petroleum Geology, v. 32, p. 382-397.

Joyce-Loebl (ed.), 1985. Image analysis: principles and practice. Short Run Press, Exeter, 250 p.

Kasvand, T., Fabbri, A. G., and Nel, L. D., 1981. Digitization and processing of large regional maps. National Research Council of Canada, Division of Electrical Engineering, ERB - 938, NRCC No. 19746, 91 p.

Kelly, M. G., and Conrod. A., 1969. Aerial photographic studies of shallow water benthic ecology. *In* Johnson, P. L. (ed.), Remote sensing in ecology. University of Georgia Press, Athens, p. 173-184.

Kershaw, S. J., 1980. Cavities and cryptic faunas beneath non-reef stromatoporoids. Lethaia, v. 13, p. 327-338.

Kershaw, S. J., and Riding, R., 1978. Parameterization of stromatoporoid shape. Lethaia, v. 11, p. 233-242.

Klapper, G., and Foster, C. T., 1986. Quantification of outlines in Frasnian (Upper Devonian) platform conodonts. Canadian Journal of Earth Sciences, v. 23, p. 1214-1222.

Kobluk, D. R., and Kozelj, M., 1985. Recognition of a relationship between depth and macroboring distribution in growth framework reef cavities, Bonaire, Netherlands Antilles. Bulletin of Canadian Petroleum Geology, v. 33, p. 462-470.

Kobluk, D. R., and Nemcsok, S., 1982. The macroboring ichnofossil *Trypanites* in colonies of the Middle Ordovician bryozoan *Prasopora*: population behaviour and reaction to environmental influences. Canadian Journal of Earth Sciences, v. 19, p. 679-688.

Kobluk, D. R., James, N. P., and Pemberton, S. G., 1978. Initial diversification of macroboring ichnofossils and exploitation of the macroboring niche in the lower Paleozoic. Paleobiology, v. 4, p. 163-170.

Kohn, A. J., and Helfrich, P., 1957. Primary organic productivity of a Hawaiian coral reef. Limnology and Oceanography, v. 2, p. 241-251.

Land, L. S., 1970. Carbonate mud: production by epibiont growth by *Thalassia testudinum*. Journal of Sedimentary Petrology, v. 40, p. 1361-1363.

Lazarus, D., 1986. Three-dimensional measurement of microfossil morphology. Journal of Paleontology, v. 60, p. 960-964.

Lepley, L. K., 1968. Coastal water clarity from space photographs. Photogrammetric Engineering, v. 34, p. 667-674.

Lessios, H. A., Cubit, J. D., Robertson, D. R., Shulman, M. J., Parker, M. R., Garrity, S. D., and Levings, S. C., 1984. Mass mortality of *Diadema antillarum* on the Caribbean coast of Panama. Coral Reefs, v. 3, p. 173-182.

Lighty, R. G., Macintyre, I. G., and Stuckenrath, R., 1982. *Acropora palmata* reef framework: a reliable indicator of sea level in the western Atlantic for the past 10,000 years. Coral Reefs, v. 1, p. 125-130.

Lison, L., 1953. Schwarzschild-Villiger effect in microspectrophotometry. Science, v. 118, p. 382-383.

Lumia, R., Haralick, R. M., Zuniga, O., Shapiro, L., Pong, T., and Wang, F., 1983. Texture analysis of aerial photographs. Pattern Recognition, v. 16, p. 39-46.

Lynts, G. W., 1966. Relationship of sediment-size distribution to ecologic factors in Buttonwood Sound, Florida Bay. Journal of Sedimentary Petrology, v. 36, p. 66-74.

MacGeachy, J. K., 1975. Boring by macro-organisms in the coral *Montastrea annularis* on Barbados reefs. Unpublished M. Sc. Thesis, McGill University, 83 p.

MacGeachy, J. K., and Stearn, C. W., 1976. Boring by macro-organisms in the coral *Montastrea annularis* on Barbados. Internationale Revue der Gesamten Hydrobiologie, v. 16, p. 715-745.

Matley, C. A., 1926. The geology of the Cayman Islands (British West Indies) and their relation to the Bartlett Trough. Quarterly Journal of the Geological Society of London, v. 82, p. 352-387.

Maxwell, E. A., 1983. Introduction to statistical thinking. Prentice-Hall, Inc., Englewood Cliffs, New Jersey, 574 p.

Mazzullo, J. K., and Kennedy, S. K., 1985. Automated measurement of the nominal sectional diameters of individual sedimentary particles. Journal of Sedimentary Petrology, v. 55, p. 593-596.

McRoy, C. P., and McMillan, C. 1977. Production ecology and physiology of seagrasses. *In* McRoy, C. P., and Helfferich, C. (eds), Seagrass ecosystems. Marcel Dekker Inc., New York, p. 53-88.

Merriam, D. F., 1981. Roots of quantitative geology. *In* Merriam, D. F. (ed.), Down-to-earth statistics: solution looking for geological problems. Syracuse University Geology Contribution 8, p. 1-15.

Michael, J. R., 1983. The stabilized probability plot. Biometrika, v. 70, p. 11-17.

Minnis, M. M., 1984. An automatic point-counting method for mineralogical assessment. American Association of Petroleum Geologists Bulletin, v. 68, p. 744-752.

Moore, C. H., 1973. Intertidal carbonate cementation, Grand Cayman, West Indies. Journal of Sedimentary Petrology, v. 43, p. 591-602.

Moore, D. R., 1963. Distribution of the sea grass, *Thalassia*, in the United States. Bulletin of Marine Science of the Gulf and Caribbean, v. 13, p. 329-342.

Moore, G. A., 1968. Automatic scanning and computer processes for the quantitative analysis of micrographs and equivalents subjects. *In* Cheng, G. C., Ledley, R. S., Pollock, D. K., and Rosenfeld, A. (eds.), Pictorial pattern recognition. Thompson Book Company, Washington, D. C., p. 275-326.

Nelsen, J. E. Jr., and Ginsburg, R. N., 1986. Calcium carbonate production by epibionts on *Thalassia* in Florida Bay. Journal of Sedimentary Petrology, v. 56, p. 622-628.

Nield, E. W., 1984. The boring of Silurian stromatoporoids-towards an understanding of larval behaviour in the *Trypanites* organism. Palaeogeography, Palaeoclimatology, Palaeoecology, v. 48, p. 229-243.

Ogden, J. C., Brown, R. A., and Salesky, N., 1973. Grazing by the echinoid *Diadema antillarum* Philippi: formation of halos around West Indian patch reefs. Science, v. 182, p. 715-717.

Paine, D. P., 1981. Aerial photography and image interpretation for resource management. John Wiley & Sons, New York, 571 p.

Paler, K., and Kittler, J., 1983. Grey level edge thinning: a new method. Pattern Recognition Letters, v. 1, p. 409-416.

Patriquin, D. G., 1972. Carbonate mud production by epibionts on *Thalassia*: an estimate based on leaf growth rate data. Journal of Sedimentary Petrology, v. 42, p. 687-689.

Patriquin, D. G., 1975. "Migration" of blowouts in seagrass beds at Barbados and Carriacou, West Indies, and its ecological and geological implications. Aquatic Botany, v. 1, p. 163-189.

Pavlidis, T., 1977. Structural pattern recognition. Springer-Verlag, New York, 302 p.

Pemberton, S. G., and Jones, B., 1988. Ichnology of the Pleistocene Ironshore Formation, Grand Cayman Island, British West Indies. Journal of Paleontology, v. 62, p. 495-505.

Pemberton, S. G., Jones, B., and Edgecombe, G., 1988. The influence of *Trypanites* in the diagenesis of Devonian stromatoporoids. Journal of Paleontology, v. 62, p. 22-31.

Pemberton, S. G., Kobluk, D. R., Yeo, R. K., and Risk, M. J., 1980. The boring *Trypanites* at the Silurian-Devonian disconformity in southern Ontario. Journal of Paleontology, v. 54, p. 1258-1266.

Perfit, M. R., and Heezen, B. C., 1978. The geology and evolution of the Cayman Trench. Bulletin of the Geological Society of America, v. 89, p. 1155-1174.

Petruk, W., 1976. The application of quantitative mineralogical analysis of ores to ore dressing. Canadian Institute of Mining and Metallurgy Bulletin, v. 69, p. 146-153.

Pettijohn, F. J., 1975. Sedimentary rocks, Third Edition. Harper & Row, New York, 628 p.

Piepe, W., and Steller, M., 1984. Characterization of coal and coal blends by automatic image analysis. Fuel, v. 63, p. 313-317.

Pleydell, S. M., 1987. Aspects of diagenesis and ichnology in the Oligocene-Miocene Bluff Formation of Grand Cayman Island, British West Indies. Unpublished M.Sc. Thesis, University of Alberta, Edmonton, 209 p.

Pleydell, S. M., and Jones, B., 1988. Boring of various faunal elements in the Oligocene-Miocene Bluff Formation of Grand Cayman, British West Indies. Journal of Paleontology, v. 62, p. 348-367.

Pong. T., Haralick, R. M., Craig, J. R., Yoon, R., and Choi, W., 1983. The application of image analysis techniques to mineral processing. Pattern Recognition Letters, v. 2, p. 117-123.

Prieur, L., and Sathyendranath, S., 1981. An optical classification of coastal and oceanic waters based on the specific absorption curves of phytoplankton pigments, dissolved organic matter, and other particulate material. Limnology and Oceanography, v. 26, p. 671-689.

Raup, D. M., and Stanley, S. M., 1978. Principles of paleontology, Second Edition. W. H. Freeman and Company, San Francisco, 481 p.

Ray, R. G., 1960. Aerial photographs in geologic interpretation and mapping. United States Geological Survey Professional Paper 373, 230 p.

Reeves, R. G. (ed.), 1975. Manual of remote sensing, Second Edition. American Society of Photogrammetry, Fall Church, Virginia, 2144 p.

Rhoads, D. C., and Stanley, D. J., 1966. Transmitted infra-red radiation: a simple method for studying sedimentary structures. Journal of Sedimentary Petrology, v. 36, p. 1144-1149.

Rigby, J. K., and Roberts, H. H., 1976. Geology, reefs and marine communities of Grand Cayman Island, British West Indies. *In* J. K. Rigby and H. H. Roberts (eds.), Grand Cayman Island: Geology, Sediments and Marine Communities. Bringham Young University Geology Studies Special Publication, No. 4, p. 1-95.

Rink, M., 1976. A computerized qualitative image analysis procedure for investigating features and an adapted image process. Journal of Microscopy, v. 107, p. 267-286.

Rink, M., and Schopper, J. R., 1978. On the application of image analysis to formation evaluation. The Log Analyst, January-February, p. 12-22.

Riseman, E. M., and Arbib, M. A., 1977. Computational techniques in the visual segmentation of static scenes. Computer Graphics and Image Processing, v. 6, p. 221-276.

Risk, M. J., and Szczuczko, R. B., 1977. A method for staining trace fossils. Journal of Sedimentary Petrology, v. 47, p. 855-859.

Roberts, H. H., 1971a. Environments and organic communities of North Sound, Grand Cayman Island, B.W.I. Caribbean Journal of Science, v. 11, p. 67-79.

Roberts, H. H., 1971b. Mineralogical variation in lagoonal carbonates from North Sound, Grand Cayman Island (British West Indies). Sedimentary Geology, v. 59, p. 85-103.

Roberts, H. H., 1976. Carbonate sedimentation in a reef-enclosed lagoon, North Sound, Grand Cayman Island. *In* J. K. Rigby and H. H. Roberts (eds.), Grand Cayman Island: Geology, Sediments and Marine Communities. Bringham Young University Geology Studies Special Publication, No. 4, p. 97-122.

Roberts, H. H., and Sneider, R. M., 1982. Reefs and associated sediments of Grand Cayman Island, B.W.I.: Recent carbonate sedimentation. Geological Society of America Field Trip Guidebook, New Orleans, Louisiana, 51 p.

Roberts, H. H., Murray, S. P., and Suhayda, J. N., 1975. Physical processes in a fringing reef system. Journal of Marine Research, v. 33, p. 233-260.

Robertson, L., 1986. Multiarea measurement from maps and soil thin sections using a microcomputer and graphic tablet. *In* Hanley, J. T., and Merriam, D. F. (eds.), Microcomputer applications in geology. Pergamon Press, New York, p. 237-255.

Robinson, I. S., 1985. Satellite oceanography. Ellis Horwood Ltd., Chichester, 455 p.

Roessler, M. A., 1971. Environmental changes associated with a Florida power plant. Marine Pollution Bulletin, v. 2, p. 87-90.

Rosenfeld, A., 1984. Image analysis: problems, progress and prospects. Pattern Recognition, v. 17, p. 3-12.

Rosenfeld, A., and Kak, A. C., 1982a. Digital picture processing, Volume 1, Second Edition. Academic Press, New York, 435 p.

Rosenfeld, A., and Kak, A. C., 1982b. Digital picture processing, Volume 2, Second Edition. Academic Press, New York, 349 p.

Rosenfield, G. H., 1982. Sample design for estimating change in land use and land cover. Photogrammetric Engineering and Remote Sensing, v. 48, p. 793-801.

Rudd, R. D., 1971. Macro land use mapping with simulated space photos. Photogrammetric Engineering, v. 37, p. 365-372.

Russ, J. C., 1985. Practical stereology. Special Printing for Dapple Systems Inc., Sunnyvale, California, 115 p.

Russ, J. C., and Russ, J. C., 1984. Image processing in a general purpose microcomputer. Journal of Microscopy, v. 135, p. 89-102.

Ruzyla, K., 1986. Characterization of pore space by quantitative image analysis. SPE Formation Evaluation, v. 1, p. 389-398.

Sabins, F. F., 1987. Remote sensing: principles and interpretation, Second Edition. W. H. Freeman and Company, San Francisco, 449 p.

Safriel, U. N., 1975. The role of vermetid gastropods in the formation of Mediterranean and Atlantic reefs. Oecologia, v. 20, p. 85-101.

Sanlaville, P., 1972. *Vermetus* dating of changes in sea-level. Underwater archaeology a nascent discipline, UNESCO, Paris, p. 185-191.

Sathyendranath, S., and Morel, A., 1983. Light emerging from the sea - interpretation and uses in remote sensing. *In* Cracknell, A. P. (ed.), Remote sensing applications in marine science and technology. D. Reidel Publishing Company, Lancaster, p. 323-357.

Schäfer, A., Weissbrod, T., and Sneh, A., 1981. Application of the Kontron Videoplan method in determining the grain-size distribution and shape of Nubian sandstones from thin sections. Geological Survey of Israel Current Research 1981, p. 15-17.

Schwarzschild, K., and Villiger, W., 1906. On the distribution of brightness of the ultra-violet light on the sun's disk. Astrophysical Journal, v. 23, p. 284-305.

Scoffin, T. P., 1970. The trapping and binding of subtidal carbonate sediments by marine vegetation in Bimini Lagoon, Bahama. Journal of Sedimentary Petrology, v. 40, p. 249-273.

Serra, J., 1982. Image analysis and mathematical morphology. Academic Press Inc., London, 610 p.

Shepard, F. P., 1963. Thirty-five thousand years of sea level. *In* Clements, T., Stevenson, R. E., and Halmeess, D. M. (eds.), Essays in marine geology in honour of K. O. Emery. University of Southern California Press, Los Angeles, p. 1-10.

Silk, J., 1979. Statistical concepts in geography. George Allen & Unwin Ltd., London, 276 p.

Simonett, D. S., 1974. Quantitative data extraction and analysis of remote sensor images. *In* Estes, J. E., and Senger, L. W. (eds.), Remote Sensing: techniques for environmental analysis. Hamilton Publishing Co., Santa Barbara, California, p. 51-81.

Srivastava, G. S., 1977. Optical processing of structural contour maps. Journal of the International Association for Mathematical Geology, v. 9, p. 3-38.

Stockman, K. W., Ginsburg, R. N., and Shinn, E. A., 1967. The production of lime mud by algae in south Florida. Journal of Sedimentary Petrology, v. 37, p. 633-648.

Stoddart, D. R., 1963. Effects of hurricane Hattie on the British Honduras reefs and cays. October 30-31, 1961. Atoll Research Bulletin, No. 95, p. 1-142.

Stone, K. H., 1956. Air photo interpretation procedures. Photogrammetric Engineering, v. 22, p. 123-132.

Story, M., and Congalton, R. G., 1986. Accuracy assessment: a user's perspective. Photogrammetric Engineering and Remote Sensing, v. 52, p. 397-399.

Suk, M., and Chung, S. M., 1983. A new image segmentation technique based on partition mode test. Pattern Recognition, v. 16, p. 469-480.

Swenson, R. A., and Attle, J. R., 1979. Counting, measuring, and classifying with image analysis. American Laboratory, April, p. 51-68.

Swinchatt, J. P., 1965. Significance of constituent composition, texture and skeletal breakdown in some recent carbonate sediments. Journal of Sedimentary Petrology, v. 35, p. 17-90.

Switzer, P., 1976. Applications of random process models to the description of spatial distributions of qualitative geologic variables. *In* Merriam, D. F. (ed.), Random processes in geology. Springer-Verlag, New York, p. 124-134.

Thomas, L.P., Moore, D. R., and Work, R. C., 1961. Effects of Hurricane Donna on the turtle grass beds of Biscayne Bay, Florida. Bulletin of Marine Science of the Gulf and Caribbean, v. 11, p. 191-197.

Thomson, E., 1930. Quantitative microscopic analysis. Journal of Geology, v. 38, p. 193.

Thomson, G. H., 1973. Photographic limitations in density slicing. The ITC Journal, p. 512-514.

Till, R., 1974. Statistical methods for the earth scientist. Macmillan Press Ltd., London, 153 p.

Tomkeieff, S. I., 1945. Linear intercepts, areas and volume. Nature, v. 155, p. 107.

Underwood, E. E., 1970. Quantitative stereology. Addison-Wesley Pub. Co., Reading, Massachusetts, 274 p.

van Genderen, J. L., and Lock, B. F., 1976. A methodology for producing small scale rural land use maps in semi-arid development countries using orbital M.S.S. imagery. Final Contractor's Report-NSSA-CR-151173, 270 p.

van Genderen, J. L., and Lock, B. F., 1977. Testing land-use map accuracy. Photogrammetric Engineering and Remote Sensing, v. 43, p. 1135-1137.

Verstappen, H. T., 1974. On quantitative image analysis and the study of terrain. The ITC Journal, p. 395-413.

Wadell, H., 1934. Volume, shape and roundness of quartz particles. Journal of Geology, v. 43, p. 250-280.

Wall, F. J., 1986. Statistical data analysis handbook. McGraw-Hill Book Company, New York, 285 p.

Wanless, H. R., 1981. Fining-upwards sedimentary sequences generated in seagrass beds. Journal of Sedimentary Petrology, v. 51, p.445-454.

Ward, L. G., Kemp, W. M., and Boynton, W. R., 1984. The influence of waves and seagrass communities on suspended particulates in an estuarine embayment. Marine Geology, v. 59, p. 85-103.

Wayne, C. J., 1974. Effect of artificial sea grass on wave energy and nearshore sand transport. Transactions of the Gulf Coast Association of Geological Societies, v. 24, p. 249-273.

Weibel, E. R., 1979. Stereological methods, Volume 1. Academic Press, London, 415 p.

Welch, B. L., 1963. From coral reef to tropical island via *Thalassia* and mangrove. Virginia Journal of Science, v. 14, p. 213-214.

White, L. P., 1977. Aerial photography and remote sensing for soil survey. Clarendon Press, Oxford, 104 p.

Wilson, M. V. H., 1983. Digitizing outlines of fossil specimens using video frame capture. Canadian Journal of Earth Sciences, v. 20, p. 1747-1751.

Wolf, P. R., 1983. Elements of photogrammetry, Second Edition. McGraw-Hill Book Company, New York, 627 p.

Woodroffe, C. D., 1981. Mangrove swamp stratigraphy and Holocene transgression, Grand Cayman Island, West Indies. Marine Geology, v. 41, p. 271-294.

Woodroffe, C. D., Stoddart, D. R., Harmon, R. S., and Spencer, T., 1983. Coastal morphology and late Quaternary history, Cayman Islands, West Indies. Quaternary Research, v. 19, p. 64-84.

Young, I. T., Pevrerini, R. L., Verbeek, P. W., and van Otterloo, P. J., 1981. A new implementation for the binary and Minkowski operators. Computer Vision, Graphics and Image Processing, v. 17, p. 189-210.

Yuan, L. P., 1987. The petrography of permeability: determination of relationships between thin section data and physical measurements. Unpublished Ph. D. Thesis, University of South Carolina, 125 p.

Zieman, J. C., 1972. Origins of circular beds of *Thalassia* (Spermatophyta: Hydrocharitaceae) in South Biscayne Bay, Florida and their relationship to mangrove hammocks. Bulletin of Marine Science, v. 22, p. 559-574.

Zieman, J. C., 1975a. Seasonal variation of turtle grass, *Thalassia testudinum* Konig, with reference to temperature and salinity effects. Aquatic Botany, v. 1, p. 107-123.

Zieman, J. C., 1975b. Tropical seagrass ecosystems and pollution. *In* Wood, E. J. F., and Johannes, R. (eds), Tropical marine pollution. Elsevier, Amsterdam, p. 75-98.

Zonneveld, I. S., 1974. Aerial photography, remote sensing and ecology. The ITC Journal, p. 553-560.

Zucker, S. W., 1977. Algorithms for image segmentation. *In* Simon, J. C., and Rosenfeld, A. (eds.), Digital image processing and analysis. Noordhoff International Publishing, Leyden, p. 169-185.